UNIVERSITY OF PARMA

Ph.D. in Biotechnology

XXIX Course

Genotoxicology of Engineered Nanomaterials (ENMs): the experience and data from a comparison of genome-wide analyses in yeast and in plant.

Supervisor:
Prof. Nelson Marmiroli

Tutors:
Prof. Marta Marmiroli
Dr. Caterina Agrimonti
Dr. Jason C. White

Candidate: Francesco Pasquali

Summary

List of abbreviations

QSAR - Quantitative Structure-Activity Relationship

QDs - Quantum Dots

ENMs - Engineered Nanomaterials

NMCC - Nanomaterial Co-Contaminant

SWCNTs - Single-Walled Carbon Nanotubes

ESEM - Environmental Scanning Electron Microscope

S/TEM - Scanning/Transmission Electron Microscope

HRTEM - High Resolution Transmission Electron Microscope

XRD - X-ray diffraction

EDX - Energy-Dispersive X-ray analysis

FWHM - Full Width at Half Maximum

YPD - Yeast extract Peptone Dextrose

YPG - Yeast extract Peptone Glycerol

TTC - 2,3,5-Triphenyltetrazolium Chloride

DAPI - 4',6-Diamidino-2-Phenylindole

GSH - Glutathione reduced form

GSSG - Glutathione oxidized form

ROS - Reactive Oxygen Species

DCF - 2'-7'-Dichlorofluorescein

H_2DCFDA - 2',7'-Dichlorodihydrofluorescein Diacetate

DTNB - 5,5'-Dithiobis-2-Nitrobenzoic Acid

TNB - 2-Nitro-5-Thiobenzoic Acid

RS - Respiratory Sufficient

RD - Respiratory Deficient

RT-qPCR - Real Time quantitative Polymerase Chain Reaction

PCA - Principal Component Analysis

ANOVA - Analysis of Variance

ICP-MS - Inductively Coupled Plasma Mass Spectrometry

HSD - Honestly Significant Difference

GO - Gene Ontology

mtRFP - mitochondrial directed Red Fluorescent Protein

1. Introduction

1.1 Abstract

Engineered nanomaterials (ENMs) are structures on the range of 1-100 nm, and are characterized by properties due to their small size and surface reactivity that make them suitable for several industrial applications. Nanotechnology is a rapidly growing industry, with a market value expected to reach US$ 55 billion by 2022 (Allied market research, 2016). Because of their wide diffusion and of the lack of information about mechanisms of biological uptake and interaction with cells, it's crucial to assess the risks linked to their spread and behaviour in the environment. A first part of this work was performed in plants, following a previous experience with *Arabidopsis thaliana* L. Heynh (Marmiroli *et al.* 2014), in which transcriptomic analysis on two Ds transposition-induced mutant lines allowed the identification of genes involved in tolerance to cadmium sulphide quantum dots (CdS QDs). Starting from here, in cooperation with CAES of New Haven, CT, the work focused on the impact of nanomaterials on crop plant *Cucurbita pepo* L. Five different nanomaterials (CeO_2, La_2O_3, CuO, ZnO, and CdS QDs) were tested singularly and in couples to determine how the interaction between different NPs could alter their effect on the transcriptome and their uptake and translocation inside plant tissues. Real-time expression analysis identified several genes that specifically respond to each of the nanomaterials tested; in particular the gene 152u, encoding for a chloroplastic electron carrier, is down-regulated in all the treatment conditions, thus representing a putative biomarker of exposure. ICP-MS analysis of metal content showed that nanomaterials are more easily translocated in stems and leaves than their bulk counterparts, probably because of their smaller size. The aim of the second part of this work was to analyse the effect of CdS QDs in the model system *Saccharomyces cerevisiae*, exploiting high-throughput genomic and transcriptomic approaches: the former consisted in screening a collection of 6000 haploid strains, with a deletion in genes that are not essential for yeast's survival; the latter consisted in a whole-transcriptome analysis of expression levels through Affymetrix GeneChip Microarray platform. A gene ontology and network analysis was performed on the data obtained,

allowing the identification of mitochondrial organization and mitosis as the main biological processes affected by CdS QD action. In particular, data collected highlighted the differences between CdS QDs and Cd^{2+} mechanisms of toxicity, while HSC82, ALD3 and DSK2 were identified as some of the key genes involved in CdS QDs response (Marmiroli *et al*. 2016). The impact of quantum dots on mitochondria was then studied from a physiological and morphological point of view: i) the respiratory activity was impaired; ii) mitochondrial membrane potential was disrupted iii) fluorescence microscopy highlighted an interruption in the mitochondrial network; iv) upon treatment, reactive oxygen species accumulation was induced, while the glutathione redox-state decreased significantly; v) CdS QD treatment impaired the ability of yeast cell to grow on non-fermentable carbon sources but, conversely from ionic cadmium, did not induce the formation of respiratory deficient mutants (Pasquali *et al*. 2016).

1.2 Nanotechnologies

According to the European Union recommendation 2011/696/EU, a nanomaterial can be defined as "*a natural, incidental or manufactured material containing particles, in an unbound state or as an aggregate or as an agglomerate and where, for 50 % or more of the particles in the number size distribution, one or more external dimensions is in the size range 1 nm - 100 nm*". Engineered nanomaterials (ENMs) are gaining more consideration in the last decades due to their peculiar properties, which make them suitable for a wide range of applications: agricultural production and crop protection (Dwivedi *et al.* 2016), food processing (Peters *et al.* 2016), environmental remediation (Louie *et al.* 2016), medicine (Li *et al.* 2016), electronics (Mohiuddin *et al.* 2016) and many more. For this reason, nanotechnology market share reached 14 billion $ in 2015, and is expected to reach 55 billion $ by 2022 (Allied market research, 2016). In terms of market share the categories with the higher income include inorganic non-metallic ENMs (like

synthetic amorphous silica, aluminium oxide, titanium dioxide), carbon based ENMs (like carbon black, carbon nanotubes), metal nanoparticles and organic, macromolecular or polymeric materials.

1.3 Engineered nanomaterials and risk assessment

ENMs behaviour is strongly influenced by their small size, high surface/volume ratio, chemical stability and composition (Wani *et al.* 2016). Furthermore, because of their peculiar properties, their fate and mechanism of action are usually different from the ones of their bulk counterparts. Another key factor playing a role in nanomaterial toxicity is their occurrence as aggregates or free particles: in the first case, the formation of agglomerates might mitigate the nano-specific properties, while in the second case exposure is likely to be more dangerous. Exposure may occur at different levels (fig. 1): i) at the production stage, where the risk is higher but easily controlled by the use of proper personal protective equipment and close systems; ii) at the use stage, where exposure is strongly influenced by the inclusion of ENMs in a matrix or their enclosure inside the products; iii) at the waste stage, after disposal and grinding of ENMs containing products. Furthermore, an additional way of exposure to ENMs derives from their presence in recycled materials. Exposure to ENMs that are proved not to be toxic and not to bio-accumulate represent a lesser risk, as they won't cause toxic effects at least at moderate doses. The same applies to those ENMs who are confined in a matrix or whose effects are prevented by applying risk management measures. Scientific Committee on Emerging and Newly Identified Health Risks (SCENIHR) stated that "*while risk assessment methodologies for the evaluation of potential risks of substances and conventional materials to man and the environment are widely used and are generally applicable to nanomaterials, specific aspects related to nanomaterials still require further development. This will remain so until there is sufficient scientific information available to characterise the harmful effects of nanomaterials on humans and the environment.*" Therefore, it is necessary to develop new tools

and procedures to assess all the risks and safety issues arising from the dispersion of this new class of materials in the environment.

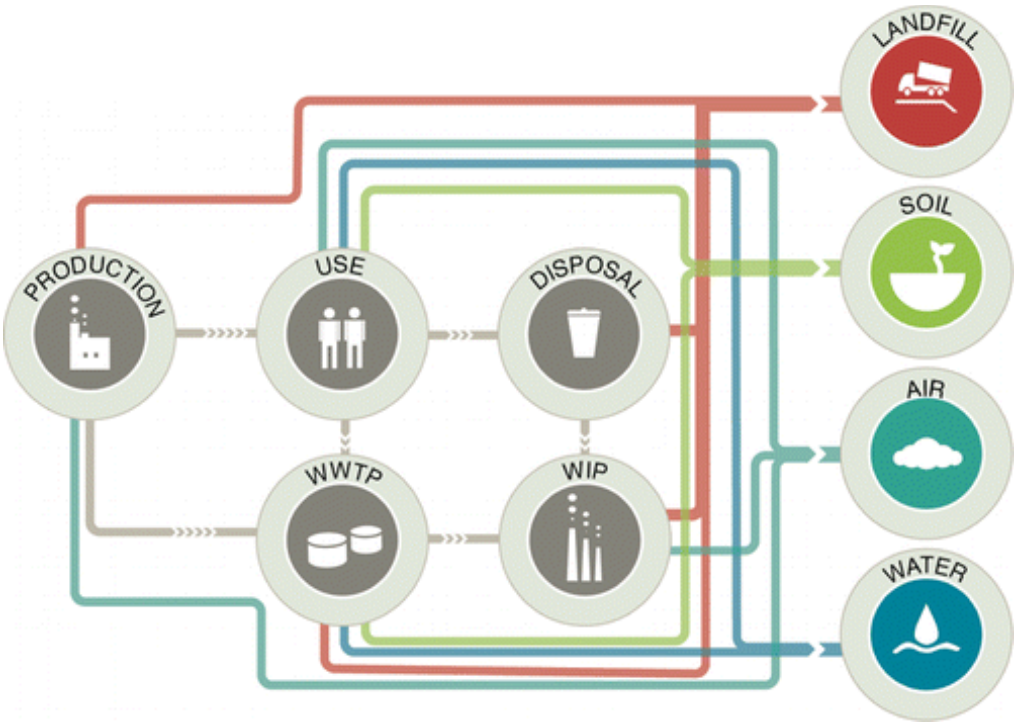

Figure 1. Routes of exposure and dispersion of ENMs in the environment (Keller *et al*. 2013).

1.4 Nanotoxicology

In this framework of risk characterization and evaluation, nanotoxicology represents a powerful tool for the study of the effect of ENMs on biological systems. In the recent years, ENMs hazards have been evaluated using both *in vitro, in vivo* and in *silico* techniques. The *in vitro* tests include the use of single cell types cultures, co-cultures, three dimensional models of tissues and cell-free assays (Stone *et al.* 2016); the abundance of tests allows the analysis of different parameters at the same time, composing an overall view of ENMs toxicity that needs the validation o n *in vivo* models and the use of a set of standards to compare different datasets. *In silico* approaches, in particular quantitative structure-activity relationship (QSAR) analysis, aim to link physiochemical properties of the ENMs to their behaviour in the biological systems, to allow the

production of "safer-by-design" ENMs and reduce the risks for human health. This kind of tests might represent a good alternative to the *in vivo* animal models, but they are still in the early stages of development (Tantra *et al*. 2015).

Considering the widespread diffusion of ENMs, their physical and chemical diversity as well as the current unreliability of the *in silico* approaches, the identification of testing platforms alternative to the expensive and ethically questionable animal models becomes crucial. Several governmental organizations, like EU (through its REACH project), the OECD (Organisation for Economic Co-operation and Development) and the US National Research Council (Krewski *et al.* 2010), are engaged in the development of alternative high-throughput tests based on simpler organisms, like *Saccharomyces cerevisiae* as a model for higher eukaryotes whereas *C. pepo* for agri-food relevant crop plants. Guidance from the international regulatory agencies (EFSA and FDA respectively for EU and US) requires a suite of *in vivo* and *in vitro* assessments that must be carried out for nanomaterial containing products. The two approaches may provide different and, sometimes, contradictive results: in fact the dose *in vitro* might not be relevant *in vivo* or the *in vitro* cell line might not be representative for the whole organism; furthermore effects of nanoparticles on health depend on individual factors such as genetics and existing disease. For these reasons, despite the respective limitation, both *in vivo* and *in vitro* tests provide necessary information that are complementarily needed to assess the ENMs mechanism of action and toxicity.

1.5 State of the art and current legislation

Even if ENMs safety regulation, recommendations and guidances are being developed to allow a safer use of ENMs, both in EU and in other countries there are still no pieces of legislation that are specific for them (Arts *et al.* 2014). For this reason ENMs are usually included in more generic categories of chemical and are subjected to pre-existing regulations. For instance, in Europe ENMs used in the different industrial sectors must meet the requirements of the REACH

(Registration, Evaluation and Authorization of Chemicals) (Regulation (EC) No 1907/2006), which regulates the production and utilization of all the chemical substances and their effects on environment and health. In many cases, the current legislation is considered to be sufficient to allow a safe use of nanotechnologies, but due to their growing heterogeneity and diffusion, a more stringent regulation might be required (Lee R.G. *et al*. 2016). At the moment, the European Parliament, Food and Drug Administration and several non-governmental organisations are actively operating in this field, developing a risk governance framework to address issues like the definition of nanomaterial, registration and authorisation procedures, risk assessment, risk management, traceability and labelling (Falkner and Jaspers, 2012).

1.6 Synthesis of engineered nanomaterials

ENMs production can exploit either bottom-up or top-down approaches (fig. 2). In the bottom-up approach, small building blocks are assembled through chemical reactions, nucleation or self-aggregation to produce complex structures. Organic synthesis, self-assembling, colloidal aggregation and laser-induced assembling techniques belong to this category. Bottom-up approach is used for the synthesis of fullerenes and carbon nanotubes (Sathish *et al*. 2009, Hitosugi *et al*. 2011). In the top-down approach, the production starts from the bulk materials which are processed through photolithography, quenching or mechanical techniques to obtain the ENMs. Top-down approaches are primarily used for the production of metal oxide nanoparticles (Yadav *et al*. 2012). The choice between the two approaches depends on the properties required for the final product: the bottom-up methods allow to precisely tune the size and the composition of the ENM, but the high complexity of these processes make them less suitable for large-scale production; on the other hand, top-down techniques have been optimized for industrial production, but result in an higher heterogeneity of the ENMs in terms of dimensions. Recently, some studies are trying to combine the advantages of both the approaches: for example, Huang *et al*. (2016) describe a manufacturing

process for hybrid anodes for lithium-ion batteries, which include a top-down synthesis of nano-silicon followed by a bottom-up inclusion in a nitrogen-doped graphene nanosheet. This process results in the production of batteries with a longer cycling lifetime and a better capacitive retention.

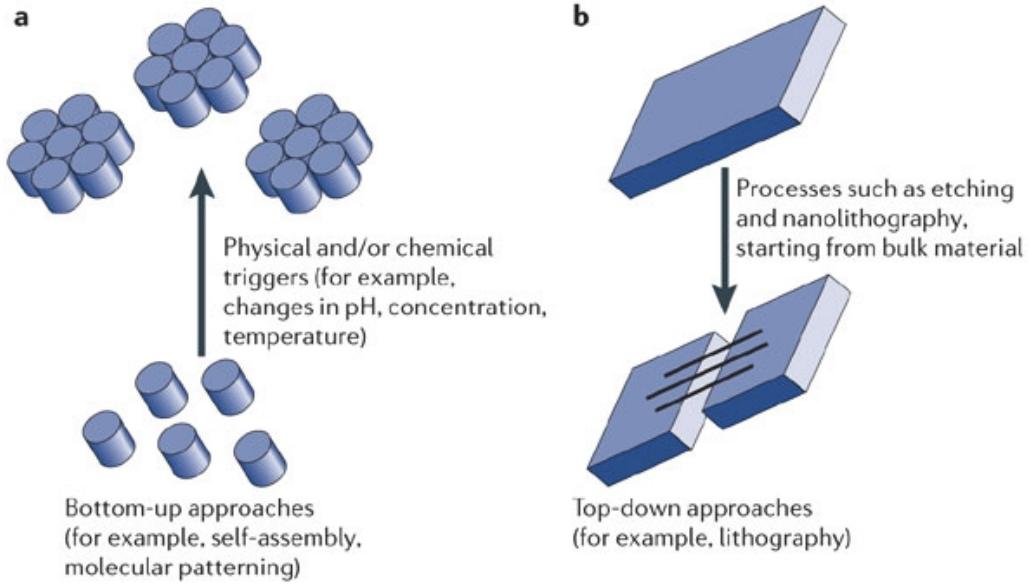

Figure 2. Bottom-up (a) and top-down (b) approaches for ENMs manufacture (Silva 2006).

1.7 Nanomaterials classification

A first classification of nanomaterials can be performed according to their natural or manufactured source. The first category includes all the nanomaterials produced by geological (e.g. chemical and physical degradation of rock materials, neoformation, volcanic eruptions) or biological (e.g. nucleic acids, peptides, viruses) processes. Living organisms evolved in an environment where these natural nanomaterials are actively released and interact with other pollutants, water and organic matter (Handy *et al*. 2008). The engineered nanomaterials are designed to meet specific properties and characteristics and are synthesized through technological processes. Engineered nanomaterials can be furthermore subdivided by their composition in: i)

carbon-based ENMs, including fullerenes, nanotubes and graphene (fig. 3); ii) metal-based ENMs, including single metals (e.g. Au and Ag nanoparticles), metal-oxides (e.g. CeO_2, La_2O_3, TiO_2 nanoparticles) and nanocrystals such as semi-conductor quantum dots; iii) hybrid ENMs, combining the two aforementioned categories through functionalization or the use of a core-shell structure to modulate ENMs reactivity and target specificity.

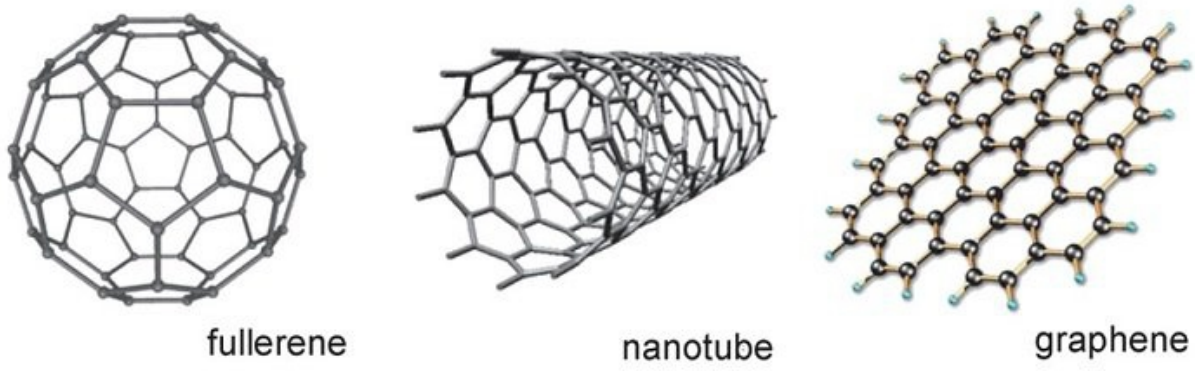

Figure 3. Different kinds of carbon based ENMs.

1.8 Metal oxide nanoparticles

Metal oxide nanoparticles are one of the most widely used ENMs for industrial applications. The high variety of oxide compound used for their synthesis along with the ease of modification and the tunability of their physical and chemical properties, makes them suitable for use in construction materials (e.g. insulators, semiconductors, paint, Lee J. *et al*. 2010), cosmetics (e.g. ZnO and TiO_2 used in sunscreen, Lu *et al*. 2015), agriculture (e.g. CuO and ZnO used as biocides, Bondarenko *et al*. 2013) and in the biomedical field (e.g. antibacterial iron oxide nanoparticles, Javanbakht *et al*. 2016). Their modifiable characteristics result in a wide range of effects, primarily dependent on charge, shape, size and degree of dispersion. For instance, semi-conductor nano-oxides seem to exert a higher toxic effect in bacteria, if compared to the non-insulators (Bohnsack *et al*. 2012); more soluble metal oxide nanoparticles, like ZnO, are easier to disperse and to be

internalized in the cell, where they induce the accumulation of reactive oxygen species and the response of cell to oxidative stress (Xia *et al*. 2008). In human lung epithelial cells, ZnO and Al_2O_3 nanoparticle exposure resulted in the activation of the NFκB pathway and induced the release of inflammatory cytokines; furthermore ZnO induced also the main mitogen-activated protein kinases (Simón-Vázquez *et al*. 2016). Patil *et al.* (2016) reported that exposure of lung fibroblasts to TiO_2 and ZnO nanoparticles resulted in a dose-dependent epigenetic alteration, as proved by the decrease in global DNA methylation and DNA methyltransferase activity. In *A. thaliana*, CuO nanoparticles significantly inhibited plant growth and induced root damage; after 2 hours of exposition, nano-CuO induced oxidative stress in roots to a greater extent if compared to the corresponding bulk material, as shown by reactive oxygen species accumulation and up-regulation of oxidative stress-related genes (Tang *et al*. 2016). CuO nanoparticles exposition induced a decrease in sees germination rates in both cucumber (Moon *et al.* 2014) and rice (Shaw and Hossain 2013). ZnO, Fe_2O_3, Al_2O_3, CuO, nanoparticles highlighted a negative impact on shoot/ root growth and elongation in many crop species such as rice, wheat, maize, tomato, and barley (Rizwan *et al.* 2017). Furthermore, metal oxide nanoparticles had been shown to induce chromosomal aberrations in maize (Castiglione *et al.* 2011) and garlic (Shaymurat *et al.* 2012).

CeO_2 nanoparticles are extensively used as semiconductors in solar cells, UV blockers, polishing agents and their photocatalytic properties are exploited in chemical and mechanical cleaning methods (Balavi *et al*. 2013). La_2O_3 nanoparticles are used in biomedical sensors for temperature, uric acid and glucose detection (Brabu *et al*. 2015). Thanks to their paramagnetic properties, La_2O_3 nanoparticles are being tested for targeted drug delivery in the human body (Zhang X. *et al*. 2016). CuO nanoparticles have applications as catalysts in chemical reactions and, thanks to their excellent electric properties, in the manufacture of superconductors, solar cells, sensors and storage devices (Singh *et al*. 2016). They also find application in agriculture as fungicides (Kanhed *et al.* 2013). ZnO nanoparticles have a potential outcome in agriculture too, as

nanofertilizers and nanopesticides (Sabir *et al*., Kah *et al*. 2014), and are used for photocatalysis and sunscreens (Faure *et al*. 2013).

1.9 Quantum dots

Quantum dots (QDs) are a class of extremely small in size semi-conductors (Ø < 10 nm), composed by metals belonging to groups II-VI or III-V of the periodic table. Conversely to traditional dyes, QDs exhibit a narrow emission and a broad excitation spectrum, making them suitable for bioimaging and biosensing approaches (Jamieson *et al*. 2007). Thanks to their tuneable absorption spectrum, combined with a high extinction coefficient, QDs find an application in the synthesis of aerogel components of photovoltaic panels (Xing *et al*. 2016). Due to their intrinsic optic, magnetic, electric and piezoelectric properties, QDs are widely used in the manufacturing of batteries, led screens and lasers (Zhai *et al*. 2010). Quantum dots' mechanism of action and possible toxicity are strongly affected by different factors, like composition, size, surface charge, presence/absence of a shell (or other surface modifications) and interactions with proteins or other bio-ligands (Oh *et al*. 2016, fig. 4).

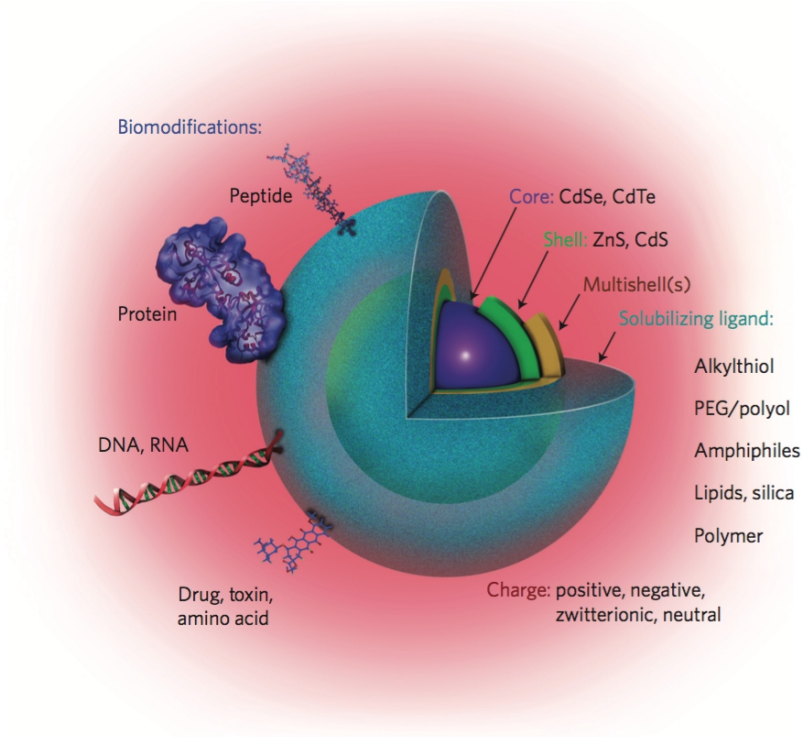

Figure 4. Schematic representation of the structure of QDs, highlighting all the factors that influence their behaviour and the possible interactions with other ligands (Oh *et al.* 2016).

The cadmium sulfide quantum dots (CdS QDs) that have been used during this study were provided by IMEM-CNR (Istituto dei Materiali per l'Elettronica e il Magnetismo, Parma, Italy). They were synthesized through a wet-chemistry approach, according to Villani *et al.* 2012, Cadmium acetate 99.99% ($Cd(CH_3CO_2)$), N,N-dimethylformamide 99% ($HCON(CH_3)_2$) and thiourea 99.5% (NH_2CSNH_2). These quantum dots have an average diameter of 4~5 nm, a density of 4.82 g cm^{-3} and an average weight of $2.5*10^{-18}$ g.

In literature there are several evidences of quantum dots' toxic impact on human health and environment, which is correlated to their surface properties, functionalization, diameter, assay type and exposure time (Oh *et al*. 2016). The study of Nguyen *et al*. (2015) analyzed the response of human hepatocellular carcinoma HepG2 cells to CdTe quantum dots exposure: QDs associate to the mitochondria, leading to a disruption of mitochondrial membrane potential and to an impairment of cellular respiration. CdTe QDs caused also a change in the activity and the levels of the enzymes of

the electron transport chain. The comparison of the response to equivalent concentrations $CdCl_2$ showed how the toxic effects of QDs were not only dependent on release of free ionic cadmium. Zhang T. *et al*. (2015) highlighted how *in vivo* and *in vitro* exposure of CdTe QDs in mice liver cells resulted in an increased level of lipid peroxide markers and in a concentration- and time-dependent cytotoxic effect. An accumulation of reactive oxygen species and the induction of apoptosis were also observed. In particular, the up-regulation of the tumor suppressor gene *p53* and of the pro-apoptotic gene *Bcl-2*, and the down-regulation of the anti-apoptosis gene *Bax*, suggested a central role of the mitochondrion in the activation of programmed cell death pathways. The study of Fan *et al*. (2016) showed how CdTe/CdS core/shell quantum dots activate autophagy instead of apoptosis in HL-7702, HepG2, HEK-293 and Raji cell lines, as confirmed by confocal and TEM microscopy. Accumulation of reactive oxygen species was suggested as one of the causes of autophagy induction and cytotoxic effects. *In vivo* tests on BALB/c mice resulted in liver injury, nephrotoxicity, and hematopoietic disorders, whose symptoms were ameliorated after administration of an autophagy repressor.

1.10 Relevance of mitochondrion in eukaryotic cells

Mitochondrion is a double-membrane organelle, which plays a central role in eukaryotic cells. They possess a circular genome, remnant of the endosymbiotic origin of these organelles. The majority of the genes required for mitochondrial biogenesis were transferred into the nuclear genome during the evolution of eukaryotes, and only a small amount is still encoded by mitochondrial DNA (mtDNA). In yeast, this genome was sequenced for the first time in 1998 (Foury *et al*. 1998): it consists of a 75 kb circular molecule, encoding for 28 proteins and 27 different ribosomal and transfer RNA. Mitochondria are considered the "powerhouse" of the cell, as they are involved in generation of ATP through the oxidative phosphorylation, controlling the basic rates of cellular metabolism (McBride *et al*. 2006). Mitochondria are also responsible for

biosynthesis of iron-sulfur clusters, heme, lipid and sterols (Lasserre *et al*. 2015). Furthermore, apoptosis could be triggered by mitochondria through three different mechanisms: the first is dependent on the caspase family of proteases, which are triggered through the release of specific proteins from the mitochondria; the other two are caspase-independent and rely on interruption of oxidative phosphorylation and alteration of cellular redox potential (fig. 5, Jin C. *et al*. 2002). As a result of evolution, mitochondrial structure and functions have been modified across the different eukaryotes, thus conserving the essential role of this organelle. So far, *Monocercomonoides* sp. is the only eukaryote devoid of functional mitochondria: some of their functions, in particular iron-sulfur cluster assembly pathway, are provided by cytosolic machinery probably acquired through bacterial lateral gene transfer (Karnkowska *et al*. 2016). In humans, defects in mitochondrial functionality are related to a number of severe diseases, including hyperglycaemia-induced coronary microvascular dysfunction, hypertensive renal disease, obesity, diabetes, muscular disease, cancer and Parkinson's disease (Nunnari *et al*. 2012, Van Houten *et al*. 2016).

In a previous study (Marmiroli *et al*. 2016), a screening of a deletion mutant collection of *Saccharomyces cerevisiae* identified mitochondrial organization as one of the main biological processes affected by CdS QD exposition. A transcriptional analysis performed on HepG2 human cell line (Paesano *et al*. 2016) highlighted that the same CdS QDs trigger mitochondria-mediated apoptotic pathway. Furthermore, in literature are reported other evidences that mitochondria is a major target of nanomaterial's toxicity: Ye *et al*. 2016 show that positively charged graphene induces mitochondrial fission and recruitment of dynamin-related protein in BV-2 cell line; TiO_2 nanoparticles affect lung mitochondrial function in animal cell lines (Freyre-Fonseca *et al*. 2011), while *in utero* exposition of rat pups induces mitochondrial dysfunction (Stapleton *et al*. 2015).

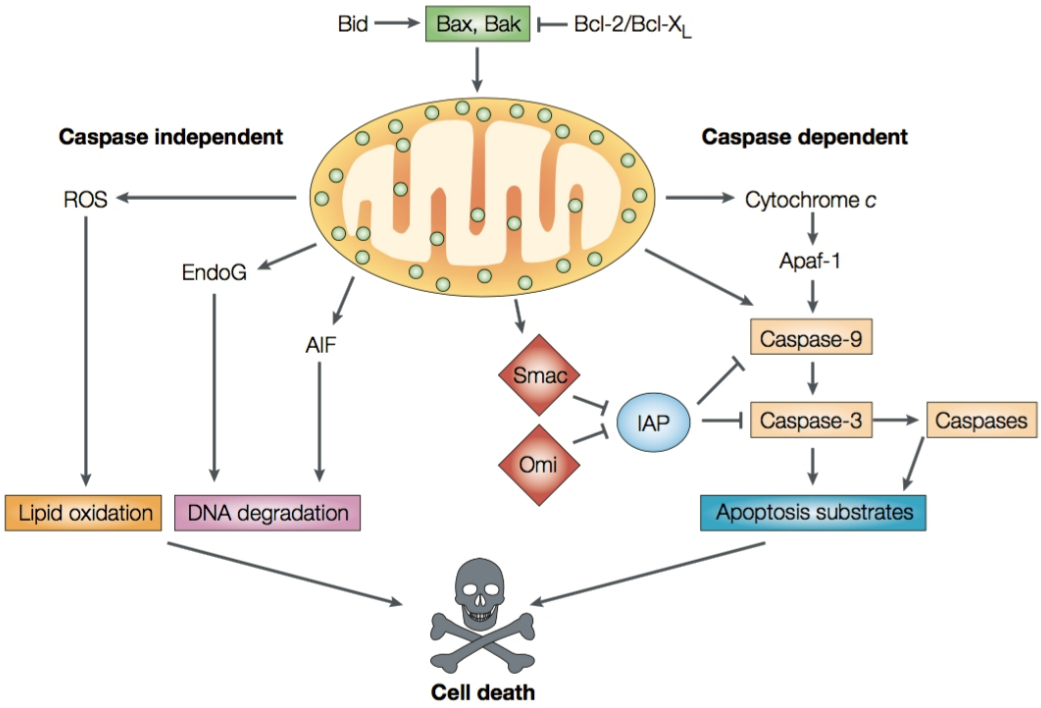

Figure 5. Mechanisms of caspase-dependent and -independent apoptosis mediated by mitochondria in mammalian cells (Jin C. *et al*. 2002).

1.11 *Cucurbita pepo* as a model organism for nanomaterial exposure in crop plants

Cucurbita pepo L. is a plant belonging to the family of *Cucurbitaceae*. It is considered as one of the most important vegetable crops from an economical and agricultural point of view, thanks to its high content in vitamins, minerals and fibers (Obrero *et al*. 2011). *C. pepo* is a monoicous species, with distinct male and female flowers on the same plant. Its genome size may vary from 945.7 to 1084.6 Mb among the different zucchini cultivars (Rayburn *et al*. 2008). Due to its wide use and distribution, in the last years *C. pepo* is gaining a growing interest as a model organism for toxicology and nanotoxicology studies: Musante and White (2010) reported that Ag

and Cu nanoparticles treatments in *C. pepo* result in a decrease in biomass and transpiration; Stampoulis *et al.* (2009) showed that Cu nanoparticles reduced emerging root length by 77% and 64% if compared to untreated control and bulk Cu treatment, while Ag nanoparticles and multiwalled carbon nanotubes negatively affected plant's biomass; Hawthorne *et al.* (2012) demonstrated that Au nanoparticles did not affect *C. pepo* growth at any particle size and concentration tested, whereas Si nanoparticle treatment resulted in a reduction of plant growth and transpiration; in addition, the solution properties were found to significantly impact the nanoparticle's effects. In the last years, in particular the focus is on transcriptional response (Pagano *et al*. 2016), uptake and translocation of pollutants in plant tissues and fruits (Tripathi *et al*. 2016), and their transfer along the food chain (Hawthorne *et al*. 2014). For this reason, several databases and bioinformatics tools are being developed: the transcriptome has been fully characterized (Blanca *et al.* 2011), and the genome sequences are available online (https://cucurbigene.upv.es/genome-v3.2/).

1.12 *Saccharomyces cerevisiae* as a model organism for nanotoxicological studies

Saccharomyces cerevisiae is a unicellular eukaryote and one of the most used model organisms for molecular biology. Its genome has a size of ~12 Mb, subdivided in 16 chromosomes, which has been completely sequenced and annotated (Goffeau, 2000). Due to its ease of use, fast life cycle (one division each 90 minutes) and to the availability of several molecular and genomic tools, yeast had been used as a platform for toxicological studies (Dos Santos *et al*. 2015). Furthermore the high level of functional conservation within higher eukaryotes genomes, in particular human, makes yeast a key model system for the assessment of the mechanisms underlying the response to environmental pollutants as ENMs. For instance, yeast cells exposed to CuO nanoparticles did not affect cellular viability, but resulted in an inhibition of metabolic activity after copper release in the growth media (Mashock *et al*. 2016). Otero-González *et al*. (2013)

studied the effects of different ENMs (TiO_2, ZrO_2, Fe^0, Fe_2O_3, and Mn_2O_3) on yeast: manganese-based ENMs had a consistent impact on inhibition of oxygen consumption and membrane integrity, whereas the others exhibited a lower or absent toxicity. Bayat *et al.* (2014) analysed the cytotoxic and morphological effects of TiO2, CuO, ZnO, Ag nanoparticles and single-walled carbon nanotubes (SWCNTs) on *S. cerevisiae*. CuO nanoparticles exerted a high cytotoxic effect, and reduced cell density by 80%; Ag and TiO_2 nanoparticles reduced cell density and localized at intracellular vacuoles, cell wall and vesicles levels. ZnO NPs were non cytotoxic and resulted in an increase of the size of the vacuoles. SWCNTs, despite the potential induction of oxidative stress evidenced in other studies, were not cytotoxic and did not induce alteration in the cell structure. As reported in other several studies (e.g. Bermejo-Nogales *et al.*, Yang *et al*., Khalid *et al*. 2016), oxidative stress induction by nanomaterial exposure affects mitochondrial functionality (disruption of mitochondrial structures, permeabilization of inner membrane). The capability to grow in mitochondrial impairment conditions makes *S. cerevisiae* a perfect model organism for the study of this "pathological mitochondria" condition.

1.13 Aim of the project

The aim of these work was to evaluate ENMs impact on *C. pepo* and *S. cerevisiae* from a molecular and physiological point of view: the first revealed the genes and biological processes most affected by ENMs exposure, while the latter focused the attention on the effects on growth and homeostasis of the two model organisms in condition of treatment; in particular, toxicity of nanomaterials was assessed in conditions of acute exposition (high concentrations and short times of exposure): these conditions are not likely to occur in the environment, but give a better understanding of ENMs mechanisms of action and toxicity and allow the identification of putative biomarkers of exposure to nanomaterials, as a part of a broader framework of risk assessment.

In the first part, the response of *C. pepo* to binary combinations of ENMs was investigated. In literature several papers analyse the response of zucchini to single types of ENMs, but currently no one has investigated how NPs-NPs interactions influence their uptake, translocation and effect on gene transcription. In particular, impact on physiological parameters (roots/shoots length, water content, photosynthetic pigments abundance), on nanoparticles uptake and translocation and on gene transcription were assessed.

The aim of the second part of the project was the in-depth investigation of the mechanism of action of CdS QDs, using *S. cerevisiae* as a model organism for higher eukaryotes. High throughput assays (deletion mutant screening and microarray transcriptome analysis) provided a general overview of the genes and biological processes involved in CdS QDs response. According to previous studies and evidences in literature, the role of mitochondria as one of the main targets of quantum dots toxicity has been analysed, using a molecular biology approach, physiological tests and fluorescence microscopy.

2. Materials and methods

2.1 CdS quantum dot synthesis and characterization

Cadmium sulphide quantum dots used were provided by IMEM-CNR (Parma, Italy) and synthesized from cadmium acetate, N,N-dimethyl formamide and thiourea through a wet-chemistry approach, according to Villani *et al.* 2012. Different analyses were carried out to determine CdS QDs properties: i) X-ray diffraction was analysed with an ARL-X'Tra device (Thermo Fisher Scientific, Waltham, MA, USA); their structure was examined with a field emission high resolution JEM-2200 FS transmission electron microscope (JEOL ltd., Tokyo, Japan) operating at 200 kV; iii) group morphology and elemental content was assessed with an environmental scanning electron microscope (ESEM) Quanta 250 FEG, FEI with Bruker QUANTAX EDS XFlash® 6T detector series and ESPRIT 2 analytical methods interface (FEI company, Hillsboro, Oregon, USA; Bruker, Berlin, Germany). For electron microscopy, single drops of an 80 mg L^{-1} solution of CdS Quantum dots were deposed on SEM stub covered with carbon tape and let dry. Scanning electron imaging and X-ray spectra acquisition were performed at a pressure of 70 Pa, a working distance of 9.9 mm, and an acceleration voltage of 20 KeV.

2.2 *Cucurbita pepo* and conditions of growth

Cerium oxide (CeO_2, nanopowder, <25 nm particle size) was purchased from Sigma Aldrich; Lanthanum oxide (La_2O_3, 10-100 nm particle size range), copper oxide (CuO, 40 nm particle size), and zinc oxide (ZnO, <100 nm particle size) were purchased from US Research Nanomaterials, Inc. CdS QDs were provided by IMEM-CNR. Every nanomaterial was characterized through z-sizer and scanning/transmission electron microscopy (S/TEM), according to Pagano *et al.* 2016. All the respective bulk materials were purchased from Sigma Aldrich.

Zucchini seeds (*Cucurbita pepo* L., cv Costata Romanesco) were purchased from Johnny's Selected Seeds (Albion, ME, USA). Seeds were sown in vermiculite for seven days. After the germination, seedlings were transferred in 100 mL of vermiculite containing 0 mg L^{-1} (untreated control), 500 mg

L^{-1} ZnO (NPs or bulk), 100 mg L^{-1} CdS (QDs or bulk), or binary combinations of the five ENMs. Prior to use, nano- and bulk materials solutions were sonicated through a Fisher Scientific model 505 sonic dismembrator (Fisher Scientific, Waltham, MA, USA) at 40% amplitude for 60-120 s. Seedlings were treated for 21 days, following Pagano *et al.* 2016.

2.3 Physiological analyses and metal content evaluation

After the exposure, plants were harvested and thoroughly washed in deionized water. For each plant, fresh weight and primary roots and shoots length were measured. For metal content analysis each plant was divided in roots, stem and leaves in five biological replicates. Samples were dried and digested in 65% HNO_3, and then analyzed with an Agilent ICP-MS CE 7500 (Agilent Technologies, Santa Clara, CA, USA), according to Pagano *et al.* 2016. 0.2 g of leaves for each plant were harvested and prepared for 2,3,5-triphenyltetrazolium chloride (TTC) and chlorophyll/carotenoids content analysis, following Marmiroli *et al.* 2014.

2.4 Gene expression analysis of *C. pepo* in response to ENM/NMCC treatment

Total RNA was extracted, in three biological replicates per treatment, from 0.1 g of fresh plant material, using a Sigma Aldrich Spectrum Plant Total RNA Kit (Sigma Aldrich). 0.1 ng of total RNA were retro-transcribed to cDNA with a RT-qPCR Qiagen QuantiTect Reverse Transcription kit (Qiagen, Velno, NL). Analysis of gene expression was performed on a subset of 38 genes, using actin β-actin of *C. pepo* as housekeeping gene, according to Pagano *et al.* 2016. The list of the 38 genes is reported in paragraph 8.1 of the appendix section.

2.5 Yeast strains and growth conditions

The majority of the experiments discussed in this thesis used *Saccharomyces cerevisiae* strain BY4742 (MATα his3Δ1 leu2Δ0 lys2Δ0 ura3Δ0). For petite induction studies, W303 (MATα leu2-3,112 trp1-1 can1-100 ura3-1 ade2-1 his3-11,15) strain was used in addition to BY4742. Yeast cells were inoculated in a liquid YPD (Yeast extract Peptone Dextrose) medium pre-culture (1% w/v yeast extract, 2% w/v peptone, 2% w/v glucose), and grown for 24 h at 28°C under shaking at 130 rpm. Pre-culture cell concentration was assessed through Burker's chamber count. 10^5 cells mL^{-1} were then inoculated in fresh YPD for negative control, treated in YPD supplemented with nystatin (0.25 mg L^{-1}), nystatin + CdS quantum dots (CdS QDs, 75, 100 or 150 mg L^{-1}), cadmium sulphate ($CdSO_4$, 10, 20 or 25 μM) or ethidium bromide (50 μg mL^{-1}), as specified for each single experiment. Nystatin is a polienic antibiotic, which binds the ergosterol of yeast cell's membrane used to encourage the uptake of CdS QDs, as described in Marmiroli *et al.* 2016. Cultures were then grown at 28°C under shaking at 130 rpm.

2.6 Yeast growth on different carbon sources

Four serial 10-fold dilutions (10^5-10^2) of either wild type and RD cells were spotted onto YPD alone, supplemented with 0.55 mg L^{-1} nystatin or 0.55 mg L^{-1} nystatin plus 100/150/200 mg L^{-1} CdS QDs. The concentrations of nystatin and CdS QDs were increased, in respect of liquid YPD treatments, due to their lower bioavailability in the solid medium, according to Marmiroli *et al.* 2016. RD mutants were used as negative control of growth on non-fermentable carbon sources. The experiment was replicated on YP agar plates where 2% w/v dextrose was replaced with other fermentable (galactose) or non-fermentable (glycerol and ethanol) carbon sources. After 72 h of incubation at 28 °C, the presence/absence of growth at each cell dilution was assessed.

2.7 Cytofluorimetric analysis of yeast response to CdS QDs

For cytofluorimetric analysis, BY4742 cells were grown in absence of treatment, or treated with 0.25 mg L^{-1} of nystatin or nystatin plus 100 mg L^{-1} CdS QDs. 10^7 cells per each treatment were then harvested by centrifugation (5000 g, 5 min) and stained with FUN1 (CAS number: 161057-69-8), a stain that is internalized in the vacuole by living cells only. Its accumulation leads to the formation of typical red-orange fluorescent structures (Wenish *et al.* 1997). For each treatment, both stained and unstained samples were analysed with an Attune NxT Flow Cytometer (Thermo Fisher Scientific, Waltham, MA, USA) using a BL1 filter.

2.8 Microarray transcriptomic analysis of yeast exposed to CdS QDs

Microarray analysis was carried out on BY4742 cells, treated for 24 h on liquid YPD without supplementation, with 0.25 mg L^{-1} nystatin, or with 0.25 mg L^{-1} nystatin plus 100 mg L^{-1} CdS QDs. Five biological replicates were performed for each treatment. Total RNA was extracted from the samples with an RNeasy Mini kit (Qiagen, Velno, NL): Extraction yield and quality was assessed through spectrophotometric analysis and electrophoresis in a 2% w/v agarose gel. For each sample, two aliquots of RNA were retro-transcribed into cDNA using a QuantiTect Reverse Transcription Kit (Qiagen, Velno, NL). Transcriptome analysis was performed through Affymetrix GeneChip Yeast genome 2.0 array platform (Affymetrix, Santa Clara, CA, USA), covering 99.93% of *S. cerevisiae*'s genome. RT-qPCR analysis of expression was performed on a subset of genes to validate microarray experiment's results, according to Marmiroli *et. al* 2014, using *PDA1* as housekeeping gene.

2.9 Analysis of oxygen consumption and assessment of respiratory cytochrome content

BY4742 cells were treated for 24 hours in YPD liquid medium, in presence of all the CdS QD and $CdSO_4$ concentrations. Around 10^{10} cells were harvested through centrifugation (5000 g, 5 min) and re-suspended in 1.5 mL of double-distilled water. The peak height of cytochrome aa3, b and c was then used to calculate the cytochrome content through the formula here reported:

Cytochrome content = (peak height*range)/(sample's dry weight).

Oxygen consumption was measured on 100 µL of the cell suspension, which were transferred into an Oxygraph reaction chamber (Hansatech Instruments, King's Lynn, UK) with 800 µL of air-saturated 0.1 M phthalate–KOH (pH 5.0) and 1.5 µM of glucose. Another 1 mL aliquot was analysed in parallel to acquire cytochrome spectra, using a Varian Cary 219 UV-VIS dual-beam spectrophotometer (Agilent Technologies, Santa Clara, CA, USA). Both assays were conducted in three biological replicates.

2.10 Analysis on the effect of mitochondrial DNA integrity

BY4742 and W303 cells were treated for 24 h in liquid YPD, in presence of nystatin, CdS QDs (all the concentrations), $CdSO_4$ (20 µM) and ethidium bromide. 100 cells per each treatment were then collected by centrifugation (5000 *g,* 5 min), washed and re-suspended in double-distilled water, and plated on YPD supplemented with agar (2% w/v). Cells were grown for 3-5 days at 28 °C. For BY4742 cells, mitochondrial function was assessed following Ogur *et al.* 1957. This assay takes advantage of the ability of respiratory sufficient (RS) cells to reduce TTC into red-pigmented 1,3,5-triphenylformazan (fig. 6). On the other hand, respiratory deficient (RD) cells are unable to reduce TTC, so their colonies remain non-pigmented. Each treatment was conducted in triplicate. To confirm the RD/RS phenotype, colonies were sub-cloned onto YPG agar (1% w/v yeast extract, 2% w/v peptone, 2% w/v glycerol), as RS (red) cells are able to grow on YPG, while RD (white)

cannot. For W303 strain, cells were cultured for 24 h on liquid YPD under the same treatment conditions, after which ~100 cells were plated onto YPD agar. For the analysis of mtDNA integrity, DNA was extracted following Harju *et. al* 2004 from $5x10^7$ BY4742 cells exposed to CdS QDs after 24 h of growth. The relative abundance of mitochondrial markers was analysed through quantitative Real Time PCR (RT-qPCR). The DNA extracted from each sample was amplified for 40 cycles of 95°C/15 s, 60°C/60 s, followed by a dissociation curve step to confirm the single amplicons. Specific primers were designed with the software package Primer 3 v 0.4.0 (bioinfo.ut.ee/primer3-0.4.0) for housekeeping gene *PDA1* and for mitochondrial genes *COX2*, *ATP6* and *COB*. Each sample was analysed in duplicate using an ABIPRISM 7000 Real-Time PCR System (Life Technologies Carlsbad, CA, USA). ΔΔCt method was used to determine the relative abundance in the different conditions of treatment, compared to the control (untreated).

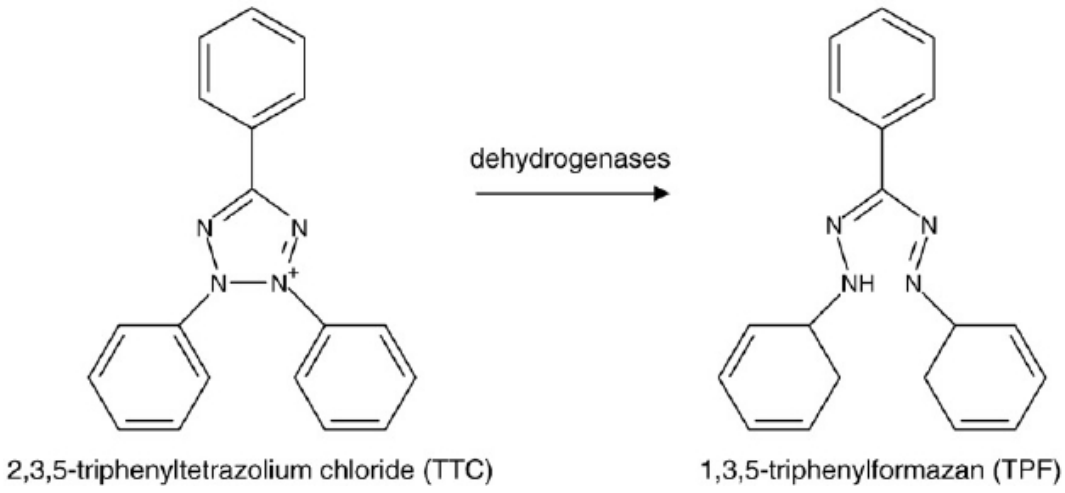

Figure 6. In the TTC assay, 2,3,5-triphenyltetrazolium chloride is reduced to 1,3,5-triphenylformazan by mitochondrial dehydrogenases.

2.11 Effect of CdS QDs on mitochondrial morphology

To assess mitochondrial integrity, wt BY4742 and RD cells were treated with nystatin alone and 100 mg L^{-1} CdS QDs. $3x10^7$ cells for each treatment were then harvested through centrifugation (5000 *g,* 5 min), and stained with two different dyes: DAPI (Sigma Aldrich), which binds A-T rich regions in DNA (including the mitochondrial genome, see Baruffini *et al.* 2010), and rhodamine B hexyl ester perchlorate (Life Technologies), which selectively binds the mitochondrial membrane (Bornhövd *et al.* 2006). Each sample was analysed with an Axio Imager 2 microscope (Carl Zeiss, Oberkochen, Germany) equipped with a DAPI filter (excitation and emission wavelengths: 359 nm and 461 nm) and a rhodamine filter (excitation and emission wavelengths: 528 and 551 nm). Mitochondrial network integrity was determined through transformation of BY4742 cells (Gietz and Woods, 2002) with the pYX142-mtRFP plasmid, provided by the laboratory of Prof. J. Winderickx. This plasmid expresses a mitochondrial-localized red fluorescent protein (Van Rossom *et al.* 2012). 10^4 cells mL^{-1} of the transformed strain were treated for 24 h in selective SC-LEU medium, in presence of either 100 mg L^{-1} CdS QDs or 20 μM $CdSO_4$. Samples were analysed with an Axio Imager 2 microscope (Carl Zeiss) equipped with an RFP filter (emission wavelength 588 nm). About 500 cells per treatment were analysed to determine the effect of treatment on the abundance of the different mitochondrial morphotypes.

2.12 Evaluation of reactive oxygen species and glutathione redox state

Accumulation of Reactive Oxygen Species (ROS) and of glutathione oxidized/reduced forms (GSSG/GSH) was assessed by measuring the formation of 2',7'-dichlorofluorescein (fig. 7 a, Bussche and Soares, 2011) and 2-nitro-5-thiobenzoate (fig. 7 b, Flattery-O'Brien and Dawes, 1998), respectively. Both assays were performed on about 10^7 cells harvested from each treatment (control, nystatin and all the CdS QDs concentrations). For ROS analysis, a cell lysate was prepared at zero, one and four hours after the beginning of the treatment. Fluorescence was measured with a

SpectraFluor Plus fluorimeter (Tecan Group Ltd., Männedorf, Switzerland, excitation and emission wavelengths: 485 nm and 535 nm). For oxidized (GSSG) and reduced (GSH) glutathione quantifications, an iMARK microplate absorbance reader (Bio-Rad, Hercules, CA, USA, emission wavelength: 415 nm) was used. The glutathione redox state was calculated from the ratio GSH/ (GSSG-GSH).

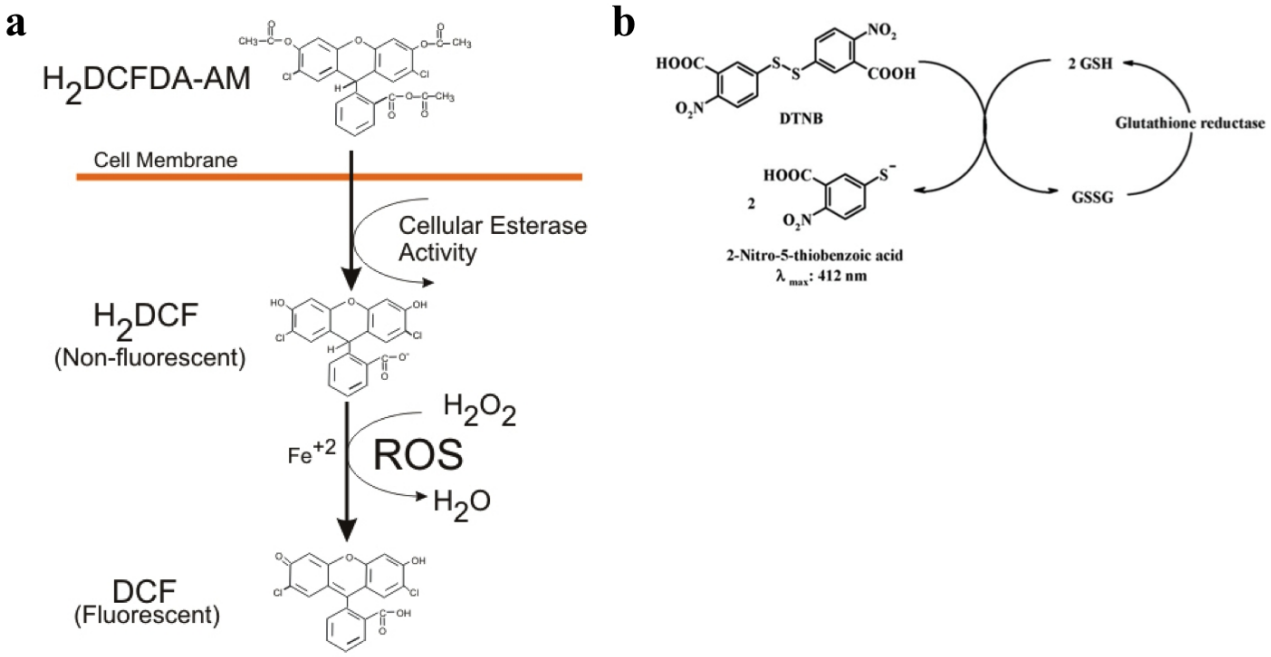

Figure 7. A) Cleavage of diacetate group from 2',7'-dichlorodihydrofluorescein diacetate (H_2DCFDA) and oxidation by reactive oxygen species (ROS) to fluorescent 2'-7'-dichlorofluorescin (DCF), source: biotek.com; b) reduced glutathione (GSH) oxidation by 5,5'-dithiobis-2-nitrobenzoic acid (DTNB) to give oxidized glutathione (GSSG), with formation of fluorescent 2-nitro-5-thiobenzoic acid (TNB), as described in Araujo *et al.* 2008.

2.13 Statistical analysis

The microarray raw data were analysed using Expression Console v1.4.0 software (www.affymetrix.com/analysis/) following protocols provided by Biolitix AG (Witterswill, SUI). Gene references were cited from Saccharomyces Genome Database (www.yeastgenome.org).

Interaction networks were built using the GeneMANIA data service (genemania.org). Cytofluorimetric data were analysed with Attune NxT software. Statistical analysis, principal component analysis, heatmaps and cluster analysis were performed with R statistical software (www.r-project.org). For each experiment, the normality of the distribution was assessed with the Shapiro-Wilk's test; variance homogeneity was determined through ANOVA; comparisons between treated and untreated samples were performed with Tukey's pairwise comparison (in the relative graphs, statistically different means are indicated with different letters).

3. *Cucurbita pepo*: results and discussion

3.1 Previous studies – *Cucurbita pepo*

A previous study (Pagano *et al*. 2016) analyzed the physiological and transcriptional response of *C. pepo* in response to 500 mg L^{-1} CeO_2, La_2O_3 and CuO NPs and to their bulk and salt counterparts. In particular, CeO_2 NPs did not dramatically impact zucchini physiology. Conversely, La_2O_3 and CuO NPs significantly decreased plant moisture content, roots/shoots length and total biomass. Treatment with bulk materials had only minor effects on zucchini plants, which highlights the particle-size specific nature of the plant response. ICP-MS metal content analysis on different plant tissues highlighted that zucchini effectively translocated La from roots to both stems and leaves, while Ce does not accumulate in leaf tissues. Not surprisingly, Cu is actively translocated in leaves too, but S/TEM analysis did identify nano-Cu aggregates. Although, bulk materials treatments also resulted in an accumulation of Ce, Cu and La in roots, stems and leaves, in general the content was lower than in the corresponding ENM. This difference was most likely due to the different particle size and element form. Transcriptional analysis focused on 38 *C. pepo* orthologs of *A. thaliana* genes that were up- or down-regulated in response to CdS QDs (Marmiroli *et al*. 2014). The analysis identified 7 genes whose expression is consistently modulated in response to CeO_2, La_2O_3 and CuO NPs treatment either. Of these, only *BIP3*, which encodes for a heat shock protein 70 (Hsp70) with ATP-binding function, was commonly up-regulated even in *A. thaliana* in response to CdS QDs, and therefore might represent a general biomarker of susceptibility.

3.2 CdS quantum dot synthesis and characterization

Figure 8 a shows QDs aggregation, observed upon solvent evaporation due to the lack of capping molecules at QDs surface. The corresponding reduced Fourier transform (FT) in the inset confirms the hexagonal structure (greenockite, P63mc) of as-synthesized CdS QDs (d=0.36 nm in agreement with JCPDS no. 80-0006). The FT of the whole HRTEM image is presented in figure 8

b: The expected ring feature coming from the random orientation of the CdS crystallites is observed, as is the overlap of (100), (002) and (101) reflections of the wurtzite structure (at high *d* values) due to low-dimension peak broadening. Such features are in agreement with XRD pattern reported in figure 8 c. All peaks have been indexed according to greenockite structure and no other reflections arising from possible impurities are observed. Scherrer calculation, based on FWHM of the three main peaks of the reported pattern, results in an average size of about 6 nm. Figures 9 a and b show SEM image of CdS QDs drop, at 29750x and 130802x magnification respectively. In these pictures, the nanocrystals are grouped into small aggregates with a diameter of 50-100 nm. EDX spectra (fig. 9 c) was performed on the point indicated in figure 9 b: Lα1 and Lβ1 emission lines are visible for cadmium at 3.133 and 3.316 eV, while Kα1 and Kβ1 lines at 2.308 and 2.464 eV are visible for sulphur.

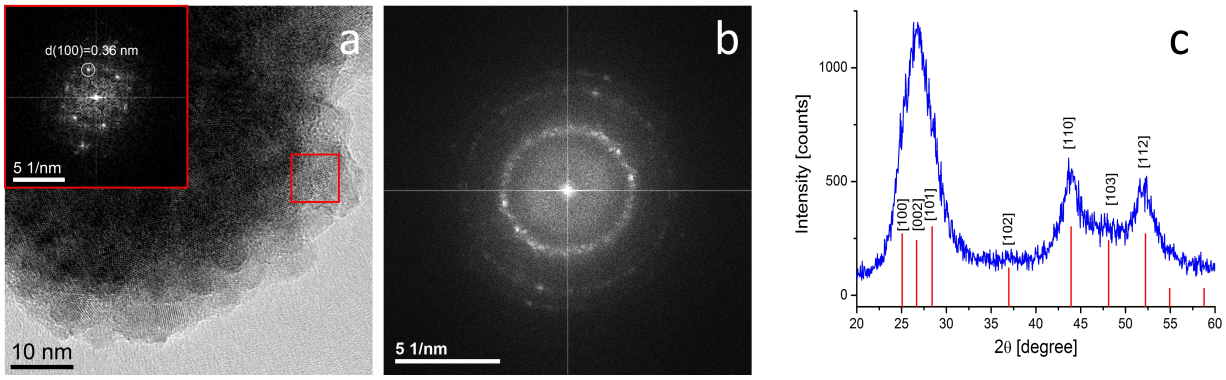

Figure 8. HRTEM image of ligand-free QDs assembly: (a) a CdS QDs aggregate upon solvent evaporation; (b) Fourier transform analysis of the whole HRTEM image. (c) X-ray diffraction pattern.

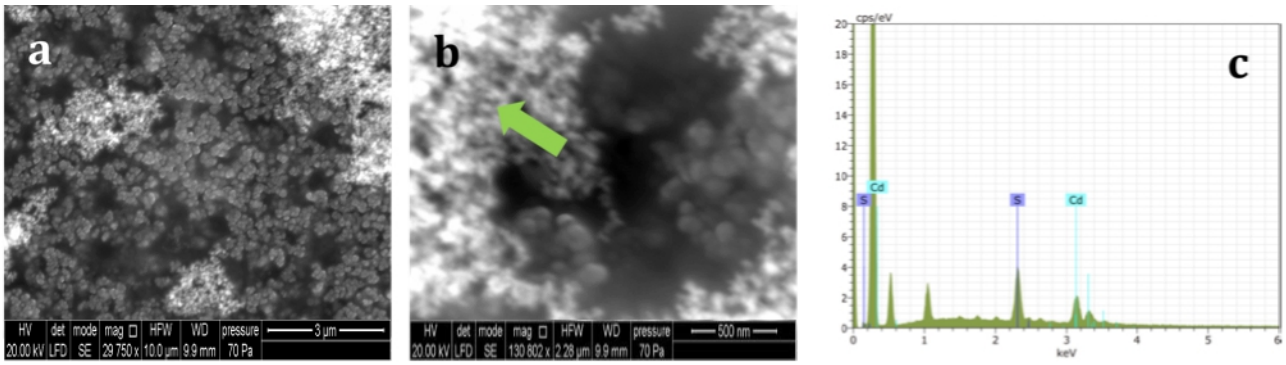

Figure 9. ESEM/EDX image of ligand-free CdS QDs assembly at 80 mg L^{-1} concentration. (a) and (b) panels show SEM images of CdS QDs at different magnifications (29750 x and 130802 x respectively). The green arrow in panel (b) indicates the point where energy-dispersive X-ray analysis (EDX) was performed. (c) EDX spectra of CdS QDs, reporting X-ray emission lines for Cd and S.

3.3 Physiological analysis of *C. pepo* upon ENMs exposure

Bulk ZnO and CdS QDs significantly affected the plant biomass. (-47.4% and -21.9% respectively, tab. 1). In general, bulk- and ENMs alone did not affect the water content in leaves, stems or roots (tab. 2); the only exception is represented by the leaves of plants treated with bulk ZnO, which showed an increase of 82.96% of the water content. Treatment with ZnO NPs resulted in an increase of 37% of the root length (tab. 3), contrary to the findings of Zhang R. *et al*. 2015 that highlighted a reduction of 17% in other *Cucurbitaceae*. However, these discrepancies might be due to the different concentrations tested (500 mg L^{-1} vs 1000 mg L^{-1}), to the different growing conditions or to species-specific effects. The other treatments did not show any significant differences in the physiological parameters analyzed. The different behavior of bulk and corresponding nano-counterparts could be in part explained considering the different amounts of Cd and Zn that were found in the different plant tissues (see paragraph 3.5 ICP-MS analysis of ENMs uptake and translocation).

Table 1. Biomass (g) of *C. pepo* treated with bulk or nano ZnO and CdS

sample	biomass	stdev	t-test
Control (untreated)	4.054	0.610	-
ZnO NPs	4.640	0.537	0.14607
ZnO Bulk	2.134	0.459	0.00064***
CdS QDs	2.762	0.280	0.00589**
CdS Bulk	3.340	0.576	0.09354

Table 2. Water content (g/g) of *C. pepo* treated with bulk or nano ZnO and CdS

sample	leaves	st dev	t-test	stems	st dev	t-test	roots	st dev	t-test
Control (untreated)	19.239	7.008	-	0.972	0.021	-	44.333	24.066	-
ZnO NPs	19.079	1.253	0.96229	0.970	0.006	0.81518	43.133	23.879	0.93886
ZnO Bulk	35.200	12.849	0.04936*	0.986	0.003	0.21584	34.600	10.526	0.44195
CdS QDs	25.448	5.555	0.16111	0.977	0.011	0.67998	31.200	9.358	0.30524
CdS Bulk	23.712	3.775	0.25461	0.977	0.005	0.62414	49.400	11.739	0.68745

Table 3. Length (cm) of stems, roots and shoots of *C. pepo* treated with bulk or nano ZnO and CdS

sample	stems	st dev	t-test	roots	st dev	t-test
Control (untreated)	18.340	24.000	-	3.669	6.255	-
ZnO NPs	18.580	33.160	0.92347	3.979	2.530	0.02698*
ZnO Bulk	14.560	24.580	0.09399	2.317	6.940	0.89306
CdS QDs	16.200	22.580	0.26803	0.967	4.115	0.68439
CdS Bulk	18.620	32.000	0.89097	2.435	5.962	0.07229

Among the binary combination treatments with each of the different ENMs, only La_2O_3 NPs + ZnO NPs induced a significant change (+27.4%) in the total biomass of the plant (tab. 4). CdS QDs and CeO_2 NPs had respectively the greatest and smallest impact on plant biomass production when combined with other ENMs. Root water content was increased by each combination with La_2O_3, while conjunction with CuO lead also to an increase of stem water content (+1.64%) (tab. 5). Root length was not significantly affected by treatment, while stem length was increased by CeO_2 in combination with CuO or ZnO (+17% and +13% respectively), by La_2O_3 in combination with ZnO

and CdS (+27.27% and +21.17% respectively) and by treatment with CuO and ZnO (+21.67%) (tab. 6).

No significant differences were highlighted in photosynthetic efficiency or cell viability, as shown by chlorophyll A, B, carotenoids and TTC content data (fig. 8). Ceriums effect on shoot length aligns with findings from previous work (Pagano *et al.* 2016, Ma *et al.* 2010), while the reduction of shoot length by La_2O_3 (Pagano *et al.* 2016) seems to be prevented by the concomitant treatment with other NPs. As reported in Ma *et al*. 2010, La_2O_3 NPs alone induced ROS production and programmed cell death, leading to a decrease in root/shoot length and total biomass. In general, each combination containing ZnO NPs caused the increase in roots water content (2.54–3.6 %).

Table 4. Biomass (g) of C. *pepo* treated with binary combination of the different ENMs. *, ** and *** indicate a *p* value respectively less than 0.05, 0.01 and 0.001.

sample	biomass	st dev	t-test
Control (untreated)	2.858	0.671	-
CeO_2 NPs + La_2O_3 NPs	3.542	0.821	0.18870
CeO_2 NPs + CuO NPs	4.174	1.065	0.05338
CeO_2 NPs + ZnO NPs	3.566	0.724	0.14771
CeO_2 NPs + CdS QDs	2.188	0.564	0.12705
La_2O_3 NPs + CuO NPs	2.96	0.275	0.76521
La_2O_3 NPs + ZnO NPs	3.938	0.774	0.04682*
La_2O_3 NPs + CdS QDs	3.624	1.082	0.22251
CuO NPs + ZnO NPs	3.412	0.935	0.31611
CuO NPs + CdS QDs	2.54	0.824	0.52297
ZnO NPs + CdS QDs	3.096	0.379	0.51450

Table 5. Water content (g/g) of *C. pepo* treated with binary combination of the different ENMs. *, ** and *** indicate a *p* value respectively less than 0.05, 0.01 and 0.001.

sample	leaves	st dev	t-test	stems	st dev	t-test	roots	st dev	t-test
Control (untreated)	22.300	5.975	-	0.971	0.003	-	0.944	0.017	-
CeO_2 NPs + La_2O_3 NPs	19.790	11.338	0.67658	0.963	0.005	0.01323*	0.953	0.013	0.38967
CeO_2 NPs + CuO NPs	12.577	1.668	0.01958*	0.950	0.010	0.00787**	0.946	0.008	0.81577
CeO_2 NPs + ZnO NPs	26.195	6.320	0.34600	0.977	0.009	0.21812	0.968	0.014	0.04122*
CeO_2 NPs + CdS QDs	24.558	12.392	0.72667	0.982	0.008	0.03423*	0.970	0.004	0.02668*
La_2O_3 NPs + CuO NPs	41.633	23.288	0.13820	0.987	0.009	0.01532*	0.981	0.003	0.00868**
La_2O_3 NPs + ZnO NPs	20.988	5.749	0.73263	0.972	0.004	0.65138	0.973	0.007	0.01612*
La_2O_3 NPs + CdS QDs	26.678	11.100	0.46631	0.978	0.006	0.06570	0.974	0.010	0.01419*
CuO NPs + ZnO NPs	29.327	7.102	0.13004	0.978	0.010	0.21173	0.977	0.009	0.00884**
CuO NPs + CdS QDs	19.973	6.575	0.57442	0.978	0.004	0.01909*	0.954	0.011	0.33531
ZnO NPs + CdS QDs	38.150	17.966	0.12161	0.976	0.006	0.12472	0.978	0.006	0.01009*

Table 6. Length (cm) of *C. pepo* treated with binary combination of the different ENMs. *, ** and *** indicate a *p* value respectively less than 0.05, 0.01 and 0.001.

sample	shoots	st dev	t-test	roots	st dev	t-test
Control (untreated)	16.06	1.22	-	29.72	7.65	-
CeO_2 NPs + La_2O_3 NPs	18.98	2.07	0.03219*	29.74	5.70	0.99638
CeO_2 NPs + CuO NPs	18.8	1.68	0.02043*	31.8	3.27	0.59840
CeO_2 NPs + ZnO NPs	18.16	1.18	0.02472*	25.62	4.47	0.33793
CeO_2 NPs + CdS QDs	14.84	0.97	0.12082	24.66	5.79	0.27446
La_2O_3 NPs + CuO NPs	17.86	2.83	0.24376	26.54	2.84	0.42272
La_2O_3 NPs + ZnO NPs	20.44	1.97	0.00431**	30.12	5.63	0.92748
La_2O_3 NPs + CdS QDs	19.46	2.28	0.02536*	25.92	2.36	0.33930
CuO NPs + ZnO NPs	19.54	1.26	0.00218**	28.12	8.55	0.76320
CuO NPs + CdS QDs	17.24	1.37	0.18971	24.3	4.52	0.21795
ZnO NPs + CdS QDs	16.66	1.46	0.50109	23.5	2.76	0.14754

3.4 Photosynthetic efficiency and cell viability assays

As reported in figure 10, colorimetric assessment of chlorophyll A, B and carotenoids did not show a significant change in comparison with the untreated control, meaning that exposure to the combinations of ENMs tested had no measurable impacts on photosynthetic efficiency. Also the 1,3,5-triphenylformazan content, which provides a measure of cell viability, was mostly unaffected by treatment except for the case of CuO NPs + ZnO NPs combination, which showed a significant

increase (+90.2%). It's important to note that the lack of statistical differences in the content of photosynthetic pigments and TTC might be due to the standard deviation in some of the analysed samples.

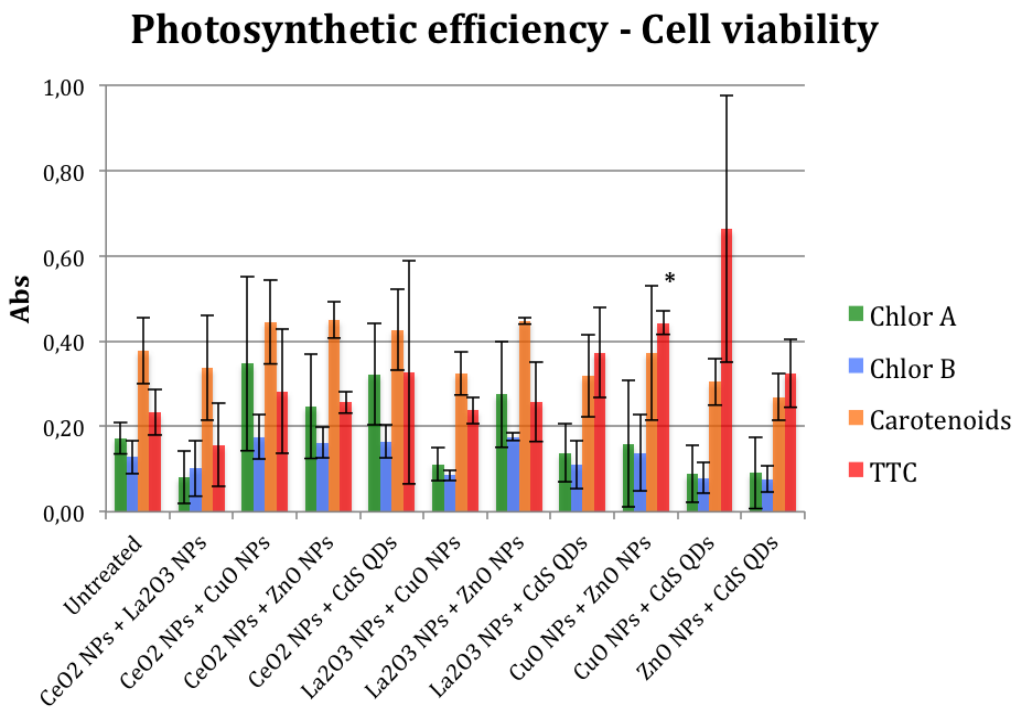

Figure 10. Chlorophyll A and B, carotenoids and 1,3,5-triphenylformazan contents in *C. pepo* plants treated with binary combinations of the five ENMs tested. (*) indicates a p value less than 0.05.

3.5 ICP-MS analysis of ENMs uptake and translocation

ICP-MS analysis performed on *C. pepo* tissues grown in absence of treatment or in presence of either bulk or nano ZnO (fig. 11) showed that: i) Zn is actively translocated in leaves; its content is higher in condition of treatment with ZnO NPs rather than with correspondent bulk material, probably because of the different size; ii) Zn content is significantly lower in NPs treatment,

probably as a result of the major translocation in the leaves; iii) there are no differences in Zn content in roots among bulk or nano treatments. Analysis on plants grown in presence of either bulk or quantum dots CdS (fig. 12), showed that Cd is poorly translocated in leaves (as already observed with cerium), while its content in stems and roots is not significantly different across the two different forms of the material. Despite the same concentration administered (500 mg L^{-1}), Zn content in all the tissues is more than two-fold higher than the one of Cd.

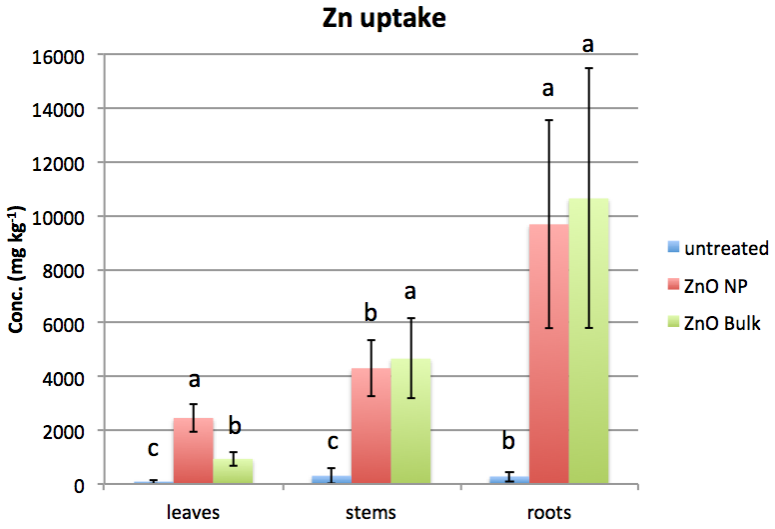

Figure 11. ICP-MS analysis of zinc content in leaves, stems and roots of plants grown in absence of treatment or in presence of 500 mg L^{-1} of either bulk or nano ZnO. The different letters indicate statistically different means, as resulting from analysis of variance.

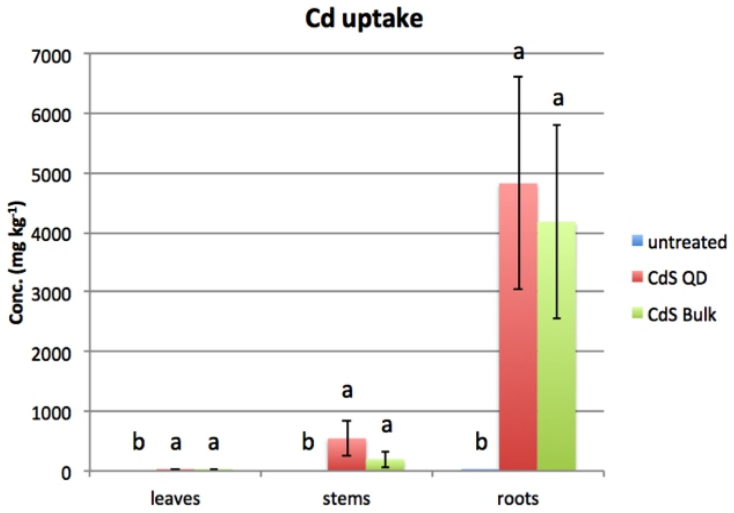

Figure 12. ICP-MS analysis of cadmium content in leaves, stems and roots of plants grown in absence of treatment or in presence of 100 mg L^{-1} of either bulk or quantum dots CdS. The different letters indicate statistically different means, as resulting from analysis of variance.

ICP-MS analysis on leaves metal content in plants treated with the different nanoparticle combinations (fig. 13 and tab. 7), partially agreed with Pagano *et al*. 2016. Specifically, Ce is poorly transferred to the leaf tissues, while La is accumulated to a greater extent. Cu and Cd content in leaves are slightly increased if compared to the untreated control. Zn translocation is consistent to what was observed for the single nanomaterial: in leaves its content is dramatically increased in all the co-contaminants treatments, especially in those with La_2O_3. This data is in contrast with what was observed for corresponding bulk materials, where La is reported to block cationic channels through which the zinc enters the cell (Reid *et al*. 1995). Metal content in stems (fig. 14 and tab. 8) shows a similar trend to the one of the leaves, with the exception of Ce, whose abundance is similar in this case to the one of La. Consistently to what was found in leaves, Zn content in stems is remarkably high in almost every treatment conditions, and seems to be increased by the presence of La. In roots (fig. 15 and tab. 9), La and Cd show similar uptake levels in all the treatments (with the

exception of CeO_2+La_2O_3 nanoparticle treatment), although CdS QDs were administered to the plants in a concentration that is 1/5 of the one of La_2O_3.

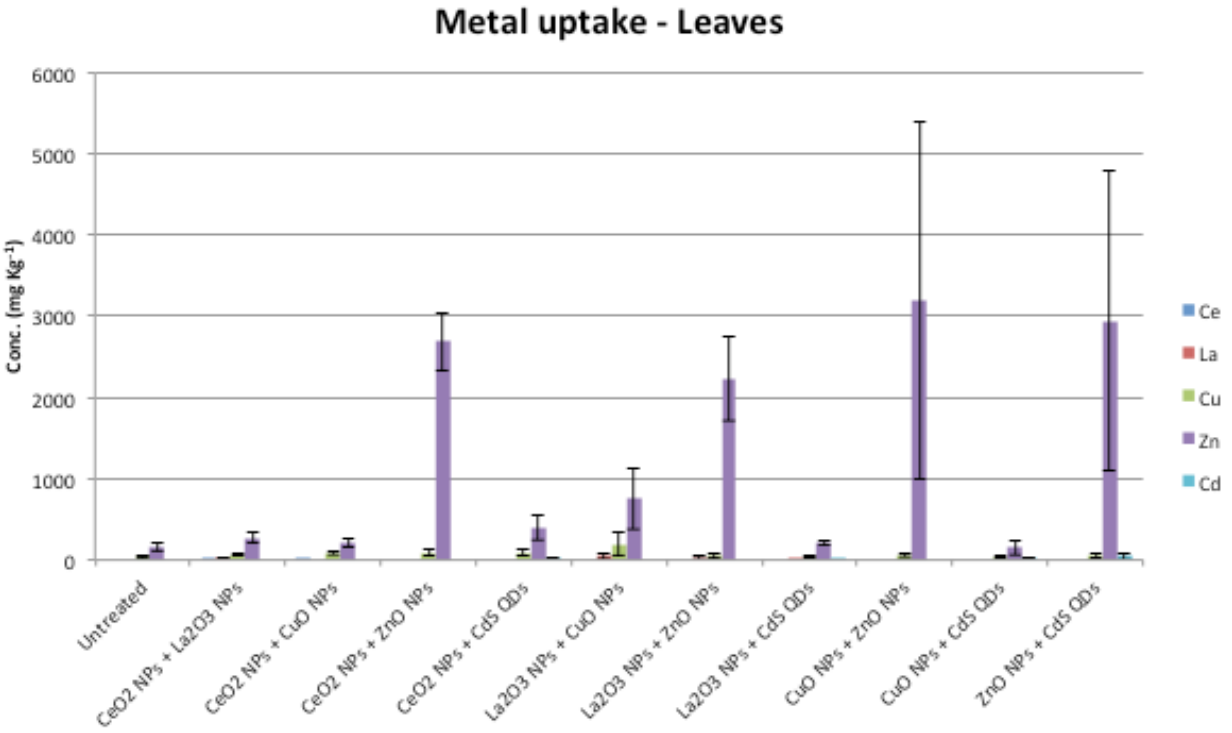

Figure 13. ICP-MS analysis of metal content in leaves upon exposure to the different ENMs combinations.

Table 7. Tukey's (HSD) pairwise multiple comparisons ($p < 0.05$) related to Ce, La, Cu, Zn and Cd uptake of NMCC treatments in leaves. Different letters represent statistically different means.

Metal uptake - Leaves	**Ce**	**La**	**Cu**	**Zn**	**Cd**
untreated	A	A	A	AB	A
CeO_2 NPs + La_2O_3 NPs	A	A	BC	B	A
CeO_2 NPs + CuO NPs	A	A	BC	B	A
CeO_2 NPs + ZnO NPs	A	A	BC	C	A
CeO_2 NPs + CdS QDs	A	A	AB	AB	A
La_2O_3 NPs + CuO NPs	A	A	BC	B	A
La_2O_3 NPs + ZnO NPs	A	A	AB	C	A
La_2O_3 NPs + CdS QDs	A	A	AB	AB	A
CuO NPs + ZnO NPs	A	A	AB	C	A
CuO NPs + CdS QDs	A	A	A	A	B
ZnO NPs + CdS QDs	A	A	A	C	B

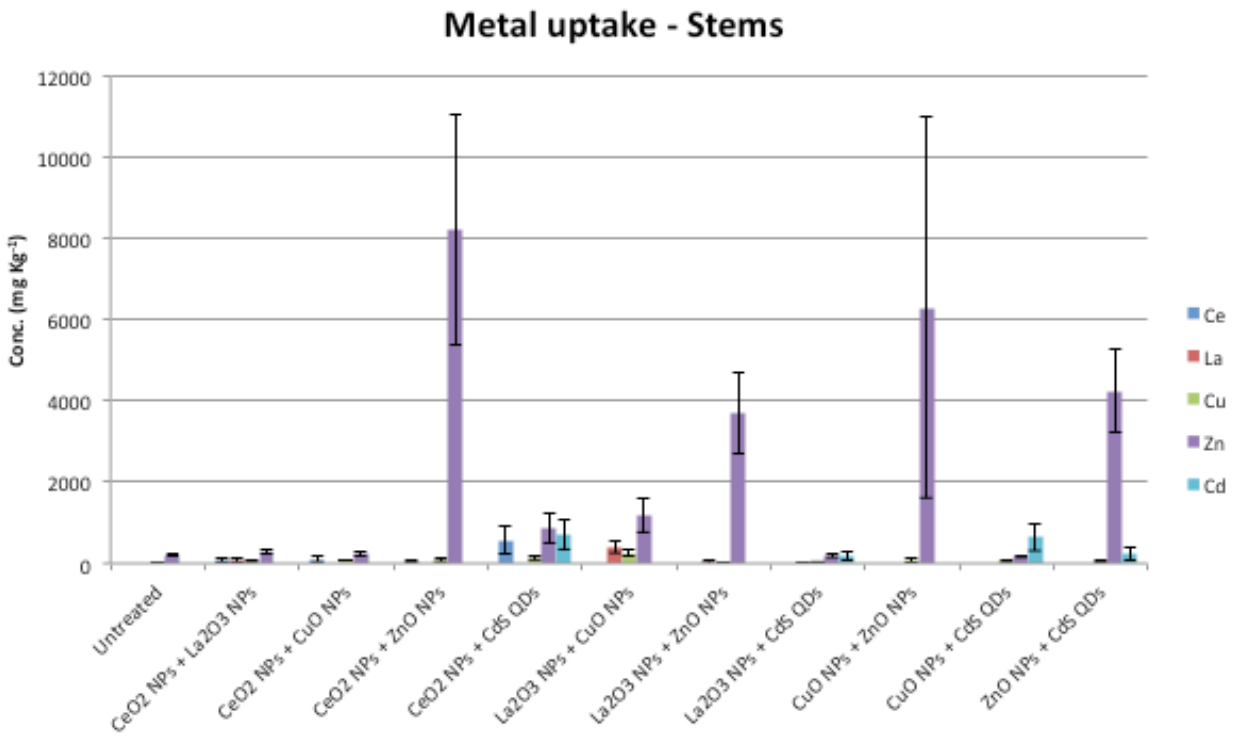

Figure 14. ICP-MS analysis of metal content in stems upon exposure to the different ENMs combinations.

Table 8. Tukey's (HSD) pairwise multiple comparisons ($p < 0.05$) related to Ce, La, Cu, Zn and Cd uptake of NMCC treatments in stems. Different letters represent statistically different means.

Metal uptake - Stems	**Ce**	**La**	**Cu**	**Zn**	**Cd**
untreated	A	A	A	A	A
CeO_2 NPs + La_2O_3 NPs	BC	C	B	B	A
CeO_2 NPs + CuO NPs	C	A	BC	B	A
CeO_2 NPs + ZnO NPs	AB	A	BC	C	A
CeO_2 NPs + CdS QDs	C	A	B	AB	BC
La_2O_3 NPs + CuO NPs	A	D	BC	B	A
La_2O_3 NPs + ZnO NPs	A	B	A	CD	A
La_2O_3 NPs + CdS QDs	A	AB	A	A	B
CuO NPs + ZnO NPs	A	A	AB	CD	A
CuO NPs + CdS QDs	A	A	A	A	C
ZnO NPs + CdS QDs	A	A	A	D	B

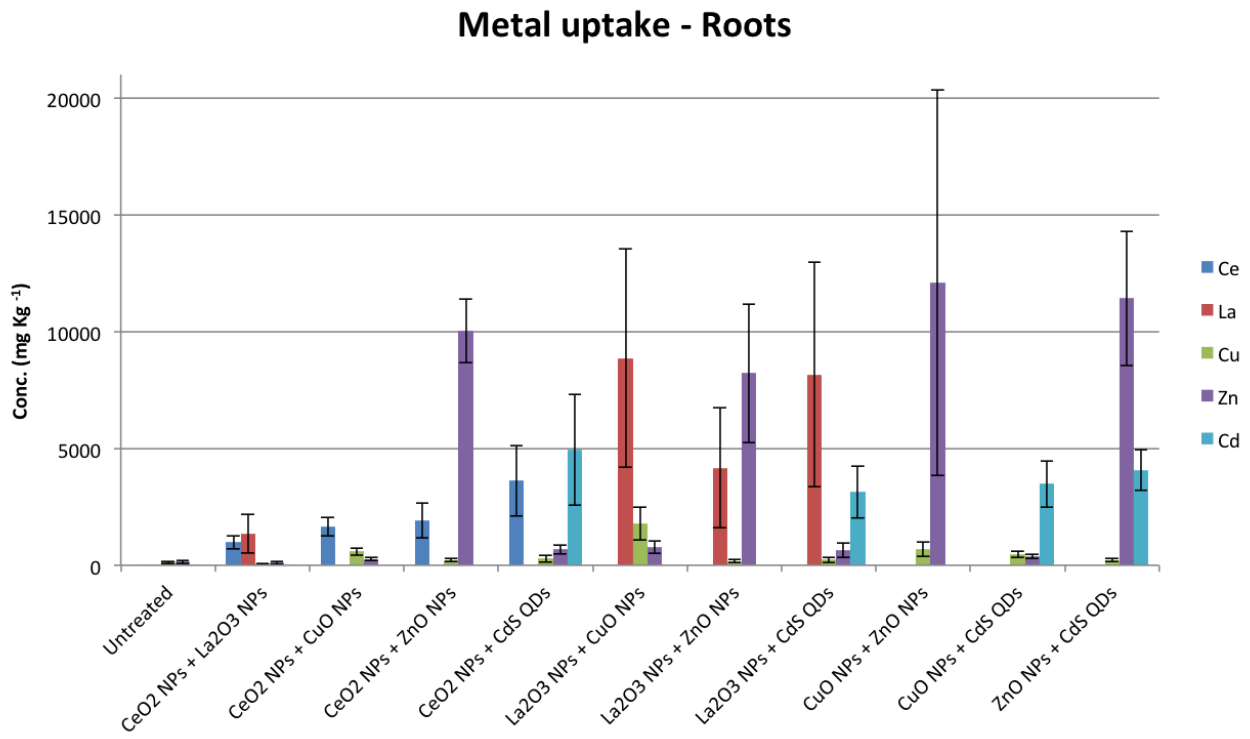

Figure 15. ICP-MS analysis of metal content in roots upon exposure to the different ENMs combinations.

Table 9. Tukey's (HSD) pairwise multiple comparisons ($p < 0.05$) related to Ce, La, Cu, Zn and Cd uptake of NMCC treatments in roots. Different letters represent statistically different means.

Metal uptake - Roots	**Ce**	**La**	**Cu**	**Zn**	**Cd**
untreated	A	A	AB	AB	A
CeO_2 NPs + La_2O_3 NPs	B	B	A	A	A
CeO_2 NPs + CuO NPs	C	A	C	B	A
CeO_2 NPs + ZnO NPs	B	A	B	D	A
CeO_2 NPs + CdS QDs	B	A	BC	BC	B
La_2O_3 NPs + CuO NPs	A	C	D	C	A
La_2O_3 NPs + ZnO NPs	A	C	B	D	A
La_2O_3 NPs + CdS QDs	A	C	BC	BC	B
CuO NPs + ZnO NPs	A	A	C	D	A
CuO NPs + CdS QDs	A	A	C	BC	B
ZnO NPs + CdS QDs	A	A	BC	D	B

3.6 Transcriptional analysis of *C. pepo* in response to ENM/NMCC treatment

For single and coupled ENMs, the transcriptional analysis was performed on a panel of 38 genes that were orthologs of *A. thaliana* genes involved in CdS QDs response (Pagano *et al.* 2016, Marmiroli *et al.* 2014), as shown in fig. 16. The only gene that was commonly down-regulated in all the conditions of treatment tested was 152u (ORF31), an electron carrier which is localized in chloroplasts endomembrane and in subunit VI of cytochrome b6f complex. As such, *ORF31* gene might represent a biomarker of exposure to ENMs. In *A. thaliana*, this gene is known to be up-regulated in response to hydrogen peroxide treatment (Davletova *et al*. 2005). Interestingly, all ENMs except ZnO are grouped in the same cluster of genes expression levels, displaying a moderate up- and down- regulation in some of the tested genes. Conversely, ZnO NPs treatment induces massive up-regulation of the tested genes (34 out of 38).

Some of the genes respond to treatment in a single ENM-dependent manner. CeO NPs alone, and all the cerium combinations, result in the up-regulation of 140u (*CUTC003431*), a cysteine proteinase I, ortholog of *A. thaliana CEP1* which is involved in pathogen and biotic stress response (Höwing *et al*. 2016). All La_2O_3 NPs treatments induce the down-regulation of 004d (*CUTC013469*) and 147u (*CUTC019875*): the first is the ortholog of *ATCCS*, a copper-zinc superoxide dismutase copper chaperone up-regulated in conditions of oxidative stress response (Zhou *et al*. 2010); the latter is the ortholog of *APRR1*, a pseudo response regulator involved in the generation of circadian rhythms which is up-regulated in response to abiotic stress (Lee B.H. *et al*. 2005). 005u (*CUTC002577*), encoding a heat shock protein 70 (Hsp 70) with ATP-binding function, was up-regulated in all the CuO NPs treatments. Five genes were up-regulated across all the ZnO NPS treatments: 043d (*CUTC049068*), 045d (*CUTC008032*), 066u (*CUTC014559*), 093u (*CUTC008356*) and 099u (*CUTC041648*). CdS QDs treatments induced the up-regulation of 150u (*CUTC021188*) and the down-regulation of 124u (*CUTC023690*): the first is the ortholog of the chloroplast gene *RPS12*, encoding ribosomal protein s12 (Chateigner-Boutin *et al*. 2007) while the

latter is the ortholog of *APRR5*, a pseudo-response regulator of clock-controlled genes like *CCA1* and *APRR1* (Norén *et al*. 2016).

Principal Component Analysis (PCA) of the transcriptional data (fig. 17) shows that CeO_2, La_2O_3 and CuO NPs treatments group in the same part of the graph, confirming the similarity of the response in these conditions of treatments, while CdS QDs and ZnO NPs group in the opposite side. Importantly, each NPs combination stands in a position between the two separate clusters. The two major components, responsible for the 54.1% of the variance, are related to the response of the genes in presence of treatment (up- or down-regulation) and to the type of ENM used in the treatment.

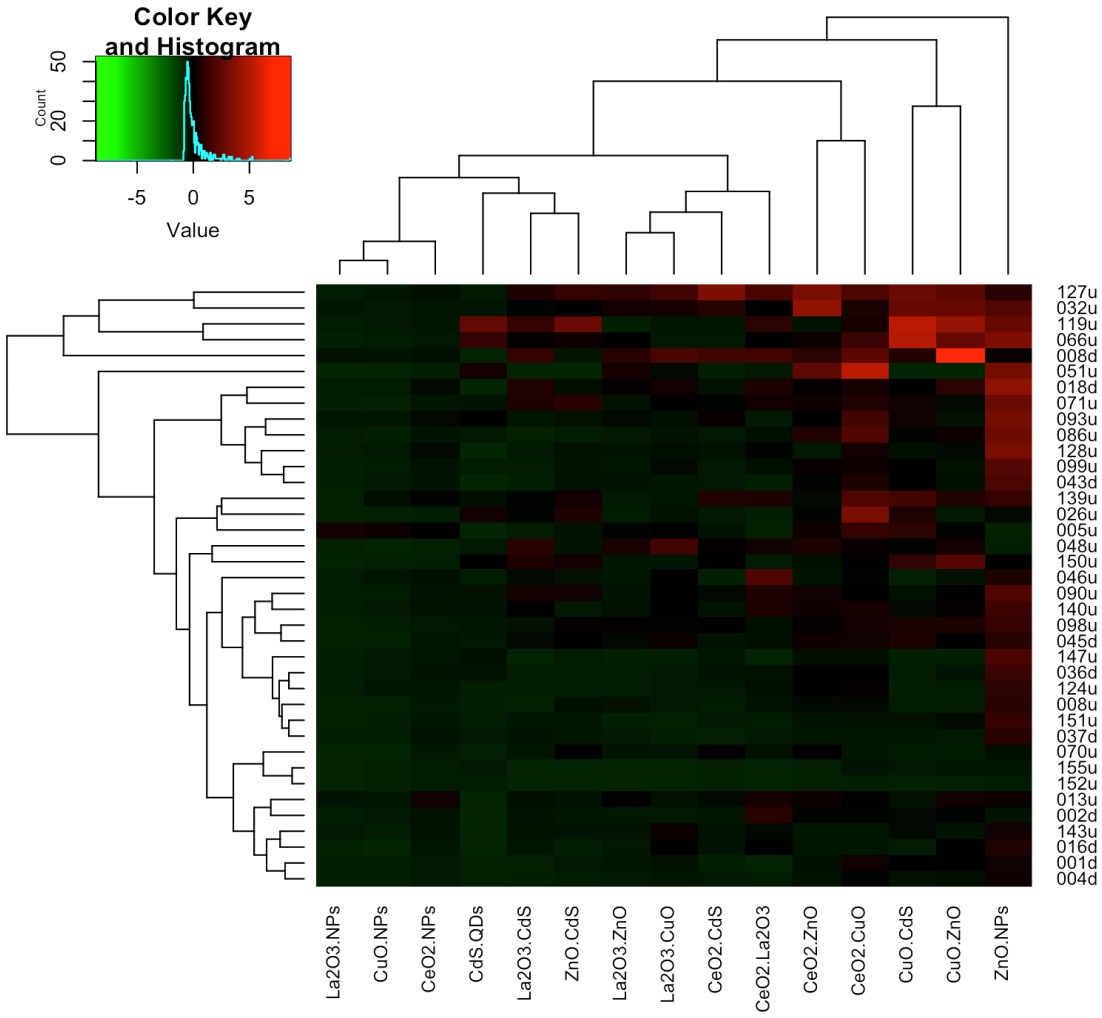

Figure 16. Comparison between gene expression levels between *C. pepo* treated with single or coupled ENMs. Up- and down-regulated genes are reported respectively in red and green.

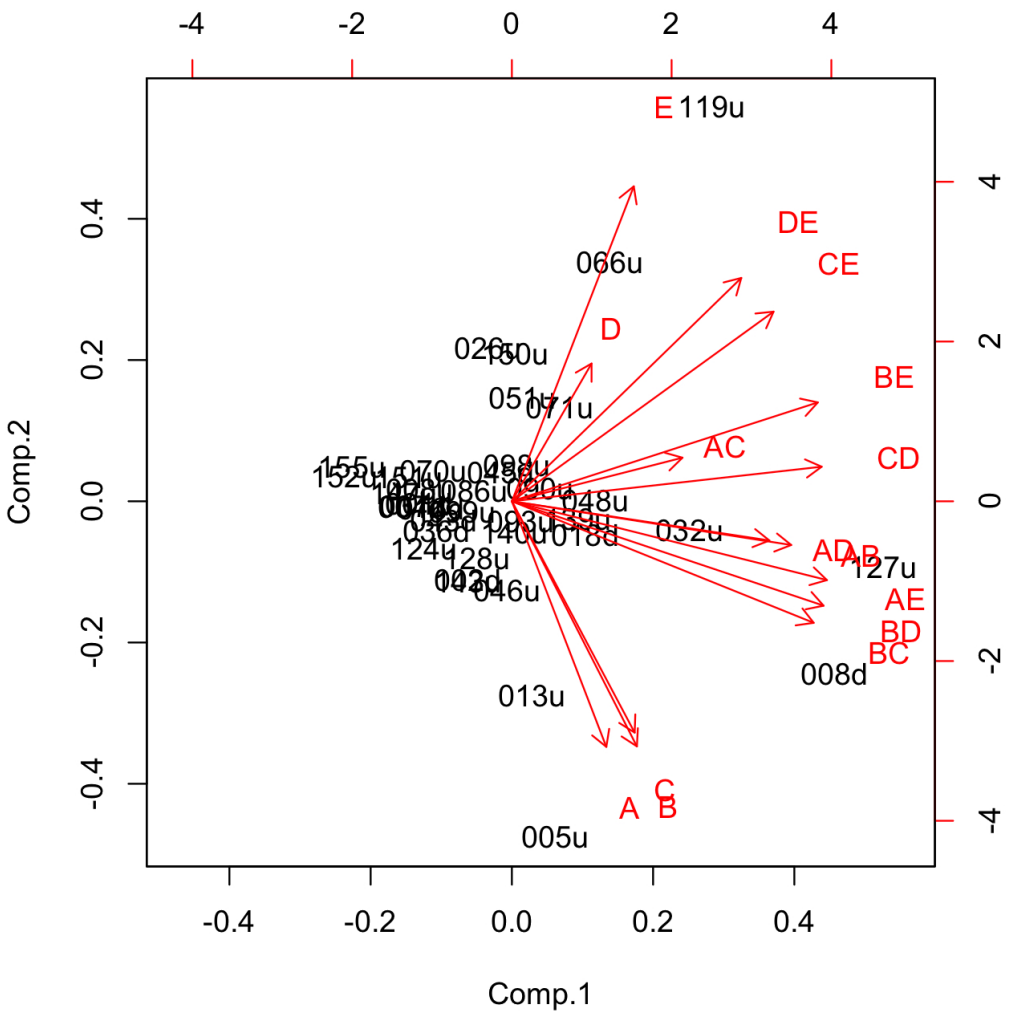


```
Importance of components:
                          Comp.1     Comp.2     Comp.3     Comp.4      Comp.5
Standard deviation     2.3166263  1.6571016  1.4289915  1.2254969  0.97172793
Proportion of Variance 0.3577838  0.1830657  0.1361345  0.1001228  0.06295034
Cumulative Proportion  0.3577838  0.5408496  0.6769840  0.7771069  0.84005720
                           Comp.6     Comp.7     Comp.8     Comp.9    Comp.10
Standard deviation     0.77609788 0.72733852 0.61640362 0.51961976 0.44782996
Proportion of Variance 0.04015519 0.03526809 0.02533023 0.01800031 0.01337011
Cumulative Proportion  0.88021239 0.91548048 0.94081071 0.95881102 0.97218114
                          Comp.11    Comp.12    Comp.13    Comp.14    Comp.15
Standard deviation     0.39547053 0.29604842 0.28350768 0.22961594 0.20035283
Proportion of Variance 0.01042646 0.00584297 0.00535844 0.00351489 0.00267608
Cumulative Proportion  0.98260760 0.98845057 0.99380902 0.99732391 1.00000000
```

Figure 17. Principal Component Analysis (PCA) of the transcriptional response in *C. pepo* in condition of treatment with single and coupled ENMs (A=CeO_2 NPs, B=La_2O_3 NPs, C=CuO NPs, D=ZnO NPs, E=CdS QDs).

For bulk material treatments, transcriptional analyses were performed on a subset of seven of the aforementioned 38 ortholog genes that were simultaneously expressed in *C. pepo* in response to CeO_2, La_2O_3 and CuO NPs (Pagano *et al*. 2016), as reported in fig. 18. CeO_2 treatments, both with the bulk- and the ENM, result in a general down-regulation of all the seven genes tested. Both ZnO treatments induce the up-regulation of 026u, (*CUTC007694*, a glucose-6-phosphate/phosphate translocator 2), 051u (*CUTC012732*, a phospholipase A 2A) and 150u. For La_2O_3 the only genes whose expression is unchanged across bulk- and ENM treatments are 048u (*CUTC008834*, a SNF1-related protein kinase 2.9) and 051u.

Once again CeO_2, La_2O_3, and CuO NPs treatments group in the same cluster, while CdS QDs and ZnO NPs response seems to be different for the seven genes analyzed.

Principal Component Analysis of this transcriptional data (fig. 19) shows that ZnO and CdS, both in their bulk and nanoscale form, are grouped in the same cluster as they induced a similar response. The other two clusters identified include the bulk and the nano-CeO_2, as well as the La_2O_3 and CuO. The first component identified, responsible of the 43.85% of the total variance, is related to the response to CdS and ZnO treatments: 051u, 026u and 150u are in fact strongly up-regulated in these conditions, while the other four genes are generally down-regulated. The second component, responsible of the 29.49% of the total variance, is dependent on the different response to bulk- and nano- CeO_2, La_2O_3 and CuO.

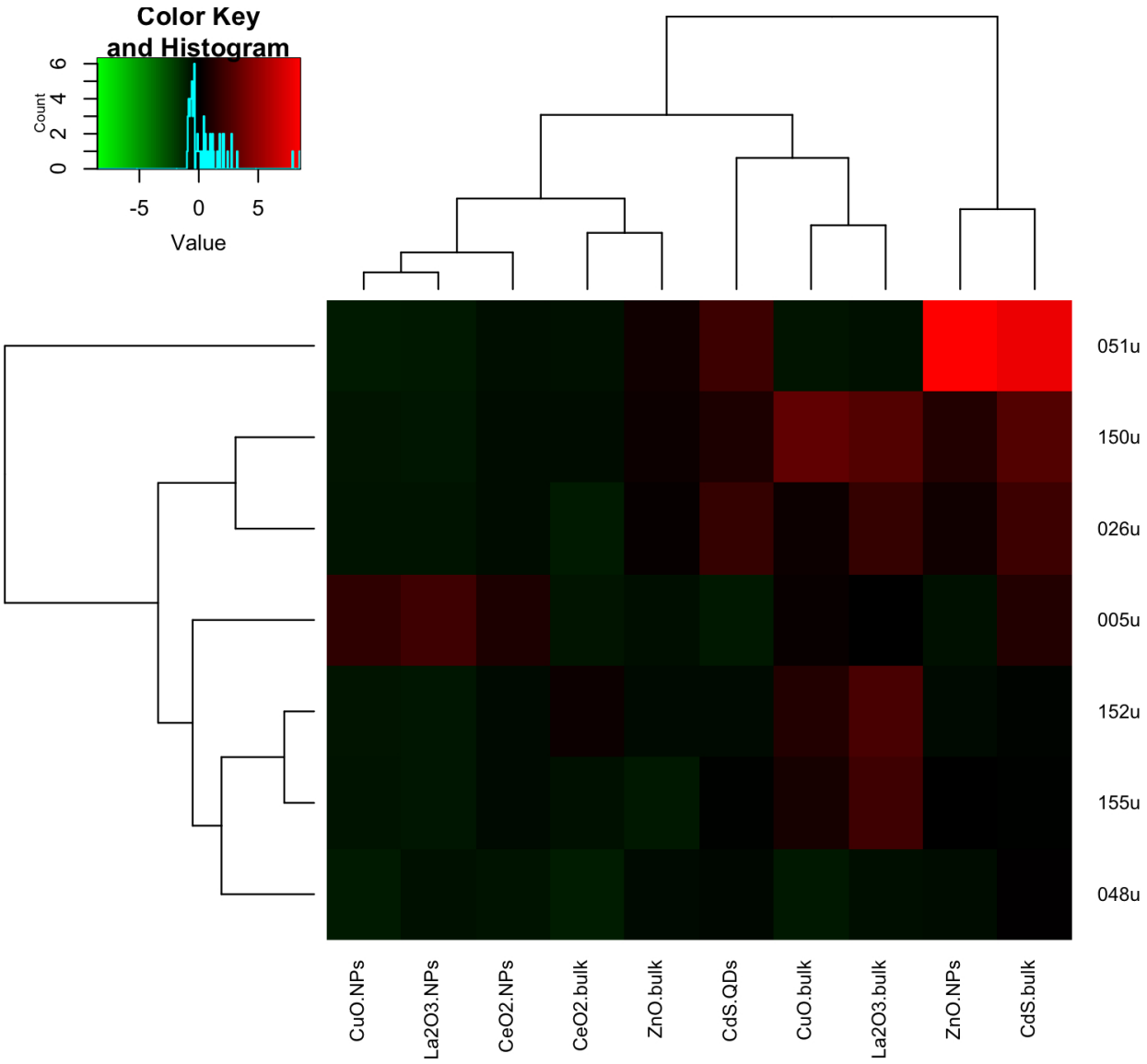

Figure 18. Comparison between gene expression levels between *C. pepo* treated with CeO_2, La_2O_3, CuO and ZnO NPs and CdS QDs. Up- and down-regulated genes are reported respectively in red and green.

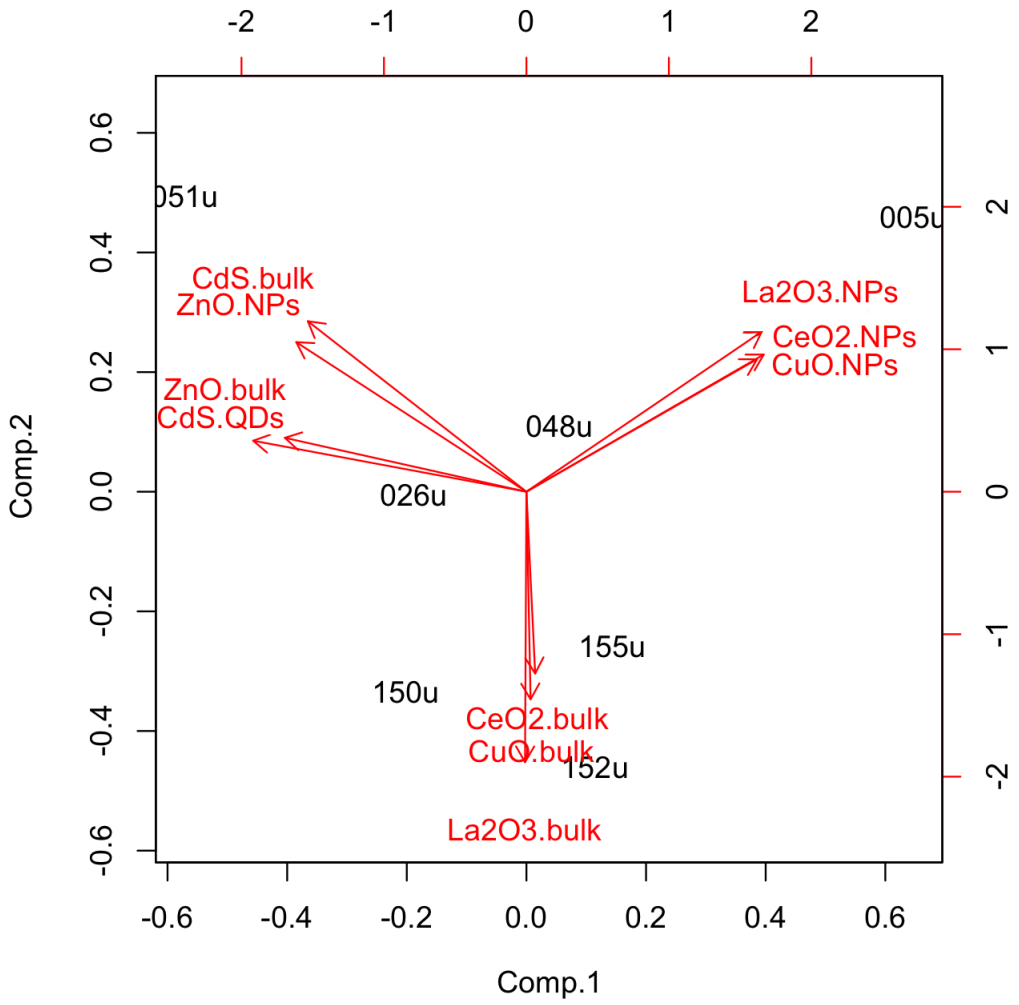


```
Importance of components:
                          Comp.1 Comp.2 Comp.3  Comp.4  Comp.5  Comp.6
Standard deviation     2.0940 1.7173 1.2461 0.89160 0.41777 0.37963
Proportion of Variance 0.4385 0.2949 0.1553 0.07949 0.01745 0.01441
Cumulative Proportion  0.4385 0.7334 0.8886 0.96813 0.98559 1.00000
                          Comp.7
Standard deviation     7.175e-17
Proportion of Variance 0.000e+00
Cumulative Proportion  1.000e+00
```

Figure 19. Principal Component Analysis (PCA) of the transcriptional response in *C. pepo* in condition of treatment with bulk material and correspondent ENM.

3.7 Comparison of the transcriptional response to CdS QDs in *C. pepo* and *A. thaliana*

The comparison between the response to CdS QDs in *A. thaliana* and *C. pepo* highlights the presence of 12 commonly up-regulated and 9 commonly down-regulated genes, amounting to 55% of the genes tested (fig. 20). It is noteworthy that in spite of the phylogenetic differences between the two plants, plant response to this ENM appears to be conserved. Among the commonly down-regulated genes are 002d (*CUTC00155*) and 018d (*CUTC015722*), encoding for two different copper/zinc superoxide dismutases, expressed in conditions of biotic and abiotic stress and involved in the detoxification of superoxide radicals (Yamasaki *et al*. 2007). 004d (*CUTC013469*), down-regulated in both plants, was also down-regulated in zucchini upon all the treatments containing La_2O_3 nanoparticles.

Among the commonly up-regulated genes are 066u (*CUTC014559*) and 093u (*CUTC008356*), which were also up-regulated upon all the treatments containing ZnO nanoparticles; 140u, up-regulated in presence of CeO_2 NPs and 150u (*CUTC021188*), which is a chloroplastic gene encoding for the ribosomal protein S12.

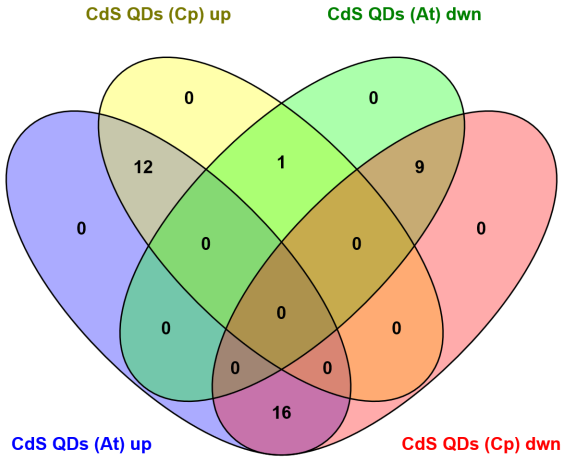

Figure 20. Comparison between the up- and down-regulated genes of *A. thaliana* (At) and *C. pepo* (Cp) in response to CdS QDs. 12 genes are commonly up-regulated in both plants, while 9 genes are commonly down-regulated.

3.8 Overall PCA of metal uptake, molecular response and biomass

Overall PCA of the experiments performed on *C. pepo* with single ENMs and their combinations (fig. 21), highlighted that the first component (responsible for the 62.2% of the total variance) is related to the presence of ZnO NPs in the treatment: in fact, Zn affected all the parameters taken into account (metal uptake, molecular response and biomass) to an greater extent if compared to the other ENMs tested. The second component, responsible for the 26.8% of the total variance, seems to be linked to the treatment with CdS QDs or CeO_2, which are once again located in opposite positions inside the biplot.

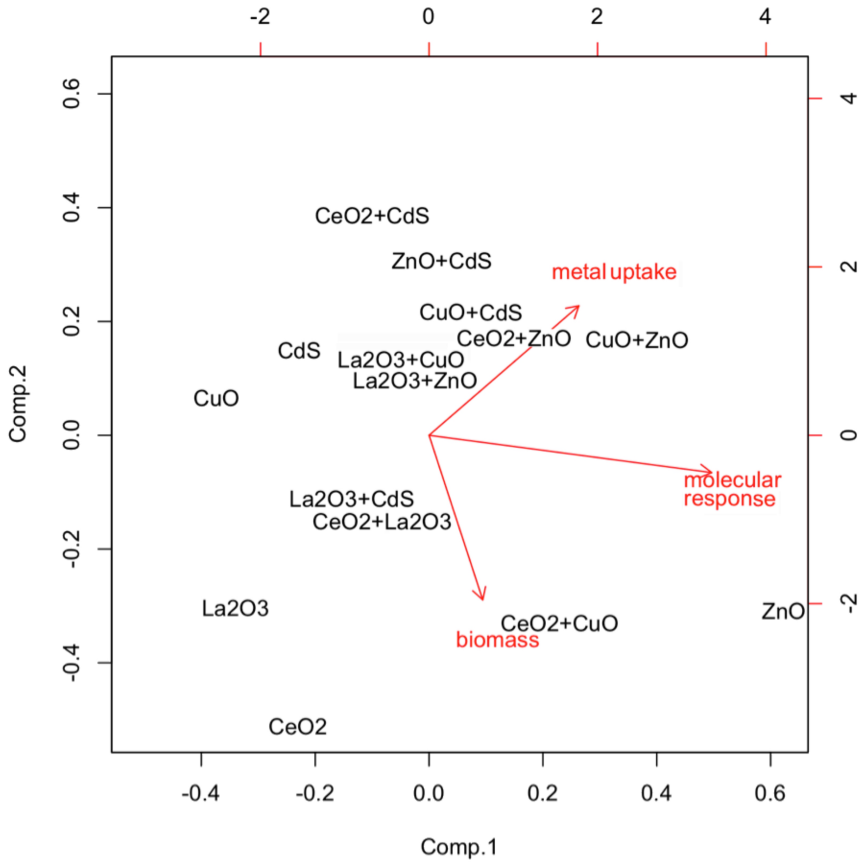


```
Importance of components:
                          Comp.1    Comp.2    Comp.3
Standard deviation     1.2426734 0.8154456 0.5235454
Proportion of Variance 0.6218517 0.2677706 0.1103777
Cumulative Proportion  0.6218517 0.8896223 1.0000000
```

Figure 21. Principal Component Analysis (PCA) of metal uptake, molecular response and biomass effects on *C. pepo* in condition of treatment with single ENMs and their different combinations.

4. *Saccharomyces cerevisiae*: results and discussion

4.1 Growth phenotype high-throughput analysis of yeast deletion mutants

Marmiroli *et al.* performed a high-throughput screening on a yeast deletion mutant collection, in condition of treatment with a sub-inhibitory concentration of CdS QDs (200 mg L^{-1} + nystatin 0.55 mg L^{-1}). This study identified 112 sensitive and 114 tolerant mutants to CdS QD exposure. Gene Ontology (GO) analysis of the two subsets of mutants identified mitochondrial organization, DNA damage repair and recombination and general stress response as some of the most represented functional categories. The comparison with a similar study performed with the correspondent salt, highlighted only a limited overlap. These findings show how, differently from $CdSO_4$, CdS QD toxicity exploits different mechanisms that are not mediated by release of free cadmium ion. The transformation of sensitive mutants with a BY4742 centromeric genomic library identified the pivotal role of *HSC82*, *DSK2* and *ALD3* in CdS QDs response.

4.2 Growth on different carbon sources

The results included in this chapter are reported in Pasquali *et al*. 2016.

Yeast cells' growth on non-fermentable carbon sources relies on respiratory metabolism, which is switched on whenever glucose or other fermentable carbon sources are not available. The last steps of respiration, Krebs cycle and the production of ATP through the electron transport chain, take place inside of the mitochondria. For this reason, the growth of BY4742 cells on both fermentable (glucose, galactose) and non-fermentable (glycerol, ethanol) carbon sources might point out to the mitochondria as one of the main targets of CdS QDs toxicity (fig. 22). Wild type (wt) and BY4742 RD cells were able to grow on glucose, at every dilution tested, unless the concentration of CdS QDs in the solid media exceeded the 100 mg L^{-1}. On galactose, RD cells were not able to grow, both in presence or absence of the CdS QD treatment. On the other hand, wt cells showed a similar behavior to the ones grown on glucose. On non-fermentable carbon media, wt

cells showed an increased sensitivity to the treatment, as they were able to grow only on the lowest concentration tested (100 mg L^{-1}) and only at the highest cell concentrations tested. As expected, RD cells were not able to grow on ethanol and glycerol due to the lack of functional mitochondria.

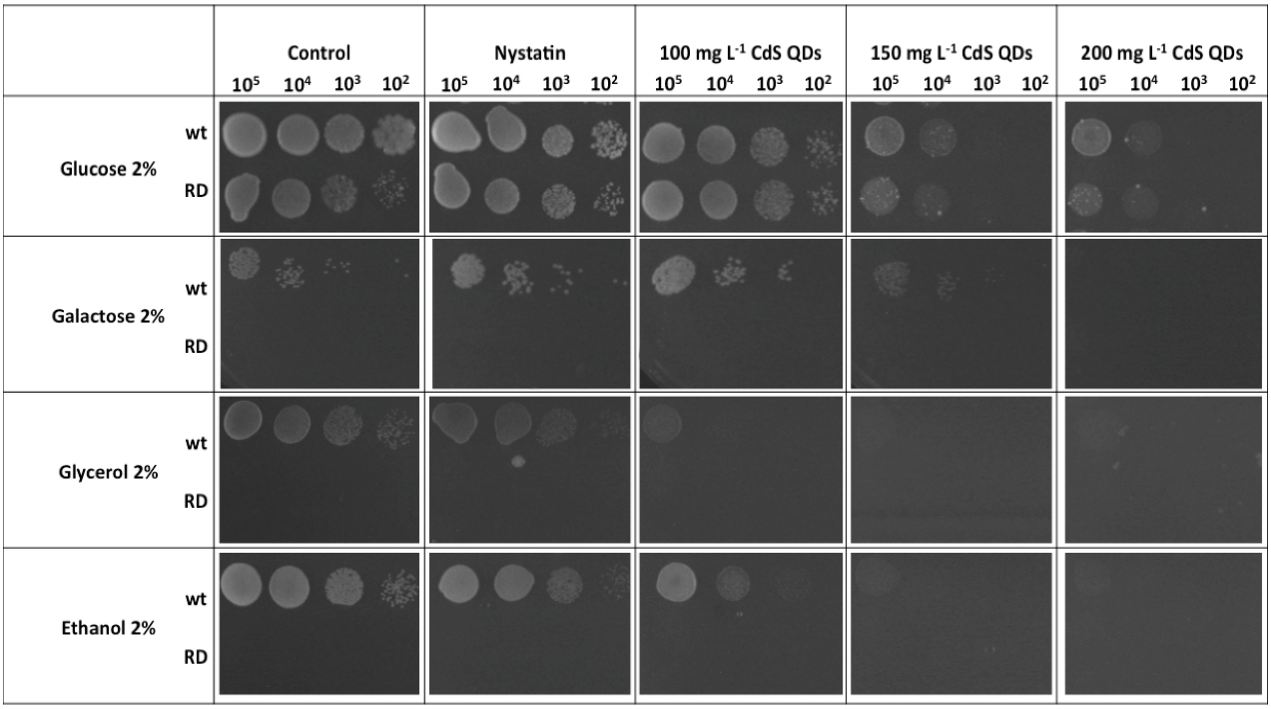

Figure 22. BY4742 wt and respiratory deficient strain (RD) were grown on different fermentable and non-fermentable carbon sources. The five panels show how the growth at the different cell dilutions was affected in the treatment conditions tested: control, 0.55 mg L^{-1} nystatin, and 0.55 mg L^{-1} nystatin with 100, 150 or 200 mg L^{-1} CdS QDs. Cell concentrations used for the different test are indicated in the first row of the table.

4.3 Cytofluorimetric analysis of yeast response to CdS QDs

Staining of the yeast cells with the vital dye FUN1, allowed the discrimination of living cells form cellular debris and CdS QDs still suspended in solution. The percentage of living cells, highlighted by the "morpho" gate (fig. 23), is about 97% for both untreated control and nystatin. In the sample treated with 0.25 mg L^{-1} nystatin plus 100 mg L^{-1} CdS QDs, the percentage decreases to 90.7% of the total events. This is due to the effect of treatment on cell viability and to the presence

of free quantum dots not internalized by yeast. The sample treated with CdS QDs highlighted a variation of side scattering, which might be due to CdS QDs internalization, and a decrease of the number of doublets/multiplets (all the events that cannot be recognized as a single one, e.g. budding cells or cell aggregates). Nystatin treated samples did not show any significant differences in side scattering or doublet/multiple events abundance, if compared to the untreated control.

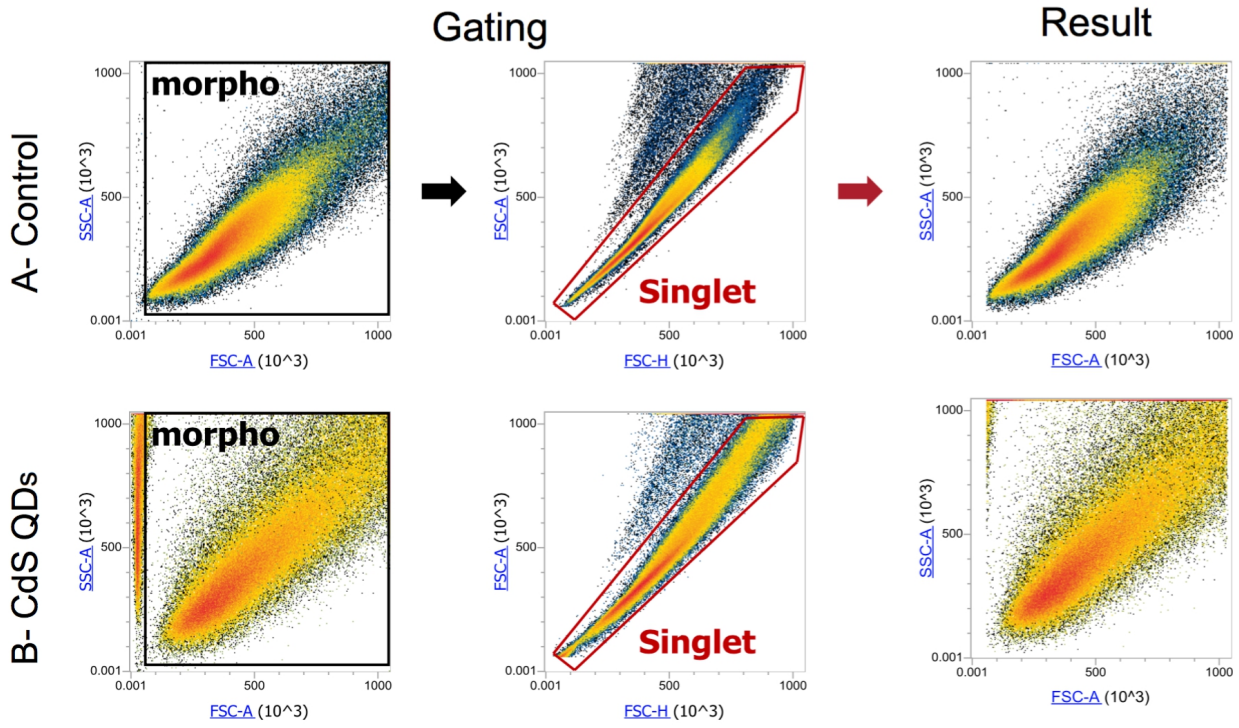

Figure 23. Cytofluorimetric analysis of cells exposed to CdS QDs

Comparison between untreated and treated (0.25 mg L^{-1} of nystatin + 100 mg L^{-1} of CdS QDs) BY4742 cells. The first gate (morpho) is applied to distinguish yeast cells from free CdS QDs in solution and cell debris, according to their size. The second gate (singlet) is applied to select only singlet events. Treatment results in a variation in side scattering upon CdS QD uptake and in an increase of singlet events.

4.4 Microarray transcriptomic analysis of yeast in response to CdS QDs

The microarray analysis of the whole transcriptome, performed on yeast cells treated with 0.25 mg L^{-1} plus 100 mg L^{-1} CdS QDs, identified 622 genes (reported here in paragraph 8.2) whose

expression levels were significantly different from the untreated control: 312 of them were up- and 310 down-regulated (fig. 24 a and b show the heatmaps of the genes whose expression was respectively 2-fold increased or decreased if compared to the untreated control). None of them was in common with the treatment with nystatin alone, which resulted in the up-regulation of only 4 genes (*YDL218W*, *IMD12*, *IMD1* and *YDR366C*) and in the down-regulation of other 4 (*DMC1*, *YOLO014W*, *MIG2* and *HXT1*); this confirms that the sub-inhibitory concentration of antibiotic used had the only effect of increase the uptake of CdS QDs, almost without affecting yeast's gene expression. The expression profiles were then compared to the one obtained in presence of 25 μM $CdSO_4$ (Jin Y.H. *et al.*, 2008). Among the genes induced or repressed by the half maximal effective concentration (EC_{50}) of this cadmium salt, only 8 were in common with the CdS QDs treatment: 4 were up-regulated (*CYS3*, *SUL2*, *FET3* and *FRE5*) and 4 down-regulated (*PHO5*, *IDP3*, *ARG1* and *YBR285W*). This confirms that cadmium in nano and ionic form exploit different mechanisms of toxicity, as reported Marmiroli *et al.* 2016. 22 genes were identified both by microarray and a deletion mutants screening as involved in CdS QD response (Marmiroli *et al.* 2016). For some of them, the phenotype can be easily correlated to the expression profile: for example, sensitive mutants are deleted in genes involved in detoxification mechanism that are likely to be up-regulated in condition of treatment with CdS QDs; the same goes for tolerant/down-regulated ones.

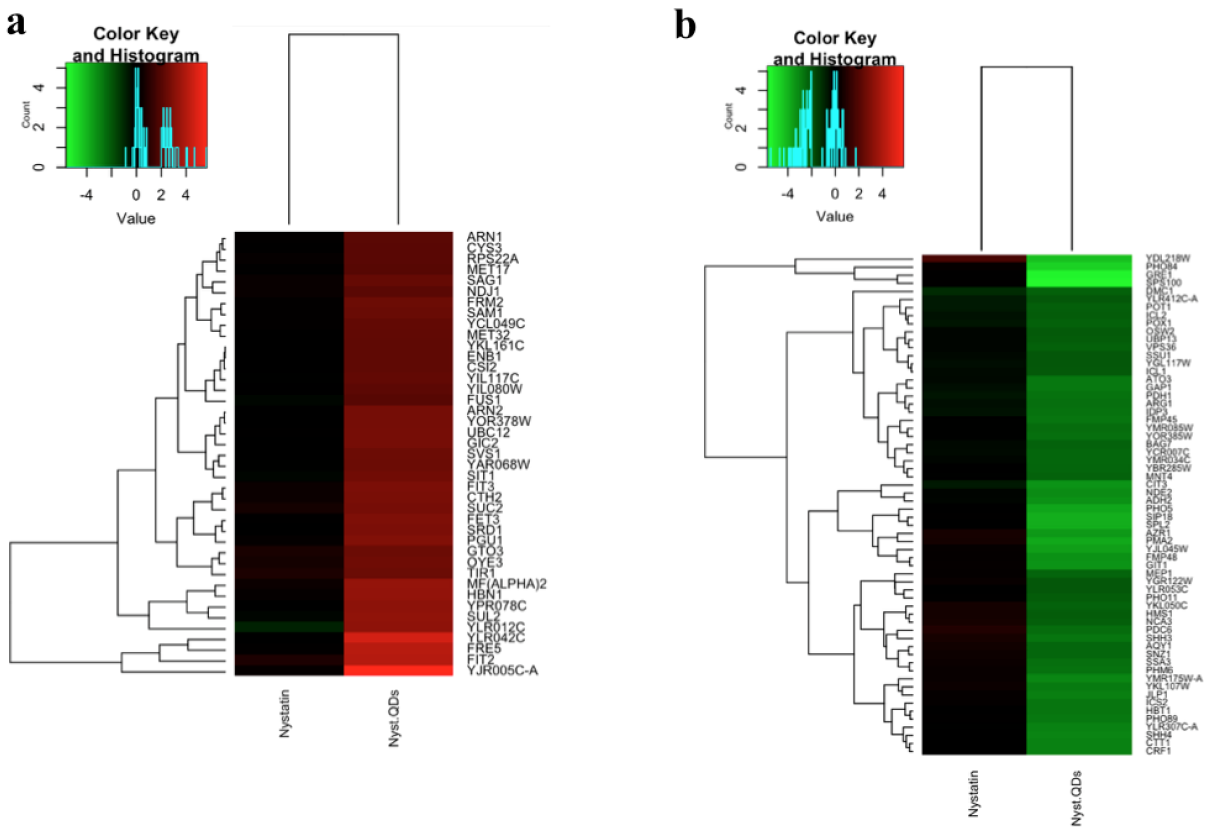

Figure 24. The heatmaps represent the effect on gene expression of nystatin (0.25 mg L^{-1}) and nystatin plus CdS QDs (100 mg L^{-1}), as generated by microarray analysis and confirmed by RT-qPCR. Over-expressed genes are indicated in red (a), while under-expressed ones are reported in green (b). Expression data from both the treatments were normalized on untreated control values.

The gene ontology (GO) analysis, performed with DAVID Bioinformatics Resources v6.7 (https://david.ncifcrf.gov), identified the biological processes that were functionally enriched in the two sets of up- and down-regulated genes: the frequency of genes annotated to these GO terms in the genome was lower than the one of the genes annotated in the sample (with *p*-value<0.01). The main biological processes enriched among the up-regulated genes (fig. 25) were translation (21.6% on sample), cellular component morphogenesis (9.5%), sexual reproduction (8.2%), ion transport (7.9%), cell wall organization (7.5%) and DNA recombination (6.5%). Translation category includes several protein components of cytosolic (40S and 60S) and mitochondrial ribosomal subunits; this category also includes *FIT2*, *FET3*, *FIT3 and SIT2*: these genes are among the most

up-regulated in response to CdS QDs, and encode for proteins involved in iron uptake and retention. Sexual reproduction category includes, among the others, the mating pheromone alpha-factor (*MF(ALPHA)1* and *MF(ALPHA)2*) and proteins whose expression is under its regulation (*FUS1* and *PRM5*) ; *FKS1* also belongs to this category: it encodes a catalytic subunit of 1,3-beta-D-glucan synthase, required for cell wall synthesis and maintenance. For the down-regulated genes, the main categories (fig. 26) included oxidation reduction (11.0%), coenzyme metabolic process (5.5%), organic acid catabolic process (4.9%) and cellular amino acid derivative metabolic process (3.2%). Oxidation reduction cluster includes both cytosolic and mitochondrial dehydrogenases (e.g. *GDH3*, *NDE2*, *GUT2*, *SHH3* and *SHH4*) and two catalases (*CTA1* and *CTT1*) with a protective role by oxidative damage. Organic acid catabolic process category includes subunits of the mitochondrial genes that encode for glycine decarboxylases (*GCV1* and *GCV2*) and for proteins involved in citrate and methylcitrate metabolism (*CIT3*, *PDH1* and *ICL2*). The last category includes *ALD3*, a cytoplasmic aldehyde dehydrogenase and *ARO10*, a phenylpyruvate decarboxylase, both involved in aminoacid metabolism; according to Marmiroli *et al.* 2016, their deletion resulted in a sensitive growth phenotype (GP) in condition of treatment with CdS QDs.

The transcriptomic data were also analysed with KEGG database (http://www.kegg.jp), to identify the metabolic pathways that are more represented among the up- and down-regulated genes lists. Of particular interest was galactose metabolism, which included 5 up-regulated genes (*MAL12*, *MAL32*, *HXK2*, *SUC2* and *IMA1*): galactose utilization partially relies on mitochondrial function, pointing out once again a possible role of mitochondria in response to CdS QDs. Furthermore, citrate cycle pathway, whose reactions occur in the mitochondrial matrix, was represented by 6 down-regulated genes (*SDH1b*, *MRPS17*, *SHH4*, *IDP3*, *MDH2* and *CIT3*).

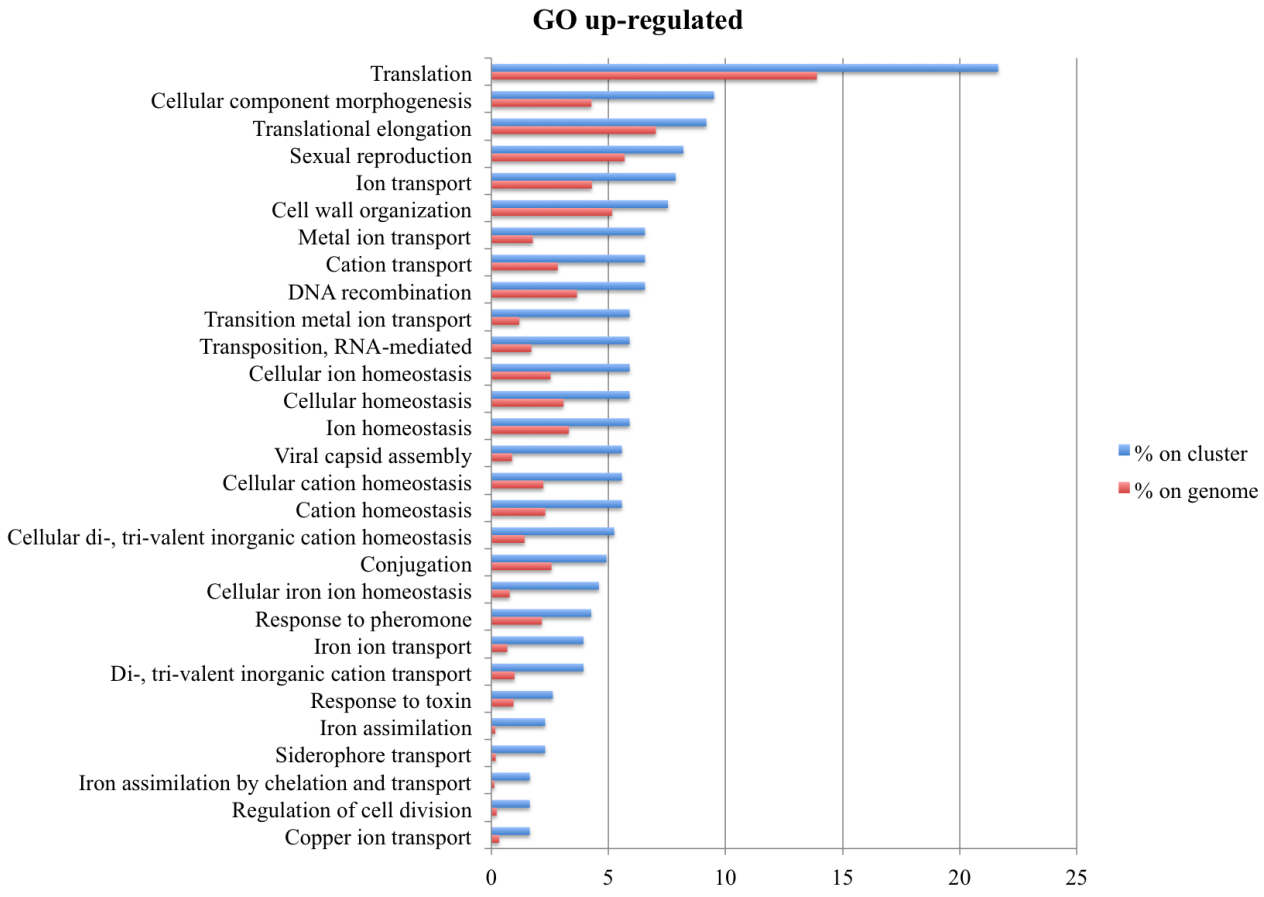

Figure 25. Gene Ontology analysis of functionally enriched biological processes among the up-regulated genes, in response to CdS QD exposure. Blue bars represent the frequency of the genes belonging to each category in the cluster, while red bars represent the frequency on the entire genome.

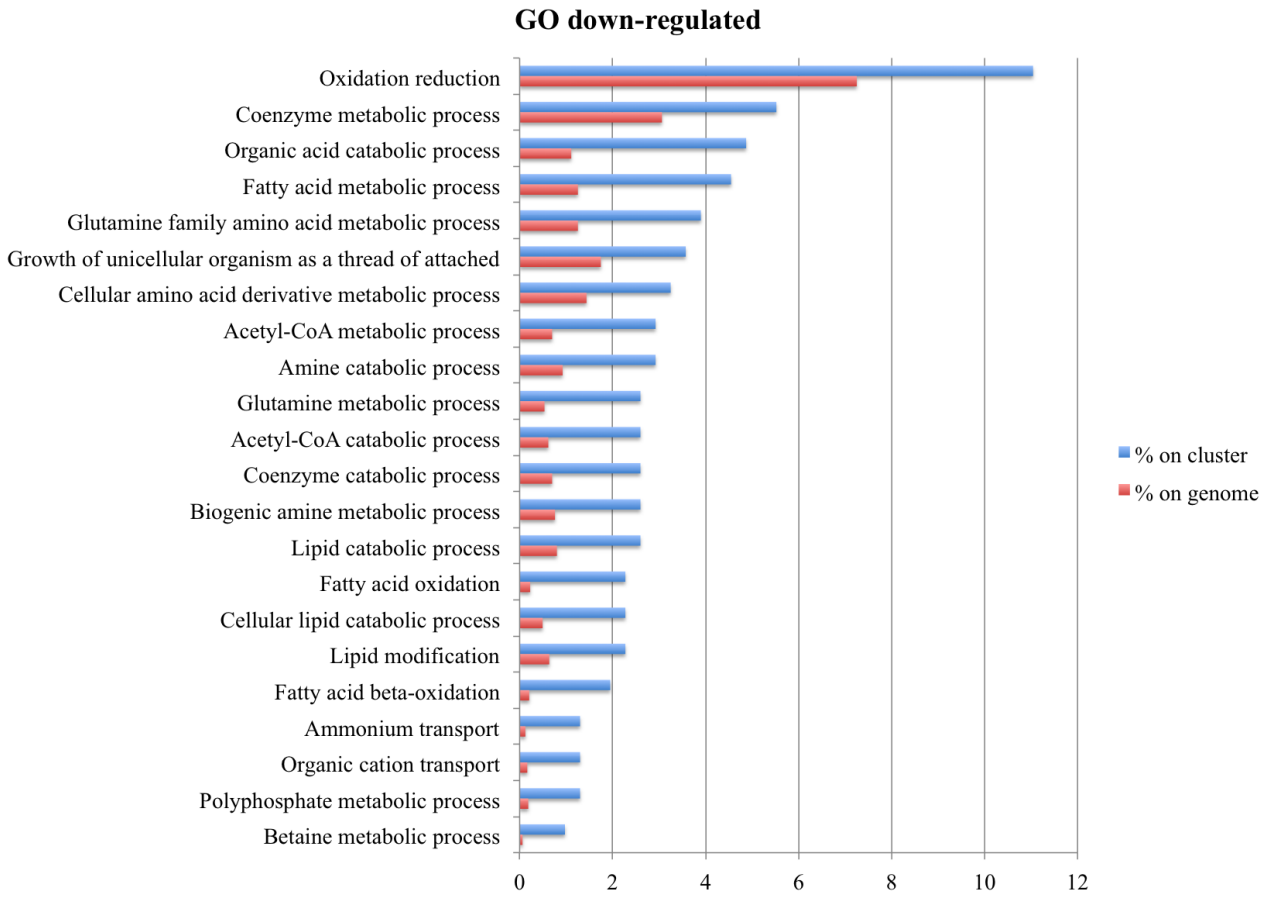

Figure 26. Gene Ontology analysis of functionally enriched biological processes among the down-regulated genes, in response to CdS QD exposure. Blue bars represent the frequency of the genes belonging to each category in the cluster, while red bars represent the frequency on the entire genome.

4.5 Analysis of oxygen consumption and assessment of respiratory cytochrome content

The analysis of the absorption spectra signature of respiratory cytochromes revealed that both CdS QD and ionic Cd^{2+} treatments have a significant impact on cellular respiratory cytochrome content, if compared to the untreated control. Exposure to CdS QDs resulted in an average reduction to 25% of cytochrome b and c content ($p<0.01$ and $p<0.001$) respectively), while

cytochrome aa3 content was reduced to 20% (p<0.0003), as shown in figure 27 a. The treatment with nystatin alone resulted in a less stressed reduction of the three cytochromes content (cytochrome c content was reduced to 35%, while b and aa3 content was reduced to 28%). Exposure of BY4742 cells to different concentrations of $CdSO_4$ negatively affected the content of each cytochrome: cytochrome b content was reduced to ~30% (p<0.004), cytochrome c was reduced to ~33% (p<0.0002), while cytochrome aa3 to ~45% (p<0.0003), as shown in figure 27 b. Furthermore, CdS QD treatment, at all the concentrations tested, reduced oxygen consumption by ~90% (fig. 27 c). In this case, presence of nystatin alone had no inhibitory effect. It's worth to consider that the residual oxygen consumption was sensitive to sodium azide, meaning that it was "primary respiration". Oxygen consumption was also significantly decreased by $CdSO_4$ treatment (88.7-96%, dependent on the salt concentration, fig. 27 d).

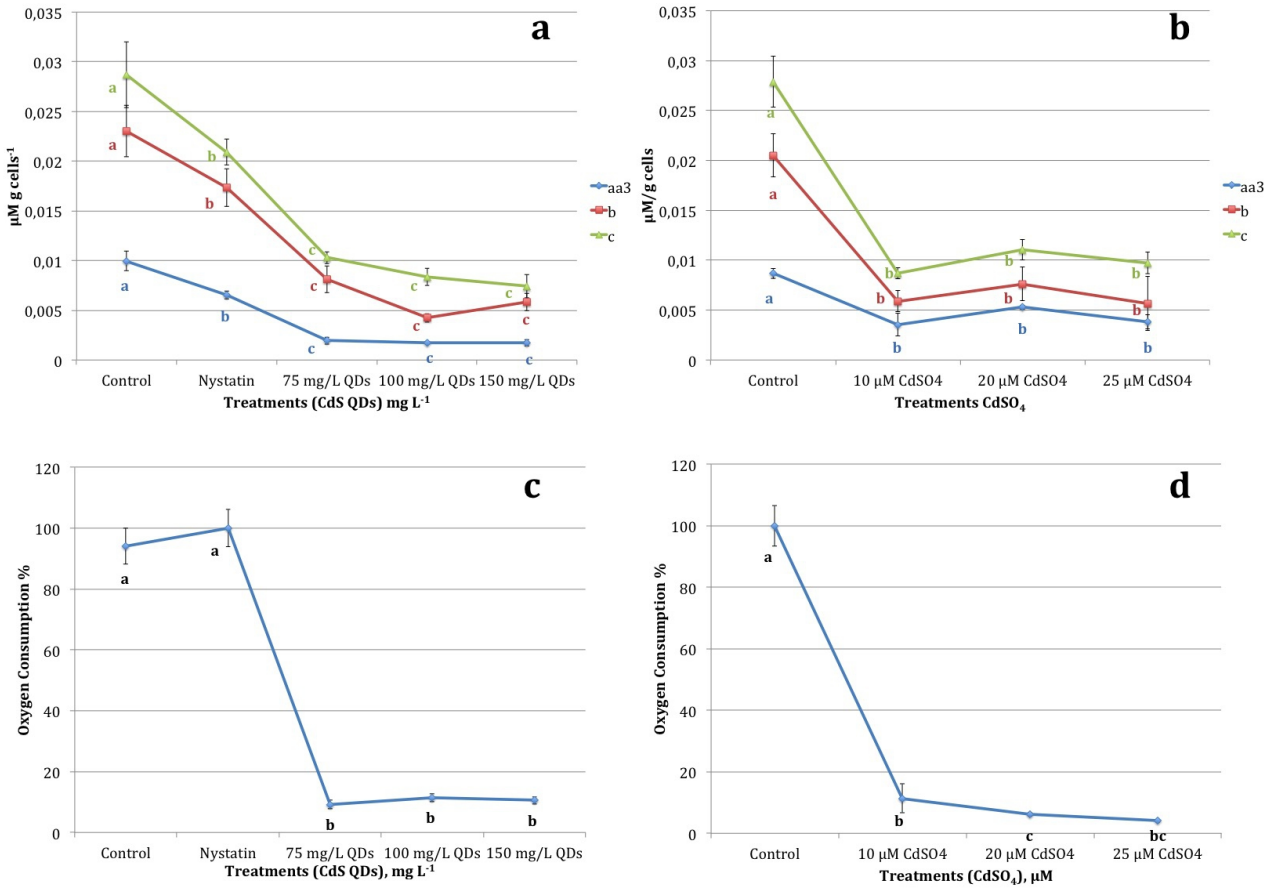

Figure 27. Cytochrome content and oxygen consumption in cells exposed to either CdS QDs or

CdSO4. CdS QDs (a) appeared to affect mainly the content of cytochrome aa3, while CdSO4 (c) affected most the content of both cytochrome b and c. The concentration of Cd in CdS QDs that inhibits 90% respiration (b) is between 58.5 and 117 mg L^{-1}, while the concentration of Cd in $CdSO_4$ to obtain the same inhibition (d) is in the range 1-2.7 mg L^{-1}. Letters (whose colour refers to the single parameter analysed) represent the results of Tukey's post-hoc comparisons of group means: different letters indicate significantly different means.

4.6 Analysis on the effect of mitochondrial DNA integrity

As reported in Pasquali *et al*. 2016, the frequency of RD cells induction was not increased either in condition of treatment with nystatin alone or with 75-150 mg L^{-1} CdS QDs. Re-culturing and re-exposing the cells did not affect RD frequency. BY4742 cells exposed to ethidium bromide, a strong mutagen, showed an RD induction of 100%. Exposure to the $CdSO_4$ salt resulted in a RD frequency of 25.5% highlighting, even in this case, a different behaviour between QDs and ionic cadmium. Similar results were obtained using the W303 strain: in this case, after treatment in a 100 mg L^{-1} CdS QDs supplemented media, about 39% of the colonies showed a pink pigmentation, which is indicative of a possible defect in oxidative phosphorylation. Despite this, the replica of the plate on YPG agar showed that the pink colonies were still able to grow on a non-fermentable media: these cells must not be considered RD cells but only RD phenocopies. Once again, the exposure of W303 cells to ethidium bromide induced 100% of RD mutants, while the frequency induced by $CdSO_4$ was similar to the one observed in BY4742 (27.5%).

4.7 Effect of CdS QDs on mitochondrial morphology

BY4742 cells were stained with DAPI and Rhodamine B, to assess mitochondrial integrity. The use of both dyes, shows that upon CdS QD exposure the mitochondrial network seems to be interrupted, but with no evidence of mitochondrial degradation (fig. 28). Mitochondrial fluorescence decreased from 98.7% of the untreated controls to 67.4% of treated cells. Fluorescence expressed by petite cells was extremely low, with no differences between treated and untreated cells. The interruption of the mitochondrial network was furthermore confirmed by the wild type strain transformed with a mitochondrial-directed RFP (mtRFP), which allowed a more directed study of the effect of treatment on the percentages of the different mitochondrial morphotypes. In particular, control cells (transformed only) showed almost 100% of long-filamentous mitochondria (fig. 29). This percentage was significantly reduced by both CdS QDs (25%) and $CdSO_4$ (28.85%) treatments. The mitochondrial network was fragmented in 71.77% of the cells treated with CdS QDs, while only 3.23% showed only an extremely low fluorescence. In case of $CdSO_4$ treatment, the fragmented morphotype represented the 46.15% of the total sample, with an increase of the low fluorescent portion to 25%.

The real-time relative quantification of mitochondrial markers *ATP6*, *COX2* and *COB* showed no differences in the abundance of mtDNA in condition of presence or absence of treatment with CdS QDs, as showed in Pasquali *et al*. 2016. This shows once again how quantum dots impact on mitochondrial functionality relies on a mechanism of action which is different from the one of the ionic cadmium: the first impairs mitochondrial respiration without any effect on mtDNA integrity, while the latter is a well-known mutagen that impairs mtDNA replication and induces petite mutant formation (Stumpf *et al*. 2014).

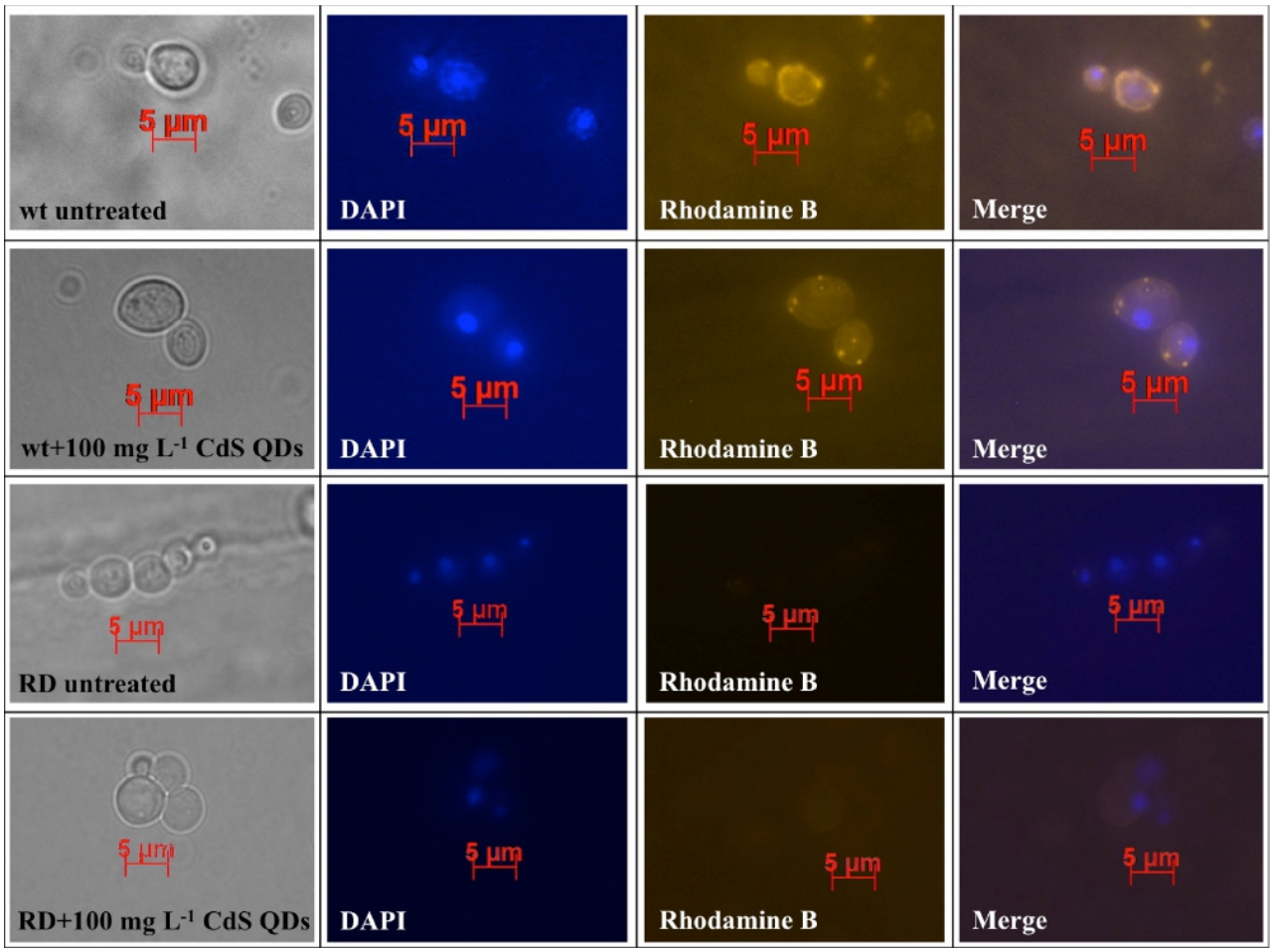

Figure 28. Comparison between RS and RD cells of the strain BY4742, after staining with DAPI and Rhodamine B, in presence or absence of 100 mg L^{-1} CdS QD treatment. DAPI staining (reported in the second column) targets both mitochondrial and nuclear DNA. Rhodamine B selectively stains mitochondrial membrane.

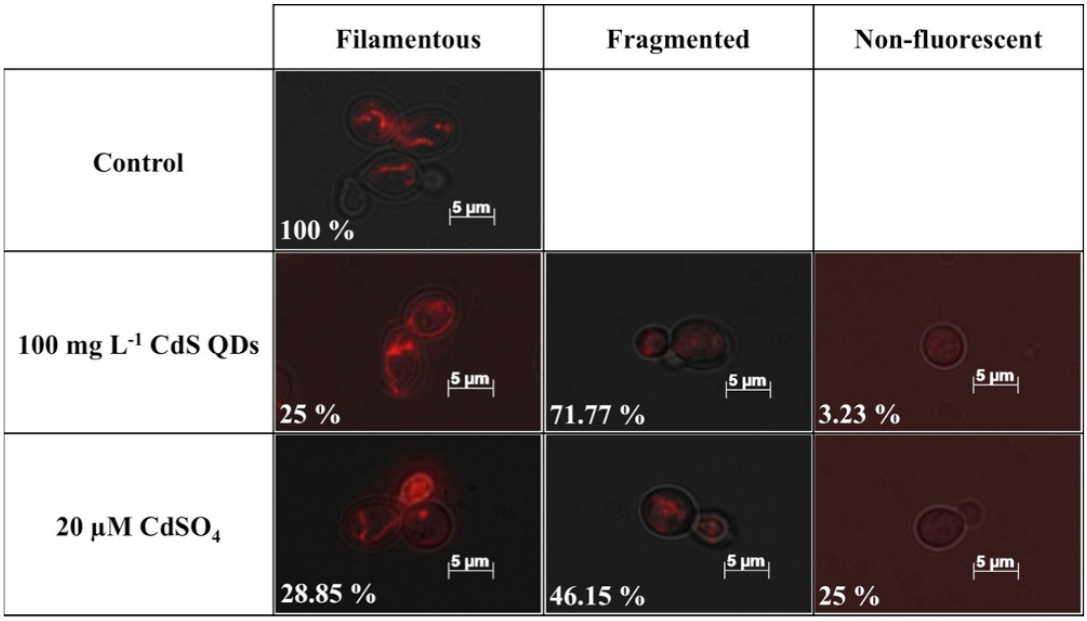

Figure 29. Comparison between BY4742 cells in absence of treatment and in presence of 100 mg L^{-1} CdS QD or 20 µM $CdSO_4$ treatments. Cells were transformed with the pYX142-mtRFP, encoding for a mitochondrial targeted red fluorescent proteins. The three columns show the percentage of the three different mitochondrial morphotypes reported.

4.8 Evaluation of reactive oxygen species and glutathione redox state

After one and four hours of exposure, all the CdS QDs concentrations tested lead to an increase in intracellular ROS content, if compared to the untreated control condition. As reported in fig. 30 a, the 150 mg L^{-1} treatment resulted in the highest induction at both the time intervals. The spectrophotometric analysis of the cell lysate, performed after 24 h of treatment (fig 30 b), showed that after exposure to a concentration higher than 75 mg L^{-1} CdS QDs resulted in a decrease of the reduced form of glutathione (GSH) with a consequent increase of its oxidized form (GSSG). Thus, the redox state of the glutathione, obtained by the ratio between GSH and total glutathione content, decreases in response to CdS QDs, consistently to the triggering of a response to oxidative stress. This is also confirmed by the up-regulation of different genes involved in glutathione metabolism and mobilization: *GTO3*, encoding for an omega class glutathione transferase; *GPX2*, encoding a

phospholipid hydroperoxide glutathione peroxidase; *GTI2*, encoding a glutathione S-transferase; *OPT1*, encoding for a proton-coupled oligopeptide transporter involved also in glutathione mobilization. These findings also confirm what is reported in literature: in particular, in mammalian cells, QDs exposure results in an accumulation of intracellular ROS and in an increase of GSSG over GSH (Nguyen *et al*. 2015).

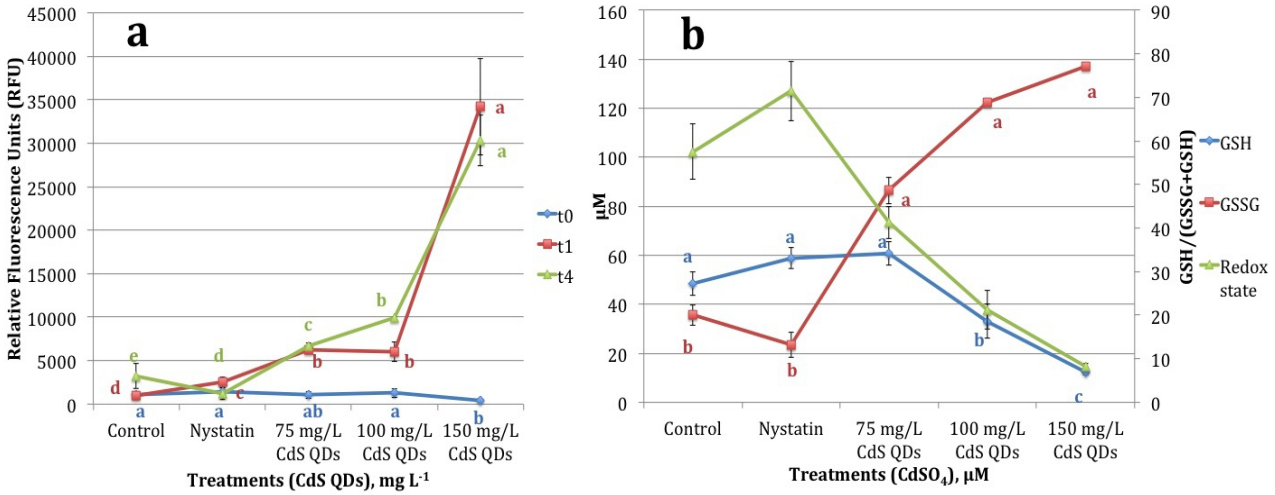

Figure 30. (a) Intracellular ROS content as affected by exposure to CdS QDs, after 0, 1 and 4 hours of exposure. (b) Content of the reduced (GSH) and oxidized (GSSG) forms of glutathione in the yeast cells, after 24 h of exposure to CdS QDs. Glutathione redox state is calculated using the formula GSH/(GSSG+GSH).

5. Conclusions

The analysis carried out in *Cucurbita pepo* showed that all the ENMs (except for CeO_2) are actively translocated from roots to stems and leaves. Nano and corresponding bulk formulations exerted a different effect on plant biomass, that might be in part explained by the different uptake and translocation among the plant tissues: this translocation frequently occurred to a greater extent than observed with the bulk counterparts; this was likely because of the smaller particle dimensions. After 21 days of treatment, the response did not trigger any other evident physiological effect, but was instead strong enough to impact on metal accumulation and modulation of gene expression.

Transcriptional analysis showed that the molecular response of the plant to ENMs is influenced by the interactions that occur between different nanoparticles upon co-exposure. Some of the genes analyzed are specifically up- or down-regulated in response to particular types of ENMs. Furthermore, the gene 152u, which encodes for a chloroplastic electron carrier, is down-regulated in all the ENP exposure conditions, thus representing a putative biomarker of ENM exposure in this organism.

CdS QDs treatment in yeast resulted in a disruption of the mitochondrial network; a deregulation of mitochondrial membrane potential; an accumulation of reactive oxygen species and the decrease of glutathione redox state; an impairment of the ability to grow on non-fermentable carbon sources; differently from ionic Cd, CdS QDs do not induce respiratory deficient mutants, showing once again how the toxic effect of bulk and ENMs is exerted through different mechanisms of action.

Saccharomyces cerevisiae proved to be a suitable model organism for nanotoxicology analysis and, thanks to the presence of a high number of orthologs conserved in higher eukaryotes, could be an ideal platform for the study of mitochondrial related pathologies in human.

In conclusion, both organisms provided further information on ENMs behavior and toxicity, useful in a risk-assessment framework. These data, combined with an in-deep characterization and mechanism-based toxicological cellular outcomes allow the determination of structure-activity relationships (SARs), which link the physicochemical properties of ENMs to their biological activity providing a powerful predictive tool for safety assessment and for safer-by-design approaches.

6. References

(2016) Nanomaterials Market by Type and End-user - Global Opportunity Analysis and Industry Forecast, 2014 – 2022.

(2011) Commission recommendation of 18 October 2011 on the definition of nanomaterial (2011/696/EU). *Official Journal of the European Union*.

Arts J.H.E., Hadi M., Keene A.M., Kreiling R., Lyon D., Maier M., Michel K., Petry T., Sauer U.G., Warheit D., Wiench K., Landsiedel R. (2014) A critical appraisal of existing concepts for the grouping of nanomaterials. *Regul Toxicol Pharmacol*. 70(2):492-506.

Balavi H., Samadanian-Isfahani S., Mehrabani-Zeinabad M., Edrissi M. (2013). Preparation and optimization of CeO_2 nanoparticles and its application in photocatalytic degradation of Reactive Orange 16 dye. *Powder technol*. 249:549-555.

Baruffini E., Ferrero I., Foury F. (2010) In vivo analysis of mtDNA replication defects in yeast. *Methods*. 51(4):426-36.

Bayat N., Rajapakse K., Marinsek-Logar R., Drobne D., Cristobal S. (2014) The effects of engineered nanoparticles on the cellular structure and growth of Saccharomyces cerevisiae. *Nanotoxicology*. 8(4):363-73.

Bermejo-Nogales A., Fernández M., Fernández-Cruz M.L., Navas J.M. (2016) Effects of a silver nanomaterial on cellular organelles and time course of oxidative stress in a fish cell line (PLHC-1). *Comp Biochem Physiol C Toxicol Pharmacol*. 190:54-65.

Blanca, J., Cañizares, J., Roig, C., Ziarsolo, P., Nuez, F., Picó, B. (2011) Transcriptome characterization and high throughput SSRs and SNPs discovery in Cucurbita pepo (Cucurbitaceae). *BMC genomics*, 12(1), 1.

Bohnsack J.P., Assemi S., Miller J.D., Furgeson D.Y. (2012) The primacy of physicochemical characterization of nanomaterials for reliable toxicity assessment: a review of the zebrafish nanotoxicology model. In Nanotoxicity: Methods and Protocols (pp. 261-316) Springer.

Bondarenko O., Juganson K., Ivask A., Kasemets K., Mortimer M., Kahru A. (2013) Toxicity of Ag, CuO and ZnO nanoparticles to selected environmentally relevant test organisms and mammalian cells in vitro: a critical review. *Arch Toxicol.* 87(7):1181–1200.

Bornhövd C., Vogel F., Neupert W., Reichert A.S. (2006) Mitochondrial membrane potential is dependent on the oligomeric state of F1F0-ATP synthase supracomplexes. *J Biol Chem*. 281(20):13990-8.

Brabu B., Haribabu S., Revathy M., Anitha S., Thangapandiyan M., Navaneethakrishnan K.R., Gopalakrishnan C., Murugan S.S., Kumaravel T.S. (2015). Biocompatibility studies on lanthanum oxide nanoparticles. *Toxicol Res*. 4(4):1037-1044.

Bussche J.V., Soares E.V. (2011) Lead induces oxidative stress and phenotypic markers of apoptosis in *Saccharomyces cerevisiae*. *Appl Microbiol Biotechnol.* 90(2), 679-87.

Castiglione M.R., Giorgetti L., Geri C., Cremonini R. (2011) The effects of nano-TiO2 on seed germination, development and mitosis of root tip cells of Vicia narbonensis L. and Zea mays L. *J Nanopart Res*. 13:2443-2449.

Chateigner-Boutin A.L., Small I. (2007) A rapid high-throughput method for the detection and quantification of RNA editing based on high-resolution melting of amplicons. *Nucleic Acids Res*. 35(17):e114.

Davletova S., Schlauch K., Coutu J., Mittler R. (2005) The zinc-finger protein Zat12 plays a central role in reactive oxygen and abiotic stress signaling in Arabidopsis. *Plant Physiol*. 139(2):847-56.

Dos Santos S.C., Sá-Correia I. (2015) Yeast toxicogenomics: lessons from a eukaryotic cell model and cell factory. *Curr Opin Biotechnol*. 33:183-91.

Dwivedi S., Saquib Q., Al-Khedhairy A.A., Musarrat J. (2016) Understanding the Role of Nanomaterials in Agriculture. In Microbial Inoculants in Sustainable Agricultural Productivity (pp. 271-288). Springer India.

Fan J., Sun Y., Wang S., Li Y., Zeng X., Cao Z., Yang P., Song P., Wang Z., Xian Z., Gao H., Chen Q., Cui D., Ju D. (2016) Inhibition of autophagy overcomes the nanotoxicity elicited by cadmium-based quantum dots. *Biomaterials*. 78:102-14.

Falkner, R., Jaspers, N., 2012. Regulating nanotechnologies: risk, uncertainty and the global governance gap. *Glob Environ Polit*. 12(1):30-55.

Faure B., Salazar-Alvarez G., Ahniyaz A., Villaluenga I., Berriozabal G., De Miguel Y.R., Bergström L. (2016). Dispersion and surface functionalization of oxide nanoparticles for transparent photocatalytic and UV-protecting coatings and sunscreens. *Sci Technol Adv Mater*. 14.

Flattery-O'Brien J.A., Dawes I.W. (1998) Hydrogen peroxide causes RAD9-dependent cell cycle arrest in G2 in *Saccharomyces cerevisiae* whereas menadione causes G1 arrest independent of RAD9 function. *J Biol Chem*. 273(15), 8564-71.

Foury F., Roganti T., Lecrenier N., Purnelle B. (1998) The complete sequence of the mitochondrial genome of Saccharomyces cerevisiae. *FEBS Lett*. 440, 325–331.

Freyre-Fonseca V., Delgado-Buenrostro N.L., Gutiérrez-Cirlos E.B., Calderón-Torres C.M., Cabellos-Avelar T., Sánchez-Pérez Y., Pinzón E., Torres I., Molina-Jijón E., Zazueta C., Pedraza-Chaverri J., García-Cuéllar C.M., Chirino Y.I. (2011) Titanium dioxide nanoparticles impair lung mitochondrial function. *Toxicol Lett.* 202(2):111-9.

Gietz R.D., Woods R.A. (2002) Transformation of yeast by lithium acetate/single-stranded carrier DNA/polyethylene glycol method. *Methods Enzymol*. 350:87-96.

Goffeau A. (2000) Four years of post-genomic life with 6,000 yeast genes. *FEBS Lett*. 480(1):37-41.

Harju S., Fedosyuk H., Peterson K.R. (2004) Rapid isolation of yeast genomic DNA: Bust n' Grab. *BMC Biotechnology*. 4:8.

Hawthorne J., De la Torre-Roche R., Xing B., Newman L.A., Ma X., Majumdar S., Gardea-Torresdey J., White J.C. (2014) Particle-size dependent accumulation and trophic transfer of cerium oxide through a terrestrial food chain. *Environ Sci Technol*. 48(22):13102-9.

Hawthorne J., Musante C., Sinha S.K., White J.C. (2012) Accumulation and phytotoxicity of engineered nanoparticles to Cucurbita pepo. *Int j phytoremediation.* 14(4):429-442.

Hitosugi S., Nakanishi W., Yamasaki T., Isobe H. (2011). Bottom-up synthesis of finite models of helical (n, m)-single-wall carbon nanotubes. *Nat Commun*. 2:492.

Höwing T., Huesmann C., Hoefle C., Nagel M.K., Isono E., Hückelhoven R., Gietl C. (2014) Endoplasmic reticulum KDEL-tailed cysteine endopeptidase 1 of Arabidopsis (AtCEP1) is involved in pathogen defense. *Front Plant Sci.* 24;5:58.

Huang Y.H., Bao Q., Duh J.G., Chang C.T. (2016) Top-down Dispersion Meets Bottom-up Synthesis: Merging Ultranano Silicon and Graphene Nanosheets for Superior Hybrid Anodes in Lithium-ion Batteries. *J Mater Chem A.* 4:9986-9997

Jamieson T., Bakhshi R., Petrova D., Pocock R., Imani M., Seifalian A.M. (2007) Biological applications of quantum dots. *Biomaterials*. 28(31):4717-32.

Javanbakht T., Laurent S., Stanicki D., Wilkinson K.J. (2016) Relating the Surface Properties of Superparamagnetic Iron Oxide Nanoparticles (SPIONs) to Their Bactericidal Effect towards a Biofilm of Streptococcus mutans. *PLoS One*. 11(4):e0154445.

Jin C., Reed J.C. (2002) Yeast and apoptosis. *Nat Rev Mol Cell Biol*. 3(6):453-459.

Jin Y.H., Dunlap P.E., McBride S.J., Al-Refai H., Bushel P.R., Freedman J.H. (2008) Global transcriptome and deletome profiles of yeast exposed to transition metals. *PLoS Genet*. 4(4):e1000053. doi: 10.1371/journal.pgen.1000053.

Kanhed P., Birla S., Gaikwad S., Gade A., Seabra A.B., Rubilar O., Duran N., Rai, M. (2014). In vitro antifungal efficacy of copper nanoparticles against selected crop pathogenic fungi. *Mater Lett*. 115:13-17.

Keller A.A., Lazareva A. (2013) Predicted releases of engineered nanomaterials: From global to regional to local. *Environ Sci Technol Lett*. 1(1):65-70.

Kah M., Hofmann T. (2014) Nanopesticide research: current trends and future priorities. *Environ Int*. 63:224-235.

Karnkowska A., Vacek V., Zubáčová Z., Treitli S.C., Petrželková R., Eme L., Novák L., Žárský V., Barlow L.D., Herman E.K., Soukal P., Hroudová M., Doležal P., Stairs C.W., Roger A.J., Eliáš M., Dacks J.B., Vlček Č., Hampl V. (2016) A Eukaryote without a Mitochondrial Organelle. *Curr Biol*. 26(10):1274-84.

Khalid H., Mukherjee S.P., O'Neill L., Byrne H.J. (2016) Structural dependence of in vitro cytotoxicity, oxidative stress and uptake mechanisms of poly(propylene imine) dendritic nanoparticles. *J Appl Toxicol*. 36(3):464-73.

Krewski D., Acosta Jr D., Andersen M., Anderson H., Bailar III J.C., Boekelheide K., Brent R., Charnley G., Cheung V.G., Green S. Jr, Kelsey K.T., Kerkvliet N.I., Li A.A., McCray L., Meyer O.,

Patterson R.D., Pennie W., Scala R.A., Solomon G.M., Stephens M., Yager J., Zeise L. (2010) Toxicity testing in the 21st century: a vision and a strategy. *J Toxicol Environ Health B Crit Rev*. 13:51–138.

Lasserre J.P., Dautant A., Aiyar R.S., Kucharczyk R., Glatigny A., Tribouillard-Tanvier D., Rytka J., Blondel M., Skoczen N., Reynier P., Pitayu L., Rötig A., Delahodde A., Steinmetz L.M., Dujardin G., Procaccio V., Pitayu L. (2015) Yeast as a system for modeling mitochondrial disease mechanisms and discovering therapies. *Dis Model Mech*. 8(6):509-526.

Lee B.H., Henderson D.A., Zhu J.K. (2005) The Arabidopsis cold-responsive transcriptome and its regulation by ICE1. *Plant Cell*. 17(11):3155-75.

Lee, J., Mahendra S., Alvarez P.J. (2010). Nanomaterials in the construction industry: a review of their applications and environmental health and safety considerations. *ACS nano* 4(7):3580-3590.

Lee R.G., Stokes E. (2016) Material Uncertainty: Nanomaterials, Regulation and Symbolic Legislation. In *Symbolic Legislation Theory and Developments in Biolaw. Springer International Publishing*, 237-252.

Li X., Zhao T., Sun L., Aifantis K.E., Fan Y., Feng Q., Cui F., Watari F. (2016) The applications of conductive nanomaterials in the biomedical field. *J Biomed Mater Res A.* 104(1):322-39.

Louie S.M., Pettibone J.M. (2016) Research highlights: engineering nanomaterial- based technologies for environmental applications. *Environ Sci: Nano* 3,11

Lu P.J., Cheng W.L., Huang S.C., Chen Y.P., Chou H.K., Cheng H.F. (2015) Characterizing titanium dioxide and zinc oxide nanoparticles in sunscreen spray. *Int J Cosmet Sci*. 37(6):620-6.

Ma Y., Kuang L., He X., Bai W., Ding Y., Zhang Z., Zhao Y., Chai, Z. (2010) Effects of rare earth oxide nanoparticles on root elongation of plants. *Chemosphere*, 78(3), 273-279.

Marmiroli M., Pagano L., Pasquali F., Zappettini A., Tosato V., Bruschi C.V., Marmiroli N. (2016) A genome-wide nanotoxicology screen of Saccharomyces cerevisiae mutants reveals the basis for cadmium sulphide quantum dot tolerance and sensitivity. *Nanotoxicology*. 10(1):84-93.

Marmiroli M., Pagano L., Savo Sardaro M.L., Villani M., Marmiroli N. (2014) Genome-wide approach in Arabidopsis thaliana to assess the toxicity of cadmium sulfide quantum dots. *Environ Sci Technol*. 48(10):5902-9.

Mashock M.J., Kappell A.D., Hallaj N., Hristova K.R. (2016) Copper oxide nanoparticles inhibit the metabolic activity of Saccharomyces cerevisiae. *Environ Toxicol Chem*. 35(1):134-43.

McBride H.M., Neuspiel M., Wasiak S. (2006) Mitochondria: more than just a powerhouse. Curr Biol. 16(14):R551-R560.

Mohiuddin M., & Tung T.T. (2016) Nanomaterials-Embedded Liquid Crystal Elastomers in Electronics Devices Application. In Flexible and Stretchable Electronic Composites (pp. 365-390). Springer International Publishing.

Moon Y.S., Park E.S., Kim T.O., Lee H.S., Lee S.E. (2014) SELDI-TOF MS-based discovery of a biomarker in Cucumis sativus seeds exposed to CuO nanoparticles. *Environ Toxicol Pharmacol*. 38:922-931.

Musante C., White J.C. (2012) Toxicity of silver and copper to Cucurbita pepo: differential effects of nano and bulk- size particles. *Environ toxicol. 27*(9):510-517.

Nguyen K.C., Rippstein P., Tayabali A.F., Willmore W.G. (2015) Mitochondrial toxicity of cadmium telluride quantum dot nanoparticles in mammalian hepatocytes. *Toxicol Sci.* 146(1):31-42.

Norén L., Kindgren P., Stachula P., Rühl M., Eriksson M.E., Hurry V., Strand Å. (2016) Circadian and Plastid Signaling Pathways Are Integrated to Ensure Correct Expression of the CBF and COR Genes during Photoperiodic Growth. *Plant Physiol*. 171(2):1392-406.

Nunnari J., Suomalainen A. (2012) Mitochondria: in sickness and in health. *Cell*. 148(6):1145-59.

Obrero Á., Die J.V., Román B., Gómez P., Nadal S., González-Verdejo C.I. (2011) Selection of reference genes for gene expression studies in zucchini (Cucurbita pepo) using qPCR. *J Agr Food Chem*. 59(10):5402-5411.

Ogur R., St. John R., Nagai S. (1957) Tetrazolium overlay technique for population studies of respiration deficiency in yeast. *Science.* 125(3254), 928-9.

Oh E., Liu R., Nel A., Gemill K.B., Bilal M., Cohen Y., Medintz I.L. (2016) Meta-analysis of cellular toxicity for cadmium-containing quantum dots. *Nat Nanotechnol*. 11(5):479-86.

Otero-González L., García-Saucedo C., Field J.A., Sierra-Álvarez R. (2013) Toxicity of TiO_2, ZrO_2, Fe_0, Fe_2O_3 and Mn_2O_3 nanoparticles to the yeast, Saccharomyces cerevisiae. Chemosphere. 93(6):1201-6.

Paesano L., Perotti A., Buschini A., Carubbi C., Marmiroli M., Maestri E., Iannotta S., Marmiroli N. (2016) Markers for toxicity to HepG2 exposed to cadmium sulphide quantum dots; damage to mitochondria. *Toxicology*. 374:18-28.

Pagano L., Servin A.D., De La Torre-Roche R., Mukherjee A., Majumdar S., Hawthorne J., Marmiroli M., Maestri E., Marra R.E., Isch S.M., Dhankher O.P., White J.C., Marmiroli N. (2016) Molecular Response of Crop Plants to Engineered Nanomaterials. *Environ Sci Technol*. 50(13):7198-207.

Pasquali F., Agrimonti C., Pagano L., Zappettini A., Villani M., Marmiroli M., White J.C., Marmiroli N. (2016) Nucleo-mitochondrial interaction of yeast in response to cadmium sulfide quantum dot exposure.Journal Of Hazardous materials. http://dx.doi.org/10.1016/j.jhazmat.2016.11.053.

Patil N.A., Gade W.N., Deobagkar D.D. (2016) Epigenetic modulation upon exposure of lung fibroblasts to TiO2 and ZnO nanoparticles: alterations in DNA methylation. *Int J Nanomedicine*. 11:4509–4519.

Penttila A., Kalimo H., Trump B.F. (1974) Influence of glutaraldehyde and/or osmium tetroxide on cell volume, ion content, mechanical stability, and membrane permeability of Ehrlich ascites tumor cells. *J Cell Biol*. 63,197-214.

Peters R.J.B., Bouwmeestera H., Gottardo S., Amenta V., Arena M., Brandhoff P., Marvin H.J.P., Mech A., Botelho Moniz F., Quiros Pesudo L., Rauscher H., Schoonjans R., Undas A.K., Vettori M.V., Weigel S., Aschberger K. (2016). Nanomaterials for products and application in agriculture, feed and food. *Trends Food Sci Tech.* 54:155-164.

Rayburn A.L., Kushad M.M., Wannarat W. (2008) Intraspecific genome size variation in pumpkin (Cucurbita pepo subsp. pepo). *Hort Science.* 43(3):949-951.

Reid R.J., Brookes J.D., Tester M.A., Smith F.A. (1996) The mechanism of zinc uptake in plants. *Planta*. 198(1):39-45.

Rizwan M., Ali S., Qayyum M.F., Ok Y.S., Adrees M., Ibrahim M., Zia-ur-Rehmand M., Faride M., Abbas F. (2017) Effect of metal and metal oxide nanoparticles on growth and physiology of globally important food crops: a critical review. *J Hazard Mater.* 322:2-16.

Sabir S., Arshad M., Chaudhari S.K. (2014) Zinc oxide nanoparticles for revolutionizing agriculture: synthesis and applications. *Scientific World J.* doi: http://dx.doi.org/10.1155/2014/925494.

Sathish M., Miyazawa K., Hill J.P., Ariga K. (2009) Solvent engineering for shape-shifter pure fullerene (C60). *J Am Chem Soc*. 131(18):6372-3.

Shaymurat T., Gu J., Xu C., Yang Z., Zhao Q., Liu Y., Liu Y. (2012) Phytotoxic and genotoxic effects of ZnO nanoparticles on garlic (Allium sativum L.):a morphological study. *Nanotoxicology* 6:241-248.

Shaw A.K., Hossain Z. (2013) Impact of nano-CuO stress on rice (Oryza sativa L.) seedlings. *Chemosphere.* 93:906-915.

Singh J., Kaur G., Rawat M. (2016) A Brief Review on Synthesis and Characterization of Copper Oxide Nanoparticles and its Applications. *J Bioelectron Nanotechnol*. 1(1):9.

Silva G.A. (2006) Neuroscience nanotechnology: progress, opportunities and challenges. *Nat Rev Neurosci*. 7:65-74.

Simón-Vázquez R., Lozano-Fernández T., Dávila-Grana A., González-Fernández A. (2016) Analysis of the activation routes induced by different metal oxide nanoparticles on human lung epithelial cells. *Future Sci OA*. 2(2): FSO118. doi: 10.4155/fso.16.2

Stampoulis D., Sinha S.K., & White, J.C. (2009) Assay-dependent phytotoxicity of nanoparticles to plants. *Environ Sci Technol. 43*(24):9473-9479.

Stapleton P.A., Nichols C.E., Yi J., McBride C.R., Minarchick V.C., Shepherd D.L., Hollander J.M., Nurkiewicz T.R. (2015) Microvascular and mitochondrial dysfunction in the female F1 generation after gestational TiO2 nanoparticle exposure. *Nanotoxicology*. 9(8):941-51.

Stone V., Johnston H.J., Balharry D., Gernand J.M., Gulumian M. (2016) Approaches to Develop Alternative Testing Strategies to Inform Human Health Risk Assessment of Nanomaterials. *Risk Anal.* 36(8):1538-50.

Stumpf J.D., Copeland W.C. (2014) MMS Exposure Promotes Increased MtDNA Mutagenesis in the Presence of Replication-Defective Disease-Associated DNA Polymerase γ Variants. *PLoS Genet*. 10(10): e1004748, doi:10.1371/journal.pgen.1004748.

Tang Y., He R., Zhao J., Nie G., Xu L., Xing B. (2016) Oxidative stress-induced toxicity of CuO nanoparticles and related toxicogenomic responses in Arabidopsis thaliana. *Environ Pollut*. 212:605-14.

Tantra R., Oksel C., Puzyn T., Wang J., Robinson K.N., Wang X.Z., Ma C.Y., Wilkins T. (2015) Nano(Q)SAR: Challenges, pitfalls and perspectives. *Nanotoxicology*. 9(5):636-42.

Tripathi D.K., Singh S., Singh S., Pandey R., Singh V.P., Sharma N.C., Prasad S.M., Dubey N.K., Chauhan D.K. (2016) An overview on manufactured nanoparticles in plants: Uptake, translocation, accumulation and phytotoxicity. *Plant Physiol Biochem*. pii: S0981-9428(16)30297-2 doi: 10.1016/j.plaphy.2016.07.030.

Van Houten B., Hunter S.E., Meyer J.N. (2016) Mitochondrial DNA damage induced autophagy, cell death, and disease. *Front Biosci*. 21:42-54.

Van Rossom S., Op de Beeck K., Franssens V., Swinnen E., Schepers A., Ghillebert R., Caldara M., Van Camp G., Winderickx J. (2012) The splicing mutant of the human tumor suppressor protein DFNA5 induces programmed cell death when expressed in the yeast Saccharomyces cerevisiae. *Front Oncol*. 2:77.

Villani M., Calestani D., Lazzarini L., Zanotti L., Mosca R., Zappettini A. (2012) Extended functionality of ZnO nanotetrapods by solution-based coupling with CdS nanoparticles. *J Mater Chem*. 22: 5694-5699.

Wani, I.A., Ahmad, T. (2016). Understanding Toxicity of Nanomaterials in Biological Systems. In Applying Nanotechnology for Environmental Sustainability (pp. 403-427). IGI global.

Wenisch C., Linnau K.F., Parschalk B., Zedtwitz-Liebenstein K., Georgopoulos A. (1997) Rapid susceptibility testing of fungi by flow cytometry using vital staining. *J Clin Microbiol.* 35(1):5-10.

Xia T., Kovochich M., Liong M., Mädler L., Gilbert B., Shi H., Yeh J.I., Zink J.I, Nel A.E. (2008) Comparison of the mechanism of toxicity of zinc oxide and cerium oxide nanoparticles based on dissolution and oxidative stress properties. *ACS nano*. 2(10):2121-2134.

Xing W., Chen Y., Wang X., Lv L., Ouyang X., Ge Z., Huang H. (2016) MoS_2 Quantum Dots with a Tunable Work Function for High-Performance Organic Solar Cells. *ACS Appl Mater Interfaces*. Epub ahead of print. DOI: 10.1021/acsami.6b06081.

Yadav T.P., Yadav R.M., Singh D.P. (2012) Mechanical milling: a top down approach for the synthesis of nanomaterials and nanocomposites. *Nanoscience and Nanotechnology* 2(3):22-48.

Yamasaki H., Abdel-Ghany S.E., Cohu C.M., Kobayashi Y., Shikanai T., Pilon M. (2007) Regulation of copper homeostasis by micro-RNA in Arabidopsis. *J Biol Chem*. 282(22):16369-78.

Yang L.Y., Gao J.L., Gao T., Dong P., Ma L., Jiang F.L., Liu Y. (2016) Toxicity of polyhydroxylated fullerene to mitochondria. *J Hazard Mater*. 301:119-26.

Ye S., Yang P., Cheng K., Zhou T., Wang Y., Hou Z., Jiang Y., Ren L. (2016) Drp1-dependent mitochondrial fission mediates toxicity of positively charged graphene in microglia. *ACS Biomater Sci Eng*. 2(5):722-733.

Zhai T., Fang X., Li L., Bando Y., Golberg D. (2010) One-dimensional CdS nanostructures: synthesis, properties, and applications. *Nanoscale*. 2:168-187.

Zhang R., Zhang H., Tu C., Hu X., Li L., Luo Y., Christie P. (2015) Phytotoxicity of ZnO nanoparticles and the released Zn(II) ion to corn (Zea mays L.) and cucumber (Cucumis sativus L.) during germination. *Environ Sci Pollut Res Int*. 22(14):11109-17.

Zhang T., Hu Y., Tang M., Kong L., Ying J., Wu T., Xue Y., Pu Y. (2015) Liver Toxicity of Cadmium Telluride Quantum Dots (CdTe QDs) Due to Oxidative Stress in Vitro and in Vivo. *Int J Mol Sci*. 16(10):23279-99.

Zhang X., Wang Y., Cheng F., Zheng Z., Du Y. (2016) Ultrathin lanthanide oxides nanomaterials: synthesis, properties and applications. *Sci Bull.* 61(18):1422-1434.

Zhou G.A., Chang R.Z., Qiu L.J. (2010) Overexpression of soybean ubiquitin-conjugating enzyme gene GmUBC2 confers enhanced drought and salt tolerance through modulating abiotic stress-responsive gene expression in Arabidopsis. *Plant Mol Biol*. 72(4-5):357-67.

7. Acknowledgements

I would like to acknowledge Prof. Nelson Marmiroli for giving me the possibility to work on this topic and to develop my research and personal skills. I also thank my tutors, Dr. Marta Marmiroli, Dr. Caterina Agrimonti and Dr. Jason C. White and my collaborators, Dr. Luca Pagano and Dr. Marina Caldara, for their help and suggestions during these three years of PhD.

I would also like to thank the Connecticut Agricultural Experiment Station of New Haven, CT, for giving me the opportunity to spend three months of my PhD in their laboratories and allowing me to gain experience in an international work environment.

I wish to thank also Dr. Andrea Zappettini and Dr. Marco Villani of the IMEM-CNR (Parma, Italy) for providing certified CdS QDs, useful comments and suggestions on the physics of nanomaterials and Fondazione Cariparma for financial support.

Last but not least, I would like to acknowledge my family, friends and colleagues for their kind support along this journey.

8. Appendix

8.1 Genes analyzed in *C. pepo*

ref	GeneID *A. thaliana*	GeneID *C. pepo*	function
005u	At1g09080	CUTC002577	BIP3, Heat shock protein 70 (Hsp 70) family protein
008u	At1g11190	CUTC008849	BFN1, ENDO1, bifunctional nuclease i
013u	At1g23730	CUTC008070	ATBCA3, BCA3, beta carbonic anhydrase 3
026u	At1g61800	CUTC007694	ATGPT2, GPT2, glucose-6-phosphate/phosphate translocator 2
032u	At1g69120	CUTC012366	AGL7, AP1, K-box region and MADS-box transcription factor family protein
046u	At2g21640	CUTC018024	Encodes a protein of unknown function that is a marker for oxidative stress response.
048u	At2g23030	CUTC008834	SNRK2-9, SNRK2.9, SNF1-related protein kinase 2.9
051u	At2g26560	CUTC012732	PLA IIA, PLA2A, PLP2, PLP2, phospholipase A 2A
066u	At3g02310	CUTC014559	AGL4, SEP2, K-box region and MADS-box transcription factor family protein
070u	At3g08860	CUTC004179	PYD4, PYRIMIDINE 4
071u	At3g12520	CUTC007045	SULTR4;2, sulfate transporter 4;2
086u	At3g59845	CUTC001470	Zinc-binding dehydrogenase family protein
090u	At4g04460	CUTC002381	Saposin-like aspartyl protease family protein
093u	At4g12280	CUTC008356	copper amine oxidase family protein
098u	At4g16370	CUTC009101	ATOPT3, OPT3, OPT3, oligopeptide transporter
099u	At4g21680	CUTC041648	NRT1.8, NITRATE TRANSPORTER 1.8
119u	At5g20240	CUTC042444	PI, K-box region and MADS-box transcription factor family protein
124u	At5g24470	CUTC023690	APRR5, PRR5, pseudo-response regulator 5
127u	At5g26220	CUTC045405	ChaC-like family protein
128u	At5g26340	CUTC013905	ATSTP13, MSS1, STP13, Major facilitator superfamily protein
139u	At5g48850	CUTC039723	ATSDI1, Tetratricopeptide repeat (TPR)-like superfamily protein
140u	At5g50260	CUTC003431	Cysteine proteinases superfamily protein
143u	At5g54960	CUTC034909	PDC2, pyruvate decarboxylase-2
147u	At5g61380	CUTC019875	APRR1, AtTOC1, PRR1, TOC1, CCT motif -containing response regulator protein
150u	AtCg00065	CUTC021188	RPS12, RPS12A, ribosomal protein S12A
151u	AtCg00360	CUTC004189	YCF3, Tetratricopeptide repeat (TPR)-like superfamily protein
152u	AtCg00590	CUTC036811	ORF31, electron carriers

155u	AtCg00700	CUTC045946	PSBN, photosystem II reaction center protein N

ref	GeneID *A. thaliana*	GeneID *C. pepo*	function
001d	At1g01060	CUTC042801	LHY, LHY1, Homeodomain-like superfamily protein
002d	At1g08830	CUTC000155	CSD1, copper/zinc superoxide dismutase 1
004d	At1g12520	CUTC013469	ATCCS, CCS, copper chaperone for SOD1
008d	At1g29660	CUTC012295	GDSL-like Lipase/Acylhydrolase superfamily protein
016d	At2g11810	CUTC015342	ATMGD3, MGD3, MGDC, monogalactosyldiacylglycerol synthase type C
018d	At2g28190	CUTC015722	CSD2, CZSOD2, copper/zinc superoxide dismutase 2
036d	At5g01600	CUTC001028	ATFER1, FER1, ferretin 1
037d	At5g02540	CUTC012876	NAD(P)-binding Rossmann-fold superfamily protein
043d	At5g43350	CUTC049068	ATPT1, PHT1;1, phosphate transporter 1;1
045d	At5g43780	CUTC008032	APS4, Pseudouridine synthase/archaeosine transglycosylase-like family protein

8.2 Microarray data

Genes up-regulated in response to 0.3 μM nystatin + 100 mg L^{-1} CdS QDs

Gene	Nyst+NPs	Description
LSO1	5,6713815	Protein with a potential role in response to iron deprivation; transcription increases during iron deprivation and during treatment with 2-(6-benzyl-2-pyridyl)quinazoline (BPQ) and copper; regulated by Aft1p and, to a lesser extent, by Aft2p; originally identified as a syntenic homolog of an Ashbya gossypii gene; localizes to nucleus and cytoplasm, and nuclear localization is enhanced under iron-replete conditions
YLR042C	4,690978	Cell wall protein of unknown function; localizes to the cytoplasm; deletion improves xylose fermentation in industrially engineered strains; YLR042C is not an essential gene
FRE5	4,0867695	Putative ferric reductase with similarity to Fre2p; expression induced by low iron levels; the authentic, non-tagged protein is detected in highly purified mitochondria in high-throughput studies
FIT2	3,9964895	Mannoprotein that is incorporated into the cell wall; incorporated via a glycosylphosphatidylinositol (GPI) anchor; involved in the retention of siderophore-iron in the cell wall
MF(ALPHA)2	3,325483	Mating pheromone alpha-factor, made by alpha cells; interacts with mating type a cells to induce cell cycle arrest and other responses leading to mating; also encoded by MF(ALPHA)1, which is more highly expressed; binds copper(II) ions
HBN1	3,320165	Protein of unknown function; similar to bacterial nitroreductases; green fluorescent protein (GFP)-fusion protein localizes to the cytoplasm and nucleus; protein becomes insoluble upon intracellular iron depletion; protein abundance increases in response to DNA replication stress
SUL2	3,263936	High affinity sulfate permease; sulfate uptake is mediated by specific sulfate transporters Sul1p and Sul2p, which control the concentration of endogenous activated sulfate intermediates
YLR012C	3,197707	Putative protein of unknown function; YLR012C is not an essential gene
YPR078C	3,180526	Putative protein of unknown function; possible role in DNA metabolism and/or in genome stability; expression is heat-inducible
PGU1	2,92913	Endo-polygalacturonase; pectolytic enzyme that hydrolyzes the alpha-1,4-glycosidic bonds in the rhamnogalacturonan chains in pectins
FET3	2,8685675	Ferro-O2-oxidoreductase; multicopper oxidase that oxidizes ferrous (Fe2+) to ferric iron (Fe3+) for subsequent cellular uptake by transmembrane permease Ftr1p; required for high-affinity iron uptake and involved in mediating resistance to copper ion toxicity, belongs to class of integral membrane multicopper oxidases; protein abundance increases in response to DNA replication stress
SRD1	2,8172025	Protein involved in the processing of pre-rRNA to mature rRNA; contains a C2/C2 zinc finger motif; srd1 mutation suppresses defects caused by the rrp1-1 mutation
FIT3	2,808425	Mannoprotein that is incorporated into the cell wall; incorporated via a glycosylphosphatidylinositol (GPI) anchor; involved in the retention of siderophore-iron in the cell wall
TIS11	2,7648905	mRNA-binding protein expressed during iron starvation; binds to a sequence element in the 3'-untranslated regions of specific mRNAs to mediate their degradation; involved in iron homeostasis; protein increases in abundance and relative distribution to the nucleus increases upon DNA replication stress; TIS11 has a paralog, CTH1, that arose from the whole genome duplication
SUC2	2,7374205	Invertase; sucrose hydrolyzing enzyme; a secreted, glycosylated form is regulated by glucose repression, and an intracellular, nonglycosylated enzyme is produced constitutively
UBC12	2,7324305	Enzyme that mediates the conjugation of Rub1p; a ubiquitin-like protein, to other proteins; related to E2 ubiquitin-conjugating enzymes

GIC2	2,721697	Redundant rho-like GTPase Cdc42p effector; involved in initiation of budding and cellular polarization; interacts with Cdc42p via the Cdc42/Rac-interactive binding (CRIB) domain and with PI(4,5)P2 via a polybasic region; GIC2 has a paralog, GIC1, that arose from the whole genome duplication
AMF1	2,6789625	Low affinity NH4+ transporter; member of the DHA2 family of drug:H+ anti porters; putative paralog of ATR1; but not required for boron tolerance; non-essential gene
ARN2	2,6742785	Transporter; member of the ARN family of transporters that specifically recognize siderophore-iron chelates; responsible for uptake of iron bound to the siderophore triacetylfusarinine C
SIT1	2,594683	Ferrioxamine B transporter; member of the ARN family of transporters that specifically recognize siderophore-iron chelates; transcription is induced during iron deprivation and diauxic shift; potentially phosphorylated by Cdc28p
OYE3	2,5360225	Conserved NADPH oxidoreductase containing flavin mononucleotide (FMN); homologous to Oye2p with different ligand binding and catalytic properties; has potential roles in oxidative stress response and programmed cell death
SVS1	2,5203655	Cell wall and vacuolar protein; required for wild-type resistance to vanadate; SVS1 has a paralog, SRL1, that arose from the whole genome duplication
FRM2	2,483154	Type II nitroreductase, using NADH as reductant; mutants are defective in fatty acid mediated repression of genes involved in fatty acid biosynthesis indicative of a role in lipid signaling; involved in the oxidative stress response; transcription induction by cadmium and selenite indicates a possible role in the metal stress response; expression induced in cells treated with the mycotoxin patulin
YAR068W	2,474727	Fungal-specific protein of unknown function; induced in respiratory-deficient cells; YAR068W has a paralog, YHR214W-A, that arose from a segmental duplication
GTO3	2,4646575	Omega class glutathione transferase; putative cytosolic localization
TIR1	2,447755	Cell wall mannoprotein; expression is downregulated at acidic pH and induced by cold shock and anaerobiosis; abundance is increased in cells cultured without shaking; member of the Srp1p/Tip1p family of serine-alanine-rich proteins
SAM1	2,417195	S-adenosylmethionine synthetase; catalyzes transfer of the adenosyl group of ATP to the sulfur atom of methionine; SAM1 has a paralog, SAM2, that arose from the whole genome duplication
SAG1	2,3276265	Alpha-agglutinin of alpha-cells; binds to Aga1p during agglutination, N-terminal half is homologous to the immunoglobulin superfamily and contains binding site for a-agglutinin, C-terminal half is highly glycosylated and contains GPI anchor
YCL049C	2,2765785	Protein of unknown function; localizes to membrane fraction; YCL049C is not an essential gene
PRM5	2,269358	Pheromone-regulated protein, predicted to have 1 transmembrane segment; induced during cell integrity signaling; PRM5 has a paralog, YNL058C, that arose from the whole genome duplication
MET32	2,2596655	Zinc-finger DNA-binding transcription factor; involved in transcriptional regulation of the methionine biosynthetic genes; targets strong transcriptional activator Met4p to promoters of sulfur metabolic genes; feedforward loop exists in the regulation of genes controlled by Met4p and Met32p; lack of such a loop for MET31 may account for the differential actions of Met32p and Met31p; MET32 has a paralog, MET31, that arose from the whole genome duplication
CSI2	2,2071155	Protein of unknown function; green fluorescent protein (GFP)- fusion protein localizes to the mother side of the bud neck and the vacuole; YOL007C is not an essential gene
ENB1	2,191336	Endosomal ferric enterobactin transporter; expressed under conditions of iron deprivation; member of the major facilitator superfamily; expression is regulated by Rcs1p and affected by chloroquine treatment
KDX1	2,190174	Protein kinase; implicated in Slt2p mitogen-activated (MAP) kinase signaling pathway; interacts with numerous components in the mating pheromone and CWI MAPK pathways; associates with Rlm1p; KDX1 has a paralog, SLT2, that arose from the whole genome duplication

YIL080W	2,1317405	n/a
NDJ1	2,1175175	Protein that regulates meiotic SPB cohesion and telomere clustering; localizes to both spindle pole bodies (SPBs) and telomeres; required for bouquet formation, effective homolog pairing, ordered cross-over distribution, sister chromatid cohesion at meiotic telomeres, chromosomal segregation and telomere-led rapid prophase movement
ARN1	2,101529	ARN family transporter for siderophore-iron chelates; responsible for uptake of iron bound to ferrirubin, ferrirhodin, and related siderophores; protein increases in abundance and relocalizes to the vacuole upon DNA replication stress
RPS22A	2,0804175	Protein component of the small (40S) ribosomal subunit; homologous to mammalian ribosomal protein S15A and bacterial S8; RPS22A has a paralog, RPS22B, that arose from the whole genome duplication
CYS3	2,0776965	Cystathionine gamma-lyase; catalyzes one of the two reactions involved in the transsulfuration pathway that yields cysteine from homocysteine with the intermediary formation of cystathionine; protein abundance increases in response to DNA replication stress
FUS1	2,019903	Membrane protein localized to the shmoo tip; required for cell fusion; expression regulated by mating pheromone; proposed to coordinate signaling, fusion, and polarization events required for fusion; potential Cdc28p substrate
MET17	2,0023105	O-acetyl homoserine-O-acetyl serine sulfhydrylase; required for Methionine and cysteine biosynthesis
MSB2	1,9911225	Mucin family member involved in various signaling pathways; functions as osmosensor in the Sho1p-mediated HOG pathway; functions in Cdc42p- and MAP kinase-dependent filamentous growth signaling pathway; processed into secreted and cell-associated forms by aspartyl protease Yps1p; potential Cdc28p substrate
MF(ALPHA)1	1,98062	Mating pheromone alpha-factor, made by alpha cells; interacts with mating type a cells to induce cell cycle arrest and other responses leading to mating; also encoded by MF(ALPHA)2, although MF(ALPHA)1 produces most alpha-factor; binds copper(II) ions
CCC2	1,919217	Cu(+2)-transporting P-type ATPase; required for export of copper from the cytosol into an extracytosolic compartment; similar to human proteins involved in Menkes and Wilsons diseases; protein abundance increases in response to DNA replication stress; affects TBSV model (+)RNA virus replication by regulating copper metabolism; human homologs ATP7A and ATP7B both complement yeast null mutant
RPL33B	1,906153	Ribosomal 60S subunit protein L33B; rpl33b null mutant exhibits normal growth while rpl33a rpl33b double null mutant is inviable; homologous to mammalian ribosomal protein L35A, no bacterial homolog; RPL33B has a paralog, RPL33A, that arose from the whole genome duplication
RPS22B	1,902249	Protein component of the small (40S) ribosomal subunit; homologous to mammalian ribosomal protein S15A and bacterial S8; RPS22B has a paralog, RPS22A, that arose from the whole genome duplication
YCL021W-A	1,8954995	Putative protein of unknown function; SWAT-GFP and mCherry fusion proteins localize to the vacuole
MAN2	1,8897575	Mannitol dehydrogenase; MAN2 has a paralog, DSF1, that arose from a segmental duplication
VMR1	1,8859685	Vacuolar membrane protein; involved in multiple drug resistance and metal sensitivity; ATP-binding cassette (ABC) family member involved in drug transport; potential Cdc28p substrate; induced under respiratory conditions; VMR1 has a paralog, YBT1, that arose from the whole genome duplication
AXL2	1,874811	Integral plasma membrane protein; required for axial budding in haploid cells; localizes to the incipient bud site and bud neck; glycosylated by Pmt4p; potential Cdc28p substrate
RPS9A	1,874456	Protein component of the small (40S) ribosomal subunit; homologous to mammalian ribosomal protein S9 and bacterial S4; RPS9A has a paralog, RPS9B, that arose from the whole genome duplication
SPT14	1,8554395	UDP-glycosyltransferase subunit of the GPI-GnT complex; UDP-GlcNAc-binding and catalytic subunit of the enzyme that mediates the first step in glycosylphosphatidylinositol (GPI) biosynthesis, mutations

		cause defects in transcription and in biogenesis of cell wall proteins
PCL1	1,855243	Cyclin, interacts with cyclin-dependent kinase Pho85p; member of the Pcl1,2-like subfamily, involved in the regulation of polarized growth and morphogenesis and progression through the cell cycle; is ubiquitinated by Dma1p; phosphorylation by Pho85p targets it for degradation; localizes to sites of polarized cell growth
DDI3	1,853148	Cyanamide hydratase that detoxifies cyanamide; member of the HD domain metalloprotein superfamily; expression is induced over 100-fold by cyanamide and by SN2-type DNA alkylating agents such as MMS and DMA; induction decreased in rad6 and rad18 mutants; gene and protein are identical to DDI2 and Ddi2p
OST5	1,8451995	Zeta subunit of the oligosaccharyltransferase complex of the ER lumen; complex catalyzes asparagine-linked glycosylation of newly synthesized proteins
PRY2	1,8260095	Sterol binding protein involved in the export of acetylated sterols; secreted glycoprotein and member of the CAP protein superfamily (cysteine-rich secretory proteins (CRISP), antigen 5, and pathogenesis related 1 proteins); sterol export function is redundant with that of PRY1; may be involved in detoxification of hydrophobic compounds; PRY2 has a paralog, PRY1, that arose from the whole genome duplication
RPL22B	1,8186325	Ribosomal 60S subunit protein L22B; homologous to mammalian ribosomal protein L22, no bacterial homolog; RPL22B has a paralog, RPL22A, that arose from the whole genome duplication
QDR2	1,805148	Plasma membrane transporter of the major facilitator superfamily; member of the 12-spanner drug:H(+) antiporter DHA1 family; exports copper; has broad substrate specificity and can transport many mono- and divalent cations; transports a variety of drugs and is required for resistance to quinidine, barban, cisplatin, and bleomycin; contributes to potassium homeostasis; expression is regulated by copper
HMX1	1,753154	ER localized heme oxygenase; involved in heme degradation during iron starvation and in the oxidative stress response; expression is regulated by AFT1 and oxidative stress; relocates to the perinuclear region in the presence of oxidants
ISU2	1,7467235	Mitochondrial protein required for iron-sulfur protein synthesis; performs scaffolding function during Fe/S cluster assembly; involved in Fe-S cluster assembly for both mitochondrial and cytosolic proteins; protein abundance increases under DNA replication stress; ISU2 has a paralog, ISU1, that arose from the whole genome duplication; isu1 isu2 double mutant is inviable; human homolog ISCU implicated in mitochondrial myopathy, can complement isu1 isu2 double mutant
YLR342W-A	1,73737	Putative protein of unknown function
YOL131W	1,727078	Putative protein of unknown function; YOL131W has a paralog, STB1, that arose from the whole genome duplication
TDA5	1,726611	Putative protein of unknown function; detected in highly purified mitochondria in high-throughput studies; proposed to be involved in resistance to mechlorethamine and streptozotocin; null mutant sensitive to expression of top1-T722A allele
SRL3	1,717006	GTB motif (G1/S transcription factor binding) containing protein; binds SBF-regulated promoters in hydroxyurea-treated cells; when overexpressed, suppresses the lethality of a rad53 null mutation; potential Cdc28p substrate; SRL3 has a paralog, WHI5, that arose from the whole genome duplication
FTR1	1,7161745	High affinity iron permease; involved in the transport of iron across the plasma membrane; forms complex with Fet3p; expression is regulated by iron; protein abundance increases in response to DNA replication stress
UTR2	1,7125045	Chitin transglycosylase; functions in the transfer of chitin to beta(1-6) and beta(1-3) glucans in the cell wall; similar to and functionally redundant with Crh1; glycosylphosphatidylinositol (GPI)-anchored protein localized to bud neck

GPX2	1,703527	Phospholipid hydroperoxide glutathione peroxidase; protects cells from phospholipid hydroperoxides and nonphospholipid peroxides during oxidative stress; induced by glucose starvation; protein abundance increases in response to DNA replication stress
ERG4	1,7026595	C-24(28) sterol reductase; catalyzes the final step in ergosterol biosynthesis; mutants are viable, but lack ergosterol
PFK27	1,7000235	6-phosphofructo-2-kinase; catalyzes synthesis of fructose-2,6-bisphosphate; inhibited by phosphoenolpyruvate and sn-glycerol 3-phosphate, expression induced by glucose and sucrose, transcriptional regulation involves protein kinase A
YGR035C	1,693885	Putative protein of unknown function, potential Cdc28p substrate; transcription is activated by paralogous transcription factors Yrm1p and Yrr1p along with genes involved in multidrug resistance; YGR035C has a paralog, YLR346C, that arose from the whole genome duplication
TUB3	1,661504	Alpha-tubulin; associates with beta-tubulin (Tub2p) to form tubulin dimer, which polymerizes to form microtubules; expressed at lower level than Tub1p; TUB3 has a paralog, TUB1, that arose from the whole genome duplication
YNL033W	1,6519085	Putative protein of unknown function; YNL033W has a paralog, YNL019C, that arose from a segmental duplication
TPO2	1,6518015	Polyamine transporter of the major facilitator superfamily; member of the 12-spanner drug:H(+) antiporter DHA1 family; specific for spermine; localizes to the plasma membrane; transcription of TPO2 is regulated by Haa1p; TPO2 has a paralog, TPO3, that arose from the whole genome duplication
CHS7	1,6272125	Protein of unknown function; may be involved in chitin biosynthesis by regulation of Chs3p export from the ER; relocalizes from bud neck to ER upon DNA replication stress
YHR214W	1,6211925	Putative protein of unknown function; predicted to be a glycosylphosphatidylinositol-modified (GPI) protein; YHR214W has a paralog, YAR066W, that arose from a segmental duplication
DRE2	1,620317	Component of the cytosolic Fe-S protein assembly (CIA) machinery; contains an Fe-S cluster that receives electrons from NADPH via the action of Tah18p in an early step in the CIA pathway; ortholog of human Ciapin1; protein abundance increases in response to DNA replication stress; inviability of the null mutant is functionally complemented by human CIAPIN1
PCL2	1,615527	Cyclin, interacts with cyclin-dependent kinase Pho85p; member of the Pcl1,2-like subfamily, involved in the regulation of polarized growth and morphogenesis and progression through the cell cycle; localizes to sites of polarized cell growth; PCL2 has a paralog, PCL9, that arose from the whole genome duplication
DSF2	1,6116215	Deletion suppressor of mpt5 mutation; relocalizes from bud neck to cytoplasm upon DNA replication stress
DOG2	1,6099945	2-deoxyglucose-6-phosphate phosphatase; member of a family of low molecular weight phosphatases, induced by oxidative and osmotic stress, confers 2-deoxyglucose resistance when overexpressed; DOG2 has a paralog, DOG1, that arose from a single-locus duplication; the last half of DOG1 and DOG2 are subject to gene conversions among S. cerevisiae, S. paradoxus, and S. mikatae
RPL14A	1,6095225	Ribosomal 60S subunit protein L14A; N-terminally acetylated; homologous to mammalian ribosomal protein L14, no bacterial homolog; RPL14A has a paralog, RPL14B, that arose from the whole genome duplication
RBS1	1,60943	Protein involved in assembly of the RNA polymerase III (Pol III) complex; high copy suppressor of Pol III assembly mutation and psk1 psk2 mutations that confer temperature-sensitivity for galactose utilization; physically interacts with Pol III; proposed to bind single-stranded nucleic acids via its R3H domain
PHO92	1,6066435	Posttranscriptional regulator of phosphate metabolism; facilitates PHO4 mRNA degradation by interacting with Pop2p; regulates PHO4 mRNA stability by binding to PHO4's 3'UTR in a phosphate-

		dependent manner; contains highly conserved YTH (YT521-B Homology) domain that exhibits RNA-binding activity; human homolog YTHDF2 can complement yeast null mutant
RPL18B	1,601797	Ribosomal 60S subunit protein L18B; homologous to mammalian ribosomal protein L18, no bacterial homolog; RPL18B has a paralog, RPL18A, that arose from the whole genome duplication
YKE4	1,597243	Zinc transporter; localizes to the ER; null mutant is sensitive to calcofluor white, leads to zinc accumulation in cytosol; ortholog of the mouse KE4 and member of the ZIP (ZRT, IRT-like Protein) family
RAX2	1,5924205	N-glycosylated protein; involved in the maintenance of bud site selection during bipolar budding; localization requires Rax1p; RAX2 mRNA stability is regulated by Mpt5p
HTA2	1,5847825	Histone H2A; core histone protein required for chromatin assembly and chromosome function; one of two nearly identical (see also HTA1) subtypes; DNA damage-dependent phosphorylation by Mec1p facilitates DNA repair; acetylated by Nat4p
MAL12	1,5516365	Maltase (alpha-D-glucosidase); inducible protein involved in maltose catabolism; encoded in the MAL1 complex locus; hydrolyzes the disaccharides maltose, turanose, maltotriose, and sucrose
CRG1	1,544924	S-AdoMet-dependent methyltransferase involved in lipid homeostasis; mediates resistance to a drug cantharidin
GIN4	1,534187	Protein kinase involved in bud growth and assembly of the septin ring; proposed to have kinase-dependent and kinase-independent activities; undergoes autophosphorylation; similar to Hsl1p; GIN4 has a paralog, KCC4, that arose from the whole genome duplication
FKS1	1,524676	Catalytic subunit of 1,3-beta-D-glucan synthase; functionally redundant with alternate catalytic subunit Gsc2p; binds to regulatory subunit Rho1p; involved in cell wall synthesis and maintenance; localizes to sites of cell wall remodeling; FKS1 has a paralog, GSC2, that arose from the whole genome duplication
RSR1	1,513076	GTP-binding protein of the Ras superfamily; required for bud site selection, morphological changes in response to mating pheromone, and efficient cell fusion; localized to the plasma membrane; significantly similar to mammalian Rap GTPases
TOS2	1,51046	Protein involved in localization of Cdc24p to the site of bud growth; may act as a membrane anchor; localizes to the bud neck and bud tip; potentially phosphorylated by Cdc28p; TOS2 has a paralog, SKG6, that arose from the whole genome duplication
GFA1	1,5043065	Glutamine-fructose-6-phosphate amidotransferase; catalyzes the formation of glucosamine-6-P and glutamate from fructose-6-P and glutamine in the first step of chitin biosynthesis; GFA1 has a paralogous region, comprising ORFs YMR084W-YMR085W, that arose from the whole genome duplication
FCY22	1,5032625	Putative purine-cytosine permease; very similar to Fcy2p but cannot substitute for its function
SLI15	1,49569	Subunit of the conserved chromosomal passenger complex (CPC); complex regulates kinetochore-microtubule attachments, activation of the spindle tension checkpoint, and mitotic spindle disassembly; other complex members are Ipl1p, Bir1p, and Nbl1p
YGL015C	1,4793585	Putative protein of unknown function; null mutants accumulate cargo in the Golgi
TRS65	1,477157	Component of transport protein particle (TRAPP) complex II; TRAPPII is a multimeric guanine nucleotide-exchange factor for the GTPase Ypt1p, regulating intra-Golgi and endosome-Golgi traffic; role in cell wall beta-glucan biosynthesis and the stress response
YHP1	1,4731845	Homeobox transcriptional repressor; binds Mcm1p and early cell cycle box (ECB) elements of cell cycle regulated genes, thereby restricting ECB-mediated transcription to the M/G1 interval; YHP1 has a paralog, YOX1, that arose from the whole genome duplication
RPS28B	1,461595	Protein component of the small (40S) ribosomal subunit; homologous to mammalian ribosomal protein S28, no bacterial homolog; has an extraribosomal function in autoregulation, in which Rps28Bp binds to a decapping complex via Edc3p, which then binds to RPS28B mRNA leading to its decapping and

		degradation; RPS28B has a paralog, RPS28A, that arose from the whole genome duplication
PDR16	1,4594295	Phosphatidylinositol transfer protein (PITP); controlled by the multiple drug resistance regulator Pdr1p; localizes to lipid particles and microsomes; controls levels of various lipids, may regulate lipid synthesis; homologous to Pdr17p; protein abundance increases in response to DNA replication stress
HOT13	1,457111	Zinc-binding mitochondrial intermembrane space (IMS) protein; involved in a disulfide relay system for IMS import of cysteine-containing proteins; binds Mia40p and stimulates its Erv1p-dependent oxidation, probably by sequestering zinc
MTM1	1,452403	Mitochondrial protein of the mitochondrial carrier family; high affinity pyridoxal 5'-phosphate (PLP) transporter, important for delivery of PLP cofactor to mitochondrial enzymes; involved in mitochondrial iron homeostasis and in activating mitochondrial Sod2p by facilitating insertion of an essential manganese cofactor
LDS2	1,45132	Protein Involved in spore wall assembly; localizes to lipid droplets found on or outside of the prospore membrane; shares similarity with Lds1p and Rrt8p, and a strain mutant for all 3 genes exhibits reduced dityrosine fluorescence relative to the single mutants; green fluorescent protein (GFP)-fusion protein localizes to the cytoplasm in a punctate pattern
YLR264C-A	1,4372255	Putative protein of unknown function
TRA1	1,4339855	Subunit of SAGA and NuA4 histone acetyltransferase complexes; interacts with acidic activators (e.g., Gal4p) which leads to transcription activation; similar to human TRRAP, which is a cofactor for c-Myc mediated oncogenic transformation
GTT2	1,4169255	Glutathione S-transferase capable of homodimerization; functional overlap with Gtt2p, Grx1p, and Grx2p; protein abundance increases in response to DNA replication stress
HSL1	1,4165625	Nim1p-related protein kinase; septin-binding kinase that localizes to the bud neck septin ring and regulates the morphogenesis checkpoint; phosphorylates Hsl7p and cooperates with Elm1p to recruit Hsl7p to the mother-bud neck, as a prerequisite for the subsequent recruitment, phosphorylation, and degradation of Swe1p; autophosphorylation enhances interactions with Hsl7p
YKL133C	1,41214	Putative protein of unknown function; not required for growth of cells lacking the mitochondrial genome; SWAT-GFP and mCherry fusion proteins localize to the mitochondria; YKL133C has a paralog, MGR3, that arose from the whole genome duplication
TOS4	1,409556	Putative transcription factor, contains Forkhead Associated domain; binds chromatin; involved in expression homeostasis, buffering of mRNA synthesis rate against gene dosage changes during S phase; target of SBF transcription factor; expression is periodic and peaks in G1; involved in DNA replication checkpoint response; interacts with Rpd3 and Set3 histone deacetylase complexes; APCC(Cdh1) substrate; relative distribution to nucleus increases upon DNA replication stress
PIC2	1,403545	Mitochondrial copper and phosphate carrier; imports copper and inorganic phosphate into mitochondria; functionally redundant with Mir1p but less abundant than Mir1p under normal conditions; expression is induced at high temperature
FET4	1,40331	Low-affinity Fe(II) transporter of the plasma membrane
INA1	1,40319	Protein of unknown function; not an essential gene; YLR413W has a paralog, FAT3, that arose from the whole genome duplication
RPS11A	1,3987555	Protein component of the small (40S) ribosomal subunit; homologous to mammalian ribosomal protein S11 and bacterial S17; N-terminally propionylated in vivo; RPS11A has a paralog, RPS11B, that arose from the whole genome duplication
YOX1	1,3983565	Homeobox transcriptional repressor; binds to Mcm1p and to early cell cycle boxes (ECBs) in the promoters of cell cycle-regulated genes expressed in M/G1 phase; expression is cell cycle-regulated;

		phosphorylated by Cdc28p; relocalizes from nucleus to cytoplasm upon DNA replication stress; YOX1 has a paralog, YHP1, that arose from the whole genome duplication
EXG2	1,3954575	Exo-1,3-beta-glucanase; involved in cell wall beta-glucan assembly; may be anchored to the plasma membrane via a glycosylphosphatidylinositol (GPI) anchor
KCH1	1,39455	Potassium transporter that mediates K+ influx; activates high-affinity Ca2+ influx system (HACS) during mating pheromone response; expression up-regulated in response to alpha factor; localized to sites of polarized growth; member of a fungal-specific gene family; potential Cdc28p substrate; KCH1 has a paralog, PRM6, that arose from the whole genome duplication
IRC4	1,3933145	Protein of unknown function; null mutant displays increased levels of spontaneous Rad52p foci; green fluorescent protein (GFP)-fusion protein localizes to the cytoplasm and nucleus
SSK22	1,391874	MAP kinase kinase kinase of HOG1 mitogen-activated signaling pathway; functionally redundant with Ssk2p; interacts with and is activated by Ssk1p; phosphorylates Pbs2p; SSK22 has a paralog, SSK2, that arose from the whole genome duplication
POP5	1,390654	Subunit of both RNase MRP and nuclear RNase P; RNase MRP cleaves pre-rRNA, while nuclear RNase P cleaves tRNA precursors to generate mature 5' ends and facilitates turnover of nuclear RNAs
YGR153W	1,387632	Putative protein of unknown function
OPT1	1,383463	Proton-coupled oligopeptide transporter of the plasma membrane; also transports glutathione and phytochelatin; member of the OPT family
RPL37A	1,358075	Ribosomal 60S subunit protein L37A; required for processing of 27SB pre-rRNA and formation of stable 66S assembly intermediates; homologous to mammalian ribosomal protein L37, no bacterial homolog; RPL37A has a paralog, RPL37B, that arose from the whole genome duplication
MID2	1,353378	O-glycosylated plasma membrane protein; acts as a sensor for cell wall integrity signaling and activates the pathway; interacts with Rom2p, a guanine nucleotide exchange factor for Rho1p, and with cell integrity pathway protein Zeo1p; MID2 has a paralog, MTL1, that arose from the whole genome duplication
YPL088W	1,3411475	Putative aryl alcohol dehydrogenase; transcription is activated by paralogous transcription factors Yrm1p and Yrr1p along with genes involved in multidrug resistance
YOL013W-A	1,339072	Putative protein of unknown function; identified by SAGE
YPS6	1,329977	Putative GPI-anchored aspartic protease; member of the yapsin family of proteases involved in cell wall growth and maintenance
YOL155W-A	1,327454	Putative protein of unknown function; identified by expression profiling and mass spectrometry
SPO16	1,3264265	Meiosis-specific protein involved in synaptonemal complex assembly; implicated in regulation of crossover formation; required for sporulation
YPL068C	1,3130155	Protein of unknown function; green fluorescent protein (GFP)-fusion protein localizes to the nucleus and is induced in response to the DNA-damaging agent MMS
RPL27B	1,3129385	Ribosomal 60S subunit protein L27B; homologous to mammalian ribosomal protein L27, no bacterial homolog; RPL27B has a paralog, RPL27A, that arose from the whole genome duplication
RPS26B	1,312343	Protein component of the small (40S) ribosomal subunit; homologous to mammalian ribosomal protein S26, no bacterial homolog; RPS26B has a paralog, RPS26A, that arose from the whole genome duplication; human homolog can partially complement an RPS26A, RPS26B double null mutant; mutations in the human gene are associated with Diamond-Blackfan anemia
RPL26B	1,311724	Ribosomal 60S subunit protein L26B; binds to 5.8S rRNA; non-essential even when paralog is also deleted; deletion has minimal affections on ribosome biosynthesis; homologous to mammalian ribosomal protein L26 and bacterial L24; RPL26B has a paralog, RPL26A, that arose from the whole genome

		duplication
YKL068W-A	1,310141	Putative protein of unknown function; identified by homology to Ashbya gossypii
GND1	1,297351	6-phosphogluconate dehydrogenase (decarboxylating); catalyzes an NADPH regenerating reaction in the pentose phosphate pathway; required for growth on D-glucono-delta-lactone and adaptation to oxidative stress; GND1 has a paralog, GND2, that arose from the whole genome duplication
TPO1	1,2968215	Polyamine transporter of the major facilitator superfamily; member of the 12-spanner drug:H(+) antiporter DHA1 family; recognizes spermine, putrescine, and spermidine; catalyzes uptake of polyamines at alkaline pH and excretion at acidic pH; during oxidative stress exports spermine, spermidine from the cell, which controls timing of expression of stress-responsive genes; phosphorylation enhances activity and sorting to the plasma membrane
YDL241W	1,2948515	Putative protein of unknown function; SWAT-GFP and mCherry fusion proteins localize to the endoplasmic reticulum; YDL241W is not an essential gene
AIM32	1,2933925	Protein of unknown function; null mutant is viable and displays elevated frequency of mitochondrial genome loss
FCY21	1,29093	Putative purine-cytosine permease; very similar to Fcy2p but cannot substitute for its function
PER33	1,290761	Protein that localizes to the endoplasmic reticulum; also associates with the nuclear pore complex; deletion extends chronological lifespan; highly conserved across species, orthologous to human TMEM33 and paralogous to Pom33p; protein abundance increases in response to DNA replication stress
HSP31	1,289241	Methylglyoxalase that converts methylglyoxal to D-lactate; involved in oxidative stress resistance, diauxic shift, and stationary phase survival; has similarity to E. coli Hsp31 and C. albicans Glx3p; member of the DJ-1/ThiJ/PfpI superfamily, which includes human DJ-1 involved in Parkinson's disease and cancer; exists as a dimer and contains a putative metal-binding site; protein abundance increases in response to DNA replication stress
CAR1	1,2889435	Arginase, catabolizes arginine to ornithine and urea; expression responds to both induction by arginine and nitrogen catabolite repression; disruption decreases production of carcinogen ethyl carbamate during wine fermentation and also enhances freeze tolerance
HSP30	1,28796	Negative regulator of the H(+)-ATPase Pma1p; stress-responsive protein; hydrophobic plasma membrane localized; induced by heat shock, ethanol treatment, weak organic acid, glucose limitation, and entry into stationary phase
CLN2	1,28763	G1 cyclin involved in regulation of the cell cycle; activates Cdc28p kinase to promote the G1 to S phase transition; late G1 specific expression depends on transcription factor complexes, MBF (Swi6p-Mbp1p) and SBF (Swi6p-Swi4p); CLN2 has a paralog, CLN1, that arose from the whole genome duplication; cell cycle arrest phenotype of the cln1 cln2 cln3 triple null mutant is complemented by any of human cyclins CCNA2, CCNB1, CCNC, CCND1, or CCNE1
RPL11A	1,286645	Ribosomal 60S subunit protein L11A; expressed at twice the level of Rpl11Bp; involved in ribosomal assembly; depletion causes degradation of 60S proteins and RNA; homologous to mammalian ribosomal protein L11 and bacterial L5; RPL11A has a paralog, RPL11B, that arose from the whole genome duplication
RPL9B	1,2843475	Ribosomal 60S subunit protein L9B; homologous to mammalian ribosomal protein L9 and bacterial L6; RPL9B has a paralog, RPL9A, that arose from a single-locus duplication
CYC7	1,284089	Cytochrome c isoform 2, expressed under hypoxic conditions; also known as iso-2-cytochrome c; electron carrier of the mitochondrial intermembrane space that transfers electrons from ubiquinone-cytochrome c oxidoreductase to cytochrome c oxidase during cellular respiration; protein abundance increases in response to DNA replication stress; CYC7 has a paralog, CYC1, that arose from the whole

		genome duplication
RPS29A	1,2840495	Protein component of the small (40S) ribosomal subunit; homologous to mammalian ribosomal protein S29 and bacterial S14; RPS29A has a paralog, RPS29B, that arose from the whole genome duplication
PDR12	1,275738	Plasma membrane ATP-binding cassette (ABC) transporter; weak-acid-inducible multidrug transporter required for weak organic acid resistance; induced by sorbate and benzoate and regulated by War1p; mutants exhibit sorbate hypersensitivity
RPS19A	1,2752105	Protein component of the small (40S) ribosomal subunit; required for assembly and maturation of pre-40 S particles; homologous to mammalian ribosomal protein S19, no bacterial homolog; mutations in human RPS19 are associated with Diamond Blackfan anemia; RPS19A has a paralog, RPS19B, that arose from the whole genome duplication
PIR3	1,267602	O-glycosylated covalently-bound cell wall protein; required for cell wall stability; expression is cell cycle regulated, peaking in M/G1 and also subject to regulation by the cell integrity pathway; coding sequence contains length polymorphisms in different strains; PIR3 has a paralog, HSP150, that arose from the whole genome duplication
COX17	1,266443	Copper metallochaperone that transfers copper to Sco1p and Cox11p; eventual delivery to cytochrome c oxidase; contains twin cysteine-x9-cysteine motifs; interacts with the MICOS complex, and interaction is promoted by copper ions; human homolog COX17 partially complements yeast null mutant
MRS4	1,259154	Iron transporter of the mitochondrial carrier family; mediates Fe2+ transport across the inner mitochondrial membrane; active under low-iron conditions; may transport other cations; protein abundance increases in response to DNA replication stress; MRS4 has a paralog, MRS3, that arose from the whole genome duplication
ELF1	1,2581945	Transcription elongation factor with a conserved zinc finger domain; implicated in the maintenance of proper chromatin structure in actively transcribed regions; deletion inhibits Brome mosaic virus (BMV) gene expression
EGO2	1,254537	Component of the EGO and GSE complexes; identified by homology to Ashbya gossypii; YCR075W-A has a paralog, YNR034W-A, that arose from the whole genome duplication
AGA1	1,2465875	Anchorage subunit of a-agglutinin of a-cells; highly O-glycosylated protein with N-terminal secretion signal and C-terminal signal for addition of GPI anchor to cell wall, linked to adhesion subunit Aga2p via two disulfide bonds; AGA1 has a paralog, FIG2, that arose from the whole genome duplication
RPS10A	1,2451375	Protein component of the small (40S) ribosomal subunit; homologous to mammalian ribosomal protein S10, no bacterial homolog; RPS10A has a paralog, RPS10B, that arose from the whole genome duplication; mutations in the human homolog associated with Diamond-Blackfan anemia
SCW10	1,2401815	Cell wall protein with similarity to glucanases; may play a role in conjugation during mating based on mutant phenotype and its regulation by Ste12p; SWC10 has a paralog, SCW4, that arose from the whole genome duplication
DBF2	1,2373035	Ser/Thr kinase involved in transcription and stress response; functions as part of a network of genes in exit from mitosis; localization is cell cycle regulated; activated by Cdc15p during the exit from mitosis; also plays a role in regulating the stability of SWI5 and CLB2 mRNAs; phosphorylates Chs2p to regulate primary septum formation and Hof1p to regulate cytokinesis; DBF2 has a paralog, DBF20, that arose from the whole genome duplication
RPS27B	1,2325345	Protein component of the small (40S) ribosomal subunit; homologous to mammalian ribosomal protein S27, no bacterial homolog; RPS27B has a paralog, RPS27A, that arose from the whole genome duplication
VAC17	1,2318005	Phosphoprotein involved in vacuole inheritance; degraded in late M phase of the cell cycle; acts as a vacuole-specific receptor for myosin Myo2p; involved in regulation of asymmetric inheritance of

		aggregated/misfolded proteins and age reset
YNR071C	1,229098	Putative aldose 1-epimerase
GAS1	1,2271195	Beta-1,3-glucanosyltransferase; required for cell wall assembly and also has a role in transcriptional silencing; localizes to cell surface via a glycosylphosphatidylinositol (GPI) anchor; also found at nuclear periphery; genetic interactions with histone H3 lysine acetyltransferases GCN5 and SAS3 indicate previously unsuspected functions for Gas1 in DNA damage response and cell cycle regulation
HXT4	1,224432	High-affinity glucose transporter; member of the major facilitator superfamily, expression is induced by low levels of glucose and repressed by high levels of glucose; HXT4 has a paralog, HXT7, that arose from the whole genome duplication
WSC2	1,223027	Sensor-transducer of the stress-activated PKC1-MPK1 signaling pathway; involved in maintenance of cell wall integrity and recovery from heat shock; required for the arrest of secretion response; WSC2 has a paralog, WSC3, that arose from the whole genome duplication
YCL002C	1,222331	Putative protein of unknown function; YCL002C is not an essential gene
SFG1	1,221379	Nuclear protein putative transcription factor; required for growth of superficial pseudohyphae (which do not invade the agar substrate) but not for invasive pseudohyphal growth; may act together with Phd1p; potential Cdc28p substrate
YPL067C	1,2213555	Putative protein of unknown function; green fluorescent protein (GFP)-fusion protein localizes to the cytoplasm; YPL067C is not an essential gene
SPT4	1,217999	Spt4p/5p (DSIF) transcription elongation factor complex subunit; the Spt4/5 complex binds to ssRNA in a sequence-specific manner, and along with RNAP I and II has multiple roles regulating transcriptional elongation, RNA processing, quality control, and transcription-coupled repair; localizes to kinetochores and heterochromatin, influencing chromosomal dynamics and silencing; required for transcription through long trinucleotide repeats in ORFs and non-protein coding regions
HLR1	1,2136615	Protein involved in regulation of cell wall composition and integrity; also involved in cell wall response to osmotic stress; overproduction suppresses a lysis sensitive PKC mutation; HLR1 has a paralog, LRE1, that arose from the whole genome duplication
MCD1	1,213317	Essential alpha-kleisin subunit of the cohesin complex; required for sister chromatid cohesion in mitosis and meiosis; apoptosis induces cleavage and translocation of a C-terminal fragment to mitochondria; expression peaks in S phase
SWE1	1,1996915	Protein kinase that regulates the G2/M transition; negative regulator of the Cdc28p kinase; morphogenesis checkpoint kinase; positive regulator of sphingolipid biosynthesis via Orm2p; phosphorylates a tyrosine residue in the N-terminus of Hsp90 in a cell-cycle associated manner, thus modulating the ability of Hsp90 to chaperone a selected clientele; localizes to the nucleus and to the daughter side of the mother-bud neck; homolog of S. pombe Wee1p; potential Cdc28p substrate
RPS8B	1,1990755	Protein component of the small (40S) ribosomal subunit; homologous to mammalian ribosomal protein S8, no bacterial homolog; RPS8B has a paralog, RPS8A, that arose from the whole genome duplication
YCR043C	1,1981165	Putative protein of unknown function; green fluorescent protein (GFP)-fusion protein localizes to the Golgi apparatus; YCR043C is not an essential gene
SRL1	1,197625	Mannoprotein that exhibits a tight association with the cell wall; required for cell wall stability in the absence of GPI-anchored mannoproteins; has a high serine-threonine content; expression is induced in cell wall mutants; SRL1 has a paralog, SVS1, that arose from the whole genome duplication
KTR2	1,196652	Mannosyltransferase involved in N-linked protein glycosylation; member of the KRE2/MNT1 mannosyltransferase family; KTR2 has a paralog, YUR1, that arose from the whole genome duplication
PLM2	1,1927605	Putative transcription factor, contains Forkhead Associated domain; found associated with chromatin;

		target of SBF transcription factor; induced in response to DNA damaging agents and deletion of telomerase; PLM2 has a paralog, TOS4, that arose from the whole genome duplication
HXK2	1,1909425	Hexokinase isoenzyme 2; phosphorylates glucose in cytosol; predominant hexokinase during growth on glucose; represses expression of HXK1, GLK1, induces expression of its own gene; antiapoptotic; phosphorylation/dephosphorylation at Ser14 by kinase Snf1p, phosphatase Glc7p-Reg1p regulates nucleocytoplasmic shuttling of Hxk2p; functions downstream of Sit4p in control of cell cycle, mitochondrial function, oxidative stress resistance, chronological lifespan; has paralog HXK1
YJL213W	1,185729	Protein of unknown function that may interact with ribosomes; periodically expressed during the yeast metabolic cycle; phosphorylated in vitro by the mitotic exit network (MEN) kinase complex, Dbf2p/Mob1p
UBC4	1,185345	Ubiquitin-conjugating enzyme (E2); key E2 partner with Ubc1p for the anaphase-promoting complex (APC); mediates degradation of abnormal or excess proteins, including calmodulin and histone H3; regulates levels of DNA Polymerase-{alpha} to promote efficient and accurate DNA replication; interacts with many SCF ubiquitin protein ligases; component of the cellular stress response; UBC4 has a paralog, UBC5, that arose from the whole genome duplication
CTR3	1,1838455	High-affinity copper transporter of the plasma membrane; acts as a trimer; gene is disrupted by a Ty2 transposon insertion in many laboratory strains of S. cerevisiae
RPS16B	1,1831595	Protein component of the small (40S) ribosomal subunit; homologous to mammalian ribosomal protein S16 and bacterial S9; RPS16B has a paralog, RPS16A, that arose from the whole genome duplication
MIG2	1,182434	Zinc finger transcriptional repressor; cooperates with Mig1p in glucose-induced gene repression; under low glucose conditions relocalizes to mitochondrion, where it interacts with Ups1p, antagonizes mitochondrial fission factor Dnm1p, indicative of a role in mitochondrial fusion or regulating morphology; regulates filamentous growth in response to glucose depletion; activated in stochastic pulses of nuclear localization in response to low glucose
RPL23B	1,179794	Ribosomal 60S subunit protein L23B; homologous to mammalian ribosomal protein L23 and bacterial L14; RPL23B has a paralog, RPL23A, that arose from the whole genome duplication
BDF2	1,1758055	Protein involved in transcription initiation; acts at TATA-containing promoters; associates with the basal transcription factor TFIID; contains two bromodomains; corresponds to the C-terminal region of mammalian TAF1; redundant with Bdf1p; protein abundance increases in response to DNA replication stress; BDF2 has a paralog, BDF1, that arose from the whole genome duplication
UTR4	1,170619	Protein with sequence similarity to acireductone synthases; involved in methionine salvage; found in both the cytoplasm and nucleus
RPL22A	1,1691065	Ribosomal 60S subunit protein L22A; required for the oxidative stress response in yeast; homologous to mammalian ribosomal protein L22, no bacterial homolog; RPL22A has a paralog, RPL22B, that arose from the whole genome duplication
ATX2	1,1672725	Golgi membrane protein involved in manganese homeostasis; overproduction suppresses the sod1 (copper, zinc superoxide dismutase) null mutation
SSQ1	1,1657645	Mitochondrial hsp70-type molecular chaperone; required for assembly of iron/sulfur clusters into proteins at a step after cluster synthesis, and for maturation of Yfh1p, which is a homolog of human frataxin implicated in Friedreich's ataxia
MAM33	1,1625835	Specific translational activator for the mitochondrial COX1 mRNA; acidic protein of the mitochondrial matrix; related to the human complement receptor gC1q-R
FSH1	1,1598925	Putative serine hydrolase; localizes to both the nucleus and cytoplasm; sequence is similar to S. cerevisiae Fsh2p and Fsh3p and the human candidate tumor suppressor OVCA2
CPR6	1,156695	Peptidyl-prolyl cis-trans isomerase (cyclophilin); catalyzes the cis-trans isomerization of peptide bonds

		N-terminal to proline residues; plays a role in determining prion variants; binds to Hsp82p and contributes to chaperone activity; protein abundance increases in response to DNA replication stress
DAL4	1,1549035	Allantoin permease; expression sensitive to nitrogen catabolite repression and induced by allophanate, an intermediate in allantoin degradation
MSF1	1,1520775	Mitochondrial phenylalanyl-tRNA synthetase; active as a monomer, unlike the cytoplasmic subunit which is active as a dimer complexed to a beta subunit dimer; similar to the alpha subunit of E. coli phenylalanyl-tRNA synthetase
CRN1	1,148095	Coronin; cortical actin cytoskeletal component that associates with the Arp2p/Arp3p complex to regulate its activity; plays a role in regulation of actin patch assembly
RPS27A	1,1464285	Protein component of the small (40S) ribosomal subunit; homologous to mammalian ribosomal protein S27, no bacterial homolog; RPS27A has a paralog, RPS27B, that arose from the whole genome duplication; protein abundance increases in response to DNA replication stress
TOS6	1,144312	Glycosylphosphatidylinositol-dependent cell wall protein; expression is periodic and decreases in respone to ergosterol perturbation or upon entry into stationary phase; depletion increases resistance to lactic acid
RPL36A	1,143997	Ribosomal 60S subunit protein L36A; N-terminally acetylated; binds to 5.8 S rRNA; homologous to mammalian ribosomal protein L36, no bacterial homolog; RPL36A has a paralog, RPL36B, that arose from the whole genome duplication
YML6	1,1397575	Mitochondrial ribosomal protein of the large subunit; has similarity to E. coli L4 ribosomal protein and human mitoribosomal MRP-L4 protein; essential for viability, unlike most other mitoribosomal proteins
CNB1	1,1385515	Calcineurin B; regulatory subunit of calcineurin, a Ca++/calmodulin-regulated type 2B protein phosphatase which regulates Crz1p (stress-response transcription factor); other calcineurin subunit encoded by CNA1 and/or CMP1; regulates function of Aly1p alpha-arrestin; myristoylation by Nmt1p reduces calcineurin activity in response to submaximal Ca signals, is needed to prevent constitutive phosphatase activity; protein abundance increases in response to DNA replication stress
FIG1	1,1384775	Integral membrane protein required for efficient mating; may participate in or regulate the low affinity Ca2+ influx system, which affects intracellular signaling and cell-cell fusion during mating
ATX1	1,138461	Cytosolic copper metallochaperone; transports copper to the secretory vesicle copper transporter Ccc2p for eventual insertion into Fet3p, which is a multicopper oxidase required for high-affinity iron uptake; human homolog ATOX1 can complement yeast atx1 mutant; overexpression of human ATOX1 suppresses lysine auxotrophy of the yeast sod1 null mutant, as does overexpression of yeast ATX1
IMA1	1,1370635	Major isomaltase (alpha-1,6-glucosidase/alpha-methylglucosidase); required for isomaltose utilization; preferred specificity for isomaltose, alpha-methylglucoside, and palatinose, but also exhibits alpha-1,2 glucosidase activity on sucrose and kojibiose, and can cleave the 1,3-alpha linkage of nigerose and turanose and the alpha-1,5 linkage of leucrose in vitro; member of the IMA isomaltase family
MTC3	1,1364695	Protein of unknown function; green fluorescent protein (GFP)-fusion protein localizes to the mitochondrion; mtc3 is synthetically sick with cdc13-1
MHF1	1,134781	Component of the heterotetrameric MHF histone-fold complex; in humans the MHF complex interacts with both DNA and Mph1p ortholog FANCM, a Fanconi anemia complementation group protein, to stabilize and remodel blocked replication forks and repair damaged DNA; mhf1 srs2 double mutants are MMS hypersensitive; ortholog of human centromere constitutive-associated network (CCAN) subunit CENP-S, also known as MHF1
PNP1	1,134763	Purine nucleoside phosphorylase; specifically metabolizes inosine and guanosine nucleosides; involved in the nicotinamide riboside salvage pathway
YBR255C-A	1,1336925	Putative protein of unknown function; may interact with respiratory chain complexes III (ubiquinol-cytochrome c reductase) or IV (cytochrome c oxidase); identified by sequence comparison with

		hemiascomycetous yeast species
FRE3	1,1306825	Ferric reductase; reduces siderophore-bound iron prior to uptake by transporters; expression induced by low iron levels
MRPS8	1,127561	Mitochondrial ribosomal protein of the small subunit
YGL039W	1,1274555	Aldehyde reductase; reduces aliphatic aldehyde substrates using NADH as cofactor; shown to reduce carbonyl compounds to chiral alcohols
PAN5	1,1272675	2-dehydropantoate 2-reductase; part of the pantothenic acid pathway, structurally homologous to E. coli panE
YLR036C	1,1264215	Putative protein predicted to have transmembrane domains; interacts with HSP90 by yeast two-hybrid analysis; YLR036C is not an essential protein
MRPL32	1,121898	Mitochondrial ribosomal protein of the large subunit; protein abundance increases in response to DNA replication stress
HHT1	1,1195685	Histone H3; core histone protein required for chromatin assembly, part of heterochromatin-mediated telomeric and HM silencing; one of two identical histone H3 proteins (see HHT2); regulated by acetylation, methylation, and phosphorylation; H3K14 acetylation plays an important role in the unfolding of strongly positioned nucleosomes during repair of UV damage
YFR018C	1,1177005	Putative protein of unknown function; SWAT-GFP and seamless GFP fusion proteins localize to the endoplasmic reticulum and mCherry fusion protein localizes to the vacuole
SST2	1,116484	GTPase-activating protein for Gpa1p; regulates desensitization to alpha factor pheromone; also required to prevent receptor-independent signaling of the mating pathway; member of the RGS (regulator of G-protein signaling) family
MSN4	1,1106795	Stress-responsive transcriptional activator; activated in stochastic pulses of nuclear localization in response to various stress conditions; binds DNA at stress response elements of responsive genes, inducing gene expression; involved in diauxic shift
ETT1	1,109975	Nuclear protein that inhibits replication of Brome mosaic virus; S. cerevisiae is a model system for studying replication of positive-strand RNA viruses in their natural hosts; deletion increases stop codon readthrough
ARI1	1,1051565	NADPH-dependent aldehyde reductase; utilizes aromatic and alophatic aldehyde substrates; member of the short-chain dehydrogenase/reductase superfamily
HCH1	1,102678	Heat shock protein regulator; binds to Hsp90p and may stimulate ATPase activity; originally identified as a high-copy number suppressor of a HSP90 loss-of-function mutation; role in regulating Hsp90 inhibitor drug sensitivity; GFP-fusion protein localizes to the cytoplasm and nucleus; protein abundance increases in response to DNA replication stress
YGR121W-A	1,100944	Putative protein of unknown function
MCD4	1,09972	Protein involved in GPI anchor synthesis; multimembrane-spanning protein that localizes to the endoplasmic reticulum; highly conserved among eukaryotes; GPI stands for glycosylphosphatidylinositol
YGL188C-A	1,09950425	Putative protein of unknown function
RPL23A	1,0975985	Ribosomal 60S subunit protein L23A; homologous to mammalian ribosomal protein L23 and bacterial L14; RPL23A has a paralog, RPL23B, that arose from the whole genome duplication
SKM1	1,096568	Member of the PAK family of serine/threonine protein kinases; similar to Ste20p; involved in down-regulation of sterol uptake; proposed to be a downstream effector of Cdc42p during polarized growth; SKM1 has a paralog, CLA4, that arose from the whole genome duplication
FCY1	1,08945	Cytosine deaminase; zinc metalloenzyme that catalyzes the hydrolytic deamination of cytosine to uracil;

		of biomedical interest because it also catalyzes the deamination of 5-fluorocytosine (5FC) to form anticancer drug 5-fluorouracil (5FU)
HOP2	1,0893105	Meiosis-specific protein that localizes to chromosomes; prevents synapsis between nonhomologous chromosomes and ensures synapsis between homologs; complexes with Mnd1p to promote homolog pairing and meiotic double-strand break repair; heterodimer of Hop2p-Mnd1p stimulates the Dmc1p-mediated strand invasion
POP8	1,0880595	Subunit of both RNase MRP and nuclear RNase P; RNase MRP cleaves pre-rRNA, while nuclear RNase P cleaves tRNA precursors to generate mature 5' ends and facilitates turnover of nuclear RNAs; relocalizes to the cytosol in response to hypoxia
SIM1	1,0865415	Protein of the SUN family (Sim1p, Uth1p, Nca3p, Sun4p); may participate in DNA replication; promoter contains SCB regulation box at -300 bp indicating that expression may be cell cycle-regulated; SIM1 has a paralog, SUN4, that arose from the whole genome duplication
RPS10A	1,0857305	Protein component of the small (40S) ribosomal subunit; homologous to mammalian ribosomal protein S10, no bacterial homolog; RPS10A has a paralog, RPS10B, that arose from the whole genome duplication; mutations in the human homolog associated with Diamond-Blackfan anemia
PCL7	1,083461	Pho85p cyclin of the Pho80p subfamily; forms a functional kinase complex with Pho85p which phosphorylates Mmr1p and is regulated by Pho81p; involved in glycogen metabolism, expression is cell-cycle regulated; PCL7 has a paralog, PCL6, that arose from the whole genome duplication
RPL27A	1,078197	Ribosomal 60S subunit protein L27A; homologous to mammalian ribosomal protein L27, no bacterial homolog; RPL27A has a paralog, RPL27B, that arose from the whole genome duplication
SMF3	1,0758445	Putative divalent metal ion transporter involved in iron homeostasis; transcriptionally regulated by metal ions; member of the Nramp family of metal transport proteins; protein abundance increases in response to DNA replication stress
ICP55	1,0756895	Mitochondrial aminopeptidase; cleaves the N termini of at least 38 imported proteins after cleavage by the mitochondrial processing peptidase (MPP), thereby increasing their stability; member of the aminopeptidase P family
RPL20B	1,075344	Ribosomal 60S subunit protein L20B; homologous to mammalian ribosomal protein L18A, no bacterial homolog; RPL20B has a paralog, RPL20A, that arose from the whole genome duplication
YOL013W-A	1,0739385	Putative protein of unknown function; identified by SAGE
CWP1	1,0735	Cell wall mannoprotein that localizes to birth scars of daughter cells; linked to a beta-1,3- and beta-1,6-glucan heteropolymer through a phosphodiester bond; required for propionic acid resistance
RPL34A	1,0672895	Ribosomal 60S subunit protein L34A; homologous to mammalian ribosomal protein L34, no bacterial homolog; RPL34A has a paralog, RPL34B, that arose from the whole genome duplication
YBL109W	1,066051	Dubious open reading frame; unlikely to encode a functional protein, based on available experimental and comparative sequence data
CDC7	1,064758	DDK (Dbf4-dependent kinase) catalytic subunit; required for origin firing and replication fork progression in mitotic S phase through phosphorylation of Mcm2-7p complexes and Cdc45p; kinase activity correlates with cyclical DBF4 expression; required for pre-meiotic DNA replication, meiotic DSB formation, recruitment of monopolin complex to kinetochores during meiosis I, regulation of meiosis-specific Ndt80p; mutation complemented by human CDC7 and DBF4 co-expression
TOM5	1,0618495	Component of the TOM (translocase of outer membrane) complex; responsible for recognition and initial import of all mitochondrially directed proteins; involved in transfer of precursors from the Tom70p and Tom20p receptors to the Tom40p pore
DOG2	1,0613285	2-deoxyglucose-6-phosphate phosphatase; member of a family of low molecular weight phosphatases, induced by oxidative and osmotic stress, confers 2-deoxyglucose resistance when overexpressed; DOG2

		has a paralog, DOG1, that arose from a single-locus duplication; the last half of DOG1 and DOG2 are subject to gene conversions among S. cerevisiae, S. paradoxus, and S. mikatae
DOG1	1,0613285	2-deoxyglucose-6-phosphate phosphatase; member of a family of low molecular weight phosphatases; confers 2-deoxyglucose resistance when overexpressed; DOG1 has a paralog, DOG2, that arose from a single-locus duplication; the last half of DOG1 and DOG2 are subject to gene conversions among S. cerevisiae, S. paradoxus, and S. mikatae
ELO3	1,058053	Elongase; involved in fatty acid and sphingolipid biosynthesis; synthesizes very long chain 20-26-carbon fatty acids from C18-CoA primers; involved in regulation of sphingolipid biosynthesis; lethality of the elo2 elo3 double null mutation is functionally complemented by human ELOVL1 and weakly complemented by human ELOVL3 or ELOV7
TAD2	1,0578135	Subunit of tRNA-specific adenosine-34 deaminase; forms a heterodimer with Tad3p that converts adenosine to inosine at the wobble position of several tRNAs
RPL20A	1,054235	Ribosomal 60S subunit protein L20A; homologous to mammalian ribosomal protein L18A, no bacterial homolog; RPL20A has a paralog, RPL20B, that arose from the whole genome duplication
MUD1	1,0536465	U1 snRNP A protein; homolog of human U1-A; involved in nuclear mRNA splicing
CLA4	1,050768	Cdc42p-activated signal transducing kinase; member of the PAK (p21-activated kinase) family, along with Ste20p and Skm1p; involved in septin ring assembly, vacuole inheritance, cytokinesis, sterol uptake regulation; phosphorylates Cdc3p and Cdc10p; CLA4 has a paralog, SKM1, that arose from the whole genome duplication
RPS18B	1,0495455	Protein component of the small (40S) ribosomal subunit; homologous to mammalian ribosomal protein S18 and bacterial S13; RPS18B has a paralog, RPS18A, that arose from the whole genome duplication; protein abundance increases in response to DNA replication stress
SPE4	1,0487255	Spermine synthase; required for the biosynthesis of spermine and also involved in biosynthesis of pantothenic acid
RSM18	1,0479085	Mitochondrial ribosomal protein of the small subunit; has similarity to E. coli S18 ribosomal protein
CIK1	1,047608	Kinesin-associated protein; required for both karyogamy and mitotic spindle organization, interacts stably and specifically with Kar3p and may function to target this kinesin to a specific cellular role; locus encodes a long and short transcript with differing functions; CIK1 has a paralog, VIK1, that arose from the whole genome duplication
YGR079W	1,043971	Putative protein of unknown function; YGR079W is not an essential gene
RPL2A	1,043255	Ribosomal 60S subunit protein L2A; homologous to mammalian ribosomal protein L2 and bacterial L2; RPL2A has a paralog, RPL2B, that arose from the whole genome duplication
NDE1	1,042849	Mitochondrial external NADH dehydrogenase; type II NAD(P)H:quinone oxidoreductase that catalyzes the oxidation of cytosolic NADH; Nde1p and Nde2p provide cytosolic NADH to the mitochondrial respiratory chain; NDE1 has a paralog, NDE2, that arose from the whole genome duplication
RPS24A	1,042443	Protein component of the small (40S) ribosomal subunit; homologous to mammalian ribosomal protein S24, no bacterial homolog; RPS24A has a paralog, RPS24B, that arose from the whole genome duplication
CMC2	1,040613	Protein involved in respiratory chain complex assembly or maintenance; protein of the mitochondrial intermembrane space; contains twin Cx9C motifs that can form coiled coil-helix-coiled-coil helix fold
RHO3	1,039	Non-essential small GTPase of the Rho/Rac family of Ras-like proteins; involved in the establishment of cell polarity; GTPase activity positively regulated by the GTPase activating protein (GAP) Rgd1p
IZH3	1,0388115	Membrane protein involved in zinc ion homeostasis; member of the four-protein IZH family, expression induced by zinc deficiency; deletion reduces sensitivity to elevated zinc and shortens lag phase,

		overexpression reduces Zap1p activity
UBP16	1,038272	Deubiquitinating enzyme anchored to the outer mitochondrial membrane; probably not important for general mitochondrial functioning, but may perform a more specialized function at mitochondria
PMU1	1,0367355	Putative phosphomutase; contains a region homologous to the active site of phosphomutases; overexpression suppresses the histidine auxotrophy of an ade3 ade16 ade17 triple mutant and the temperature sensitivity of a tps2 mutant
BSC4	1,036556	Protein of unknown function; protein-coding gene that evolved de novo via a series of point mutations in noncoding sequence; ORF exhibits genomic organization compatible with a translational readthrough-dependent mode of expression; readthrough is increased upon depletion of Sup35p; may be involved in DNA repair pathway during stationary phase and contribute to robustness of cells when shifted to a nutrient-poor environment
AAC3	1,0352855	Mitochondrial inner membrane ADP/ATP translocator; exchanges cytosolic ADP for mitochondrially synthesized ATP; expressed under anaerobic conditions; similar to Aac1p; has roles in maintenance of viability and in respiration; AAC3 has a paralog, PET9, that arose from the whole genome duplication
DUS3	1,03431	Dihydrouridine synthase; member of a widespread family of conserved proteins including Smm1p, Dus1p, and Dus4p; contains a consensus oleate response element (ORE) in its promoter region; forms nuclear foci upon DNA replication stress
JJJ3	1,03333	Protein of unknown function; contains a CSL Zn finger and a DnaJ-domain; involved in diphthamide biosynthesis; ortholog human Dph4
CDC6	1,0308255	Essential ATP-binding protein required for DNA replication; component of the pre-replicative complex (pre-RC) which requires ORC to associate with chromatin and is in turn required for Mcm2-7p DNA association; homologous to S. pombe Cdc18p; relocalizes from nucleus to cytoplasm upon DNA replication stress; degraded in response to plasma membrane stress
YOS1	1,03003	Integral membrane protein required for ER to Golgi transport; localized to the Golgi, the ER, and COPII vesicles; interacts with Yip1p and Yif1p
SIL1	1,0283255	Nucleotide exchange factor for the ER lumenal Hsp70 chaperone Kar2p; required for protein translocation into the endoplasmic reticulum (ER); homolog of Yarrowia lipolytica SLS1; GrpE-like protein
YNR014W	1,0271715	Putative protein of unknown function; expression is cell-cycle regulated, Azf1p-dependent, and heat-inducible; YNR014W has a paralog, YMR206W, that arose from the whole genome duplication
MATALPHA1	1,024831	Transcriptional co-activator that regulates mating-type-specific genes; targets the transcription factor Mcm1p to the promoters of alpha-specific genes; one of two genes encoded by the MATalpha mating type cassette
RPL11B	1,021004	Ribosomal 60S subunit protein L11B; expressed at half the level of Rpl11Ap; involved in ribosomal assembly; depletion causes degradation of 60S proteins and RNA; homologous to mammalian ribosomal protein L11 and bacterial L5; RPL11B has a paralog, RPL11A, that arose from the whole genome duplication
YOR389W	1,0199125	Putative protein of unknown function; expression regulated by copper levels
YGL101W	1,016208	Protein of unknown function; non-essential gene; interacts with the DNA helicase Hpr5p; YGL101W has a paralog, YBR242W, that arose from the whole genome duplication
MCM2	1,015069	Protein involved in DNA replication; component of the Mcm2-7 hexameric helicase complex that binds chromatin as a part of the pre-replicative complex; relative distribution to the nucleus increases upon DNA replication stress
YKL018C-A	1,0133075	Putative protein of unknown function; identified by homology; green fluorescent protein (GFP)-fusion protein localizes to the cytoplasm

YLR225C	1,01165	Putative protein of unknown function; green fluorescent protein (GFP)-fusion protein localizes to the cytoplasm; not an essential gene; YLR225C has a paralog, YDR222W, that arose from the whole genome duplication
YLR179C	1,010958	Protein of unknown function with similarity to Tfs1p; transcription is activated by paralogous proteins Yrm1p and Yrr1p along with proteins involved in multidrug resistance; GFP-tagged protein localizes to the cytoplasm and nucleus
SER3	1,010645	3-phosphoglycerate dehydrogenase and alpha-ketoglutarate reductase; 3PG dehydrogenase that catalyzes the first step in serine and glycine biosynthesis; also functions as an alpha-ketoglutarate reductase, converting alpha-ketoglutarate to D-2-hydroxyglutarate (D-2HG); localizes to the cytoplasm; SER3 has a paralog, SER33, that arose from the whole genome duplication
YMR045C	1,0068835	n/a
YDR210W	1,006153	Predicted tail-anchored plasma membrane protein; contains a conserved CYSTM module; related proteins in other organisms may be involved in response to stress; green fluorescent protein (GFP)-fusion protein localizes to the cell periphery
TOM7	1,004941	Component of the TOM (translocase of outer membrane) complex; responsible for recognition and initial import steps for all mitochondrially directed proteins; promotes assembly and stability of the TOM complex
MET3	1,001377	ATP sulfurylase; catalyzes the primary step of intracellular sulfate activation, essential for assimilatory reduction of sulfate to sulfide, involved in methionine metabolism; human homolog PAPSS2 complements yeast null mutant
TMT1	1,0002965	Trans-aconitate methyltransferase; cytosolic enzyme that catalyzes the methyl esterification of 3-isopropylmalate, an intermediate of the leucine biosynthetic pathway, and trans-aconitate, which inhibits the citric acid cycle

Genes down-regulated in response to 0.3 μM nystatin + 100 mg L^{-1} CdS QDs

Gene	Nyst+NPs	Description
YPR159C-A	-1,0026205	Protein of unknown function; SWAT-GFP and mCherry fusion proteins localize to the cytosol; identified by gene-trapping, microarray-based expression analysis, and genome-wide homology searching
TES1	-1,002946	Peroxisomal acyl-CoA thioesterase; likely to be involved in fatty acid oxidation rather than fatty acid synthesis; conserved protein also found in human peroxisomes; TES1 mRNA levels increase during growth on fatty acids
GPT2	-1,004993	Glycerol-3-phosphate/dihydroxyacetone phosphate sn-1 acyltransferase; located in lipid particles and the ER; involved in the stepwise acylation of glycerol-3-phosphate and dihydroxyacetone in lipid biosynthesis; the most conserved motifs and functionally relevant residues are oriented towards the ER lumen
MPC54	-1,006654	Component of the meiotic outer plaque; a membrane-organizing center which is assembled on the cytoplasmic face of the spindle pole body during meiosis II and triggers the formation of the prospore membrane; potential Cdc28p substrate

MAL33	-1,0091315	MAL-activator protein; part of complex locus MAL3; nonfunctional in genomic reference strain S288C
ELP3	-1,01024	Subunit of Elongator complex; Elongator is required for modification of wobble nucleosides in tRNA; exhibits histone acetyltransferase activity that is directed to histones H3 and H4; disruption confers resistance to K. lactis zymotoxin; human homolog ELP3 can partially complement yeast elp3 null mutant
RIM9	-1,010717	Plasma membrane protein of unknown function; involved in the proteolytic activation of Rim101p in response to alkaline pH; interacts with Rim21p and Dfg16p to form a pH-sensing complex in the Rim101 pathway and is required to maintain Rim21p levels; has similarity to A. nidulans PalI;
YNL034W	-1,0110035	Putative protein of unknown function; not an essential gene; YNL034W has a paralog, YNL018C, that arose from a segmental duplication
BIO2	-1,0114825	Biotin synthase; catalyzes the conversion of dethiobiotin to biotin, which is the last step of the biotin biosynthesis pathway; complements E. coli bioB mutant
PML39	-1,0129765	Protein required for nuclear retention of unspliced pre-mRNAs; required along with Mlp1p and Pml1p; anchored to nuclear pore complex via Mlp1p and Mlp2p; found with the subset of nuclear pores farthest from the nucleolus; may interact with ribosomes
BLM10	-1,014454	Proteasome activator; binds the core proteasome (CP) and stimulates proteasome-mediated protein degradation by inducing gate opening; required for sequestering CP into proteasome storage granule (PSG) during quiescent phase and for nuclear import of CP in proliferating cells; required for resistance to bleomycin, may be involved in protecting against oxidative damage; similar to mammalian PA200
BNS1	-1,0149345	Protein of unknown function; overexpression bypasses need for Spo12p, but not required for meiosis; BNS1 has a paralog, SPO12, that arose from the whole genome duplication
DML1	-1,014949	Essential protein involved in mtDNA inheritance; may also function in the partitioning of the mitochondrial organelle or in the segregation of chromosomes, exhibits regions similar to members of a GTPase family
ECM27	-1,0213	Protein involved in calcium homeostasis and exit from quiescence; required for proper trehalose levels during quiescence; may play a role in cell wall biosynthesis, mutants are hypersensitive to antifungal, Papulacandin B; null mutants have increased plasmid loss; interacts with Pdr5p
TOD6	-1,0216295	PAC motif binding protein involved in rRNA and ribosome biogenesis; subunit of the RPD3L histone deacetylase complex; Myb-like HTH transcription factor; hypophosphorylated by rapamycin treatment in a Sch9p-dependent manner; activated in stochastic pulses of nuclear localization
ATG14	-1,0224375	Autophagy-specific subunit of phosphatidylinositol 3-kinase complex I; Atg14p targets complex I to the phagophore assembly site (PAS); required for localizing additional ATG proteins to the PAS; required for overflow degradation of misfolded proteins when ERAD is saturated; homolog of human Barkor; other members are Vps34, Vps15, and Vps30p
PEX32	-1,0237365	Peroxisomal integral membrane protein; involved in negative regulation of peroxisome size; partially functionally redundant with Pex31p; genetic interactions suggest action at a step downstream of steps mediated by Pex28p and Pex29p
ESBP6	-1,025602	Protein with similarity to monocarboxylate permeases; appears not to be involved in transport of monocarboxylates such as lactate, pyruvate or acetate across the plasma membrane
FMP16	-1,02657	Protein of unknown function; may be involved in responding to conditions of stress; the authentic, non-tagged protein is detected in highly purified mitochondria in high-throughput studies; protein abundance increases in response to DNA replication stress
PEX1	-1,0311765	AAA-peroxin; heterodimerizes with AAA-peroxin Pex6p and participates in the recycling of peroxisomal signal receptor Pex5p from the peroxisomal membrane to the cystosol; induced by oleic acid and upregulated during anaerobiosis; mutations in human PEX1 can lead to severe peroxisomal disorders and early death
KRE29	-1,0336425	Subunit of the SMC5-SMC6 complex; this complex is involved in removal of X-shaped DNA structures that arise between sister chromatids during DNA replication and repair; heterozygous mutant shows haploinsufficiency in K1 killer toxin resistance
ASH1	-1,0347785	Component of the Rpd3L histone deacetylase complex; zinc-finger inhibitor of HO transcription; mRNA is localized and

		translated in the distal tip of anaphase cells, resulting in accumulation of Ash1p in daughter cell nuclei and inhibition of HO expression; potential Cdc28p substrate
PEP7	-1,039581	Adaptor protein involved in vesicle-mediated vacuolar protein sorting; multivalent adaptor protein; facilitates vesicle-mediated vacuolar protein sorting by ensuring high-fidelity vesicle docking and fusion, which are essential for targeting of vesicles to the endosome; required for vacuole inheritance
SLD7	-1,0445075	Protein with a role in chromosomal DNA replication; interacts with Sld3p and reduces its affinity for Cdc45p; deletion mutant has aberrant mitochondria
YKU80	-1,047416	Subunit of telomeric Ku complex (Yku70p-Yku80p); involved in telomere length maintenance, structure and telomere position effect; required for localization of telomerase ribonucleoprotein via interaction with TLC1 guide RNA; relocates to sites of double-strand cleavage to promote nonhomologous end joining during DSB repair; colocalizes with quiescent cell telomere hyperclusters
ALR1	-1,0495835	Plasma membrane Mg(2+) transporter; expression and turnover are regulated by Mg(2+) concentration; overexpression confers increased tolerance to Al(3+) and Ga(3+) ions; magnesium transport defect of the null mutant is functionally complemented by either of the human genes MAGT1 and TUSC3 that are not orthologous to ALR1
ELP6	-1,0529295	Subunit of hexameric RecA-like ATPase Elp456 Elongator subcomplex; which is required for modification of wobble nucleosides in tRNA; required for Elongator structural integrity
TRR2	-1,0570845	Mitochondrial thioredoxin reductase; involved in protection against oxidative stress, required with Glr1p to maintain the redox state of Trx3p; contains active-site motif (CAVC) present in prokaryotic orthologs; binds NADPH and FAD; TRR2 has a paralog, TRR1, that arose from the whole genome duplication
PAU22	-1,0582715	Protein of unknown function; member of the seripauperin multigene family encoded mainly in subtelomeric regions; SWAT-GFP fusion protein localizes to the endoplasmic reticulum and vacuole, while mCherry fusion localizes to just the vacuole; identical to Pau21p; encodes two proteins that are translated from two different start codons
CLB1	-1,0598395	B-type cyclin involved in cell cycle progression; activates Cdc28p to promote the transition from G2 to M phase; accumulates during G2 and M, then targeted via a destruction box motif for ubiquitin-mediated degradation by the proteasome; CLB1 has a paralog, CLB2, that arose from the whole genome duplication
RCK1	-1,064701	Protein kinase involved in oxidative stress response; promotes pseudohyphal growth via activation of Ubp3p phosphorylation; identified as suppressor of S. pombe cell cycle checkpoint mutations; RCK1 has a paralog, RCK2, that arose from the whole genome duplication
ROT2	-1,067337	Glucosidase II catalytic subunit; required to trim the final glucose in N-linked glycans; required for normal cell wall synthesis; mutations in rot2 suppress tor2 mutations, and are synthetically lethal with rot1 mutations
ENA5	-1,0683035	Protein with similarity to P-type ATPase sodium pumps; member of the Na+ efflux ATPase family
YCR100C	-1,068902	Putative protein of unknown function
LYS4	-1,0718735	Homoaconitase; catalyzes the conversion of homocitrate to homoisocitrate, which is a step in the lysine biosynthesis pathway
SAS5	-1,0728705	Subunit of the SAS complex (Sas2p, Sas4p, Sas5p); acetylates free histones and nucleosomes and regulates transcriptional silencing; stimulates Sas2p HAT activity
ATG5	-1,0774075	Conserved protein involved in autophagy and the Cvt pathway; undergoes conjugation with Atg12p to form a complex involved in Atg8p lipidation; Atg5p-Atg12p conjugate enhances E2 activity of Atg3 by rearranging its catalytic site, also forms a complex with Atg16p; the Atg5-Atg12/Atg16 complex binds to membranes and is essential for autophagosome formation; also involved in methionine restriction extension of chronological lifespan in an autophagy-dependent manner
IMD3	-1,0778935	Inosine monophosphate dehydrogenase; catalyzes the rate-limiting step in the de novo synthesis of GTP; member of a four-gene family in S. cerevisiae, constitutively expressed; IMD3 has a paralog, IMD4, that arose from the whole genome duplication
CLD1	-1,0799005	Mitochondrial cardiolipin-specific phospholipase; functions upstream of Taz1p to generate monolyso-cardiolipin; transcription increases upon genotoxic stress; involved in restricting Ty1 transposition; has homology to mammalian CGI-58

HXT2	-1,0858735	High-affinity glucose transporter of the major facilitator superfamily; expression is induced by low levels of glucose and repressed by high levels of glucose
SGE1	-1,086781	Plasma membrane multidrug transporter; member of the major facilitator superfamily; acts as an extrusion permease; partial multicopy suppressor of gal11 mutations
PMC1	-1,087065	Vacuolar Ca2+ ATPase involved in depleting cytosol of Ca2+ ions; prevents growth inhibition by activation of calcineurin in the presence of elevated concentrations of calcium; similar to mammalian PMCA1a
YDR366C	-1,0890875	Putative protein of unknown function
NCW2	-1,090407	Structural constituent of the cell wall; attached to the plasma membrane by a GPI-anchor; expression is upregulated in response to cell wall stress; null mutant is sensitive to the antifungal agent polyhexamethylene biguanide, resistant to zymolyase treatment and has increased chitin deposition
JEN1	-1,09052	Monocarboxylate/proton symporter of the plasma membrane; transport activity is dependent on the pH gradient across the membrane; mediates high-affinity uptake of carbon sources lactate, pyuvate, and acetate, and also of the micronutrient selenite, whose structure mimics that of monocarboxylates; expression and localization are tightly regulated, with transcription repression, mRNA degradation, and protein endocytosis and degradation all occurring in the presence of glucose
IRC10	-1,094315	Protein of unknown function; subunit of the leading edge protein (LEP) complex (Ssp1-Ady3-Don1-Irc10) that forms a ring-like structure at the leading edge of the prospore membrane during meiosis II; null mutant displays increased levels of spontaneous Rad52p foci
PCI8	-1,095053	Possible shared subunit of Cop9 signalosome (CSN) and eIF3; binds eIF3b subunit Prt1p, has possible dual functions in transcriptional and translational control, contains a PCI (Proteasome-COP9 signalosome (CSN)-eIF3) domain
MEP2	-1,100153	Ammonium permease involved in regulation of pseudohyphal growth; belongs to a ubiquitous family of cytoplasmic membrane proteins that transport only ammonium (NH4+); expression is under the nitrogen catabolite repression regulation
NAR1	-1,1014335	Subunit of the cytosolic iron-sulfur (FeS) protein assembly machinery; required for maturation of cytosolic and nuclear FeS proteins and for normal resistance to oxidative stress; deficiency results in shortened lifespan and sensitivity to paraquat; homologous to human Narf
STE2	-1,1022595	Receptor for alpha-factor pheromone; seven transmembrane-domain GPCR that interacts with both pheromone and a heterotrimeric G protein to initiate the signaling response that leads to mating between haploid a and alpha cells
MDM36	-1,105577	Mitochondrial protein; required for normal mitochondrial morphology and inheritance; component of the mitochondria-ER-cortex-ancor (MECA); interacts with Num1p to link the ER and mitochondria at the cell cortex; proposed involvement in the formation of Dnm1p and Num1p-containing cortical anchor complexes that promote mitochondrial fission
RIO1	-1,105586	Serine kinase involved in cell cycle regulation and rDNA integrity; associated with late pre-40S particles via its conserved C-terminal domain and participates in late 40S biogenesis; association with pre-40S particles regulated by its catalytic ATPase site and likely occurs after the release of Rio2p from these particles; involved in cell cycle progression and processing of the 20S pre-rRNA into mature 18S rRNA; phosphorylates Rpa43p in anaphase to remove Pol I from rDNA
YNL034W	-1,109006	Putative protein of unknown function; not an essential gene; YNL034W has a paralog, YNL018C, that arose from a segmental duplication
VPS51	-1,1126275	Component of the GARP (Golgi-associated retrograde protein) complex; GARP is required for the recycling of proteins from endosomes to the late Golgi, and for mitosis after DNA damage induced checkpoint arrest; links the (VFT/GARP) complex to the SNARE Tlg1p; members of the GARP complex are Vps51p-Vps52p-Vps53p-Vps54p
YLR297W	-1,1183025	Protein of unknown function; green fluorescent protein (GFP)-fusion protein localizes to the vacuole; not an essential gene; induced by treatment with 8-methoxypsoralen and UVA irradiation; relocalizes from nucleus to vacuole upon DNA replication stress; YLR297W has a paralog, YOR186W, that arose from the whole genome duplication
RSA1	-1,1285055	Protein involved in the assembly of 60S ribosomal subunits; functionally interacts with Dbp6p; functions in a late nucleoplasmic step of the assembly
TYE7	-1,1300565	Serine-rich protein that contains a bHLH DNA binding motif; binds E-boxes of glycolytic genes and contributes to their activation; may function as a transcriptional activator in Ty1-mediated gene expression; bHLH stands for basic-helix-loop-helix

RCN1	-1,1356415	Protein involved in calcineurin regulation during calcium signaling; has similarity to H. sapiens DSCR1 which is found in the Down Syndrome candidate region
SNO1	-1,138153	Protein of unconfirmed function; involved in pyridoxine metabolism; expression is induced during stationary phase; forms a putative glutamine amidotransferase complex with Snz1p, with Sno1p serving as the glutaminase
RTS2	-1,141759	Basic zinc-finger protein; similar to human and mouse Kin17 proteins which are chromatin-associated proteins involved in UV response and DNA replication
YPR127W	-1,144172	Putative pyridoxine 4-dehydrogenase; differentially expressed during alcoholic fermentation; expression activated by transcription factor YRM1/YOR172W; green fluorescent protein (GFP)-fusion protein localizes to both the cytoplasm and the nucleus
SUT1	-1,145768	Zn(II)2Cys6 family transcription factor; positively regulates sterol uptake genes under anaerobic conditions; involved in hypoxic gene expression; represses filamentation-inducing genes during vegetative growth; positively regulates mating with SUT2 by repressing expression of genes that act as mating inhibitors; repressed by STE12; relocalizes from the nucleus to the cytoplasm upon DNA replication stress; SUT1 has a paralog, SUT2, that arose from the whole genome duplication
ITR1	-1,1475655	Myo-inositol transporter; member of the sugar transporter superfamily; expression is repressed by inositol and choline via Opi1p and derepressed via Ino2p and Ino4p; relative distribution to the vacuole increases upon DNA replication stress; ITR1 has a paralog, ITR2, that arose from the whole genome duplication
YPL107W	-1,155235	Putative protein of unknown function; green fluorescent protein (GFP)-fusion protein localizes to mitochondria; YPL107W is not an essential gene
ASN1	-1,160141	Asparagine synthetase; catalyzes the synthesis of L-asparagine from L-aspartate in the asparagine biosynthetic pathway; ASN1 has a paralog, ASN2, that arose from the whole genome duplication
PRP28	-1,160385	RNA binding protein; involved in RNA isomerization at the 5' splice site and for exchange of U6 for U1 snRNA at the 5' splice site; similar to the RNA helicases of the DEAD-box family
UPC2	-1,1606675	Sterol regulatory element binding protein; induces sterol biosynthetic genes, upon sterol depletion; acts as a sterol sensor, binding ergosterol in sterol rich conditions; relocates from intracellular membranes to perinuclear foci upon sterol depletion; redundant activator of filamentation with ECM22, up-regulating the expression of filamentous growth genes; contains a Zn[2]-Cys[6] binuclear cluster; UPC2 has a paralog, ECM22, that arose from the whole genome duplication
BDH2	-1,165025	Putative medium-chain alcohol dehydrogenase with similarity to BDH1; transcription induced by constitutively active PDR1 and PDR3
PTK1	-1,1662825	Putative serine/threonine protein kinase; regulates spermine uptake; involved in polyamine transport; possible mitochondrial protein; PTK1 has a paralog, PTK2, that arose from the whole genome duplication
MMS21	-1,1672015	Highly conserved SUMO E3 ligase component of SMC5-SMC6 complex; required for anchoring of double-strand breaks to nuclear periphery; SMC5-SMC6 complex plays a key role in removal of X-shaped DNA structures that arise between sister chromatids during DNA replication and repair; required for efficient sister chromatid cohesion; mutants are sensitive to methyl methanesulfonate, show increased spontaneous mutation and mitotic recombination; SUMOylates and inhibits Snf1p function
GRX6	-1,1695075	Cis-golgi localized monothiol glutaredoxin, binds Fe-S cluster; more similar in activity to dithiol than other monothiol glutaredoxins; involved in the oxidative stress response; GRX6 has a paralog, GRX7, that arose from the whole genome duplication
CMK2	-1,172259	Calmodulin-dependent protein kinase; may play a role in stress response, many CA++/calmodulan dependent phosphorylation substrates demonstrated in vitro, amino acid sequence similar to mammalian Cam Kinase II; CMK2 has a paralog, CMK1, that arose from the whole genome duplication
NOP14	-1,1742575	Nucleolar protein; forms a complex with Noc4p that mediates maturation and nuclear export of 40S ribosomal subunits; also present in the small subunit processome complex, which is required for processing of pre-18S rRNA
MMS1	-1,1780475	Subunit of E3 ubiquitin ligase complex involved in replication repair; stabilizes protein components of the replication fork such as the fork-pausing complex and leading strand polymerase, preventing fork collapse and promoting efficient recovery during replication stress; regulates Ty1 transposition; involved with Rtt101p in nonfunctional rRNA decay

IMP2	-1,1790555	Catalytic subunit of mitochondrial inner membrane peptidase complex; required for maturation of mitochondrial proteins of the intermembrane space; complex contains two catalytic subunits (Imp1p and Imp2p that differ in substrate specificity), and Som1p
YPL108W	-1,1800705	Cytoplasmic protein of unknown function; non-essential gene that is induced in a GDH1 deleted strain with altered redox metabolism; GFP-fusion protein is induced in response to the DNA-damaging agent MMS
PXP1	-1,185017	Peroxisomal matrix protein; well-conserved in fungi; contains tripartite homology domain of thiamine pyrophosphate (TPP) enzymes; targeted to peroxisomes by Pex5p; contains low sequence identity with Pdc1p; mRNA identified as translated by ribosome profiling data
XBP1	-1,191038	Transcriptional repressor; binds promoter sequences of cyclin genes, CYS3, and SMF2; not expressed during log phase of growth, but induced by stress or starvation during mitosis, and late in meiosis; represses 15% of all yeast genes as cells transition to quiescence; important for maintaining G1 arrest and for longevity of quiescent cells; member of Swi4p/Mbp1p family; phosphorylated by Cdc28p; relative distribution to nucleus increases upon DNA replication stress
PEX28	-1,191954	Peroxisomal integral membrane peroxin; involved in the regulation of peroxisomal size, number and distribution; genetic interactions suggest that Pex28p and Pex29p act at steps upstream of those mediated by Pex30p, Pex31p, and Pex32p
YIR016W	-1,2001495	Putative protein of unknown function; expression directly regulated by the metabolic and meiotic transcriptional regulator Ume6p; overexpression causes a cell cycle delay or arrest; non-essential gene; YIR016W has a paralog, YOL036W, that arose from the whole genome duplication
MPD2	-1,202552	Member of the protein disulfide isomerase (PDI) family; exhibits chaperone activity; overexpression suppresses the lethality of a pdi1 deletion but does not complement all Pdi1p functions; undergoes oxidation by Ero1p
ECM3	-1,2049025	Non-essential protein of unknown function; involved in signal transduction and the genotoxic response; induced rapidly in response to treatment with 8-methoxypsoralen and UVA irradiation; relocalizes from ER to cytoplasm upon DNA replication stress; ECM3 has a paralog, YNL095C, that arose from the whole genome duplication
LEE1	-1,209655	Zinc-finger protein of unknown function
MCP1	-1,210383	Mitochondrial protein of unknown function involved in lipid homeostasis; integral membrane protein that localizes to the mitochondrial outer membrane; involved in mitochondrial morphology; interacts genetically with MDM10, and other members of the ERMES complex; contains five predicted transmembrane domains
GCV2	-1,2105075	P subunit of the mitochondrial glycine decarboxylase complex; glycine decarboxylase is required for the catabolism of glycine to 5,10-methylene-THF; expression is regulated by levels of 5,10-methylene-THF in the cytoplasm
RRG8	-1,211998	Protein of unknown function; required for mitochondrial genome maintenance; null mutation results in a decrease in plasma membrane electron transport
POP7	-1,2151285	Subunit of RNase MRP, nuclear RNase P and telomerase; forms a soluble heterodimer with Pop6p that binds P3 domain of RNase MRP and RNase P RNAs; RNase MRP cleaves pre-rRNA, nuclear RNase P cleaves tRNA precursors to generate mature 5' ends and facilitates turnover of nuclear RNAs, while telomerase replenishes telomeric DNA
FMS1	-1,2225985	Polyamine oxidase; converts spermine to spermidine, which is required for the essential hypusination modification of translation factor eIF-5A; also involved in pantothenic acid biosynthesis
RTC2	-1,227038	Putative vacuolar membrane transporter for cationic amino acids; likely contributes to amino acid homeostasis by exporting cationic amino acids from the vacuole; positive regulation by Lys14p suggests that lysine may be the primary substrate; member of the PQ-loop family, with seven transmembrane domains; similar to mammalian PQLC2 vacuolar transporter; RTC2 has a paralog, YPQ1, that arose from the whole genome duplication
ATG16	-1,2275715	Conserved protein involved in autophagy; interacts with Atg12p-Atg5p conjugates to form Atg12p-Atg5p-Atg16p multimers, which binds to membranes and localizes to the pre-autophagosomal structure and are required for autophagy; relocalizes from nucleus to cytoplasmic foci upon DNA replication stress
CTF19	-1,2365515	Outer kinetochore protein, needed for accurate chromosome segregation; component of kinetochore sub-complex COMA (Ctf19p, Okp1p, Mcm21p, Ame1p) that functions as platform for kinetochore assembly; required for spindle assembly checkpoint; minimizes potentially deleterious centromere-proximal crossovers by preventing meiotic DNA break formation

		proximal to centromere; homolog of human centromere constitutive-associated network (CCAN) subunit CENP-P and fission yeast fta2
DSE4	-1,238095	Daughter cell-specific secreted protein with similarity to glucanases; degrades cell wall from the daughter side causing daughter to separate from mother
RPR2	-1,2393815	Subunit of nuclear RNase P; nuclear RNase P cleaves tRNA precursors to generate mature 5' ends and facilitates turnover of nuclear RNAs; not shared between RNase MRP and RNase P, in contrast to all other RNase P protein subunits; protein abundance increases in response to DNA replication stress
YNL195C	-1,23958	Protein of unknown function; shares a promoter with YNL194C; the authentic, non-tagged protein is detected in highly purified mitochondria in high-throughput studies; YNL195C has a paralog, HBT1, that arose from the whole genome duplication
GEX1	-1,24074	Proton:glutathione antiporter; localized to the vacuolar and plasma membranes; imports glutathione from the vacuole and exports it through the plasma membrane; has a role in resistance to oxidative stress and modulation of the PKA pathway; GEX1 has a paralog, GEX2, that arose from a segmental duplication
TPH3	-1,244046	Putative protein of unknown function; GFP-fusion protein localizes to the cytoplasm; contains two adjacent PH-like domains; conserved in closely related Saccharomyces species
CBF1	-1,2453105	Basic helix-loop-helix (bHLH) protein; forms homodimer to bind E-box consensus sequence CACGTG present at MET gene promoters and centromere DNA element I (CDEI); affects nucleosome positioning at this motif; associates with other transcription factors such as Met4p and Isw1p to mediate transcriptional activation or repression; associates with kinetochore proteins, required for chromosome segregation; protein abundance increases in response to DNA replication stress
VTC1	-1,2465155	Regulatory subunit of the vacuolar transporter chaperone (VTC) complex; VTC complex is involved in membrane trafficking, vacuolar polyphosphate accumulation, microautophagy and non-autophagic vacuolar fusion; also has mRNA binding activity; protein abundance increases in response to DNA replication stress
YBR056W-A	-1,248532	Protein of unknown function; mRNA identified as translated by ribosome profiling data; partially overlaps dubious ORF YBR056C-B; YBR056W-A has a paralog, YDR034W-B, that arose from the whole genome duplication
COX19	-1,2489265	Protein required for cytochrome c oxidase assembly; located in the cytosol and mitochondrial intermembrane space; putative copper metallochaperone that delivers copper to cytochrome c oxidase; contains twin cysteine-x9-cysteine motifs
LYS9	-1,2506295	Saccharopine dehydrogenase (NADP+, L-glutamate-forming); catalyzes the formation of saccharopine from alpha-aminoadipate 6-semialdehyde, the seventh step in lysine biosynthesis pathway; exhibits genetic and physical interactions with TRM112
REX3	-1,251462	RNA exonuclease; required for maturation of the RNA component of RNase MRP; functions redundantly with Rnh70p and Rex2p in processing of U5 snRNA and RNase P RNA; member of RNase D family of exonucleases
YCR101C	-1,2521335	Putative protein of unknown function; localizes to the membrane fraction; YCR101C is not an essential gene
MCM10	-1,255126	Essential chromatin-associated protein; involved in initiation of DNA replication; required for association of MCM2-7 complex with replication origins; required to stabilize catalytic subunit of DNA polymerase-alpha; self-associates through its N-terminal domain
PEX11	-1,259644	Peroxisomal protein required for medium-chain fatty acid oxidation; also required for peroxisome proliferation, possibly by inducing membrane curvature; localization regulated by phosphorylation; transcription regulated by Adr1p and Pip2p-Oaf1p
RAD55	-1,2667995	Protein that stimulates strand exchange; stimulates strand exchange by stabilizing the binding of Rad51p to single-stranded DNA; involved in the recombinational repair of double-strand breaks in DNA during vegetative growth and meiosis; forms heterodimer with Rad57p
YIL166C	-1,273121	Putative protein with similarity to allantoate permease; similar to the allantoate permease (Dal5p) subfamily of the major facilitator superfamily; mRNA expression is elevated by sulfur limitation; YIL166C is a non-essential gene
ROG1	-1,2735835	Lipase with specificity for monoacylglycerol; preferred substrate is 1-oleoylglycerol; null mutation affects lipid droplet morphology and overexpression causes increased accumulation of reactive oxygen species
ECM21	-1,277457	Protein involved in regulating endocytosis of plasma membrane proteins; identified as a substrate for ubiquitination by Rsp5p and deubiquitination by Ubp2p; promoter contains several Gcn4p binding elements; ECM21 has a paralog, CSR2, that arose

		from the whole genome duplication
SPG4	-1,27926	Protein required for high temperature survival during stationary phase; not required for growth on nonfermentable carbon sources
YNL040W	-1,283731	Protein of unknown function; has strong similarity to alanyl-tRNA synthases from Eubacteria; null mutant displays decreased translation rate and increased readthrough of premature stop codons; green fluorescent protein (GFP)-fusion protein localizes to the cytoplasm; YNL040W is not an essential gene
LAP3	-1,286305	Cysteine aminopeptidase with homocysteine-thiolactonase activity; protects cells against homocysteine toxicity; has bleomycin hydrolase activity in vitro; transcription is regulated by galactose via Gal4p; orthologous to human BLMH
YER053C-A	-1,287466	Protein of unknown function; green fluorescent protein (GFP)-fusion protein localizes to the endoplasmic reticulum; protein abundance increases in response to DNA replication stress
CCC1	-1,290218	Vacuolar Fe2+/Mn2+ transporter; suppresses respiratory deficit of yfh1 mutants, which lack the ortholog of mammalian frataxin, by preventing mitochondrial iron accumulation; relative distribution to the vacuole decreases upon DNA replication stress
CSM4	-1,3007455	Protein required for accurate chromosome segregation during meiosis; involved in meiotic telomere clustering (bouquet formation) and telomere-led rapid prophase movements; functions with meiosis-specific telomere-binding protein Ndj1p; CSM4 has a paralog, MPS2, that arose from the whole genome duplication
CIN5	-1,3035955	Basic leucine zipper (bZIP) transcription factor of the yAP-1 family; physically interacts with the Tup1-Cyc8 complex and recruits Tup1p to its targets; mediates pleiotropic drug resistance and salt tolerance; nuclearly localized under oxidative stress and sequestered in the cytoplasm by Lot6p under reducing conditions; CIN5 has a paralog, YAP6, that arose from the whole genome duplication
IMO32	-1,3062005	Conserved mitochondrial protein of unknown function; processed by both mitochondrial processing peptidase and mitochondrial octapeptidyl aminopeptidase; gene contains the nested antisense gene NAG1
HRP1	-1,3131135	Subunit of cleavage factor I; cleavage factor I is a five-subunit complex required for the cleavage and polyadenylation of pre-mRNA 3' ends; RRM-containing heteronuclear RNA binding protein and hnRNPA/B family member that binds to poly (A) signal sequences; required for genome stability
EGT2	-1,313471	Glycosylphosphatidylinositol (GPI)-anchored cell wall endoglucanase; required for proper cell separation after cytokinesis; expression is activated by Swi5p and tightly regulated in a cell cycle-dependent manner
YJR115W	-1,317752	Putative protein of unknown function; YJR115W has a paralog, ECM13, that arose from the whole genome duplication
YNR064C	-1,3196125	Epoxide hydrolase; member of the alpha/beta hydrolase fold family; may have a role in detoxification of epoxides
ARO10	-1,321806	Phenylpyruvate decarboxylase; catalyzes decarboxylation of phenylpyruvate to phenylacetaldehyde, which is the first specific step in the Ehrlich pathway; involved in protein N-terminal Met and Ala catabolism
VTC3	-1,327303	Regulatory subunit of the vacuolar transporter chaperone (VTC) complex; involved in membrane trafficking, vacuolar polyphosphate accumulation, microautophagy and non-autophagic vacuolar fusion; VTC3 has a paralog, VTC2, that arose from the whole genome duplication
DSE3	-1,3287805	Daughter cell-specific protein, may help establish daughter fate; relocalizes from bud neck to cytoplasm upon DNA replication stress
ACS1	-1,329375	Acetyl-coA synthetase isoform; along with Acs2p, acetyl-coA synthetase isoform is the nuclear source of acetyl-coA for histone acetylation; expressed during growth on nonfermentable carbon sources and under aerobic conditions
RNR2	-1,340037	Ribonucleotide-diphosphate reductase (RNR), small subunit; the RNR complex catalyzes the rate-limiting step in dNTP synthesis and is regulated by DNA replication and DNA damage checkpoint pathways via localization of the small subunits; RNR2 has a paralog, RNR4, that arose from the whole genome duplication
DBR1	-1,342279	RNA lariat debranching enzyme; catalyzes debranching of lariat introns formed during pre-mRNA splicing; required for efficient Ty1 transposition; knockdown of human homolog Dbr1 rescues toxicity of RNA-binding proteins TDP-43 and FUS which are implicated in amyotrophic lateral sclerosis (ALS), suggests potential therapeutic target for ALS and related TDP-43

		proteinopathies; human homolog DBR1 can complement yeast dbr1 null mutant
HPF1	-1,3474865	Haze-protective mannoprotein; reduces the particle size of aggregated proteins in white wines
HXT5	-1,348125	Hexose transporter with moderate affinity for glucose; induced in the presence of non-fermentable carbon sources, induced by a decrease in growth rate, contains an extended N-terminal domain relative to other HXTs; HXT5 has a paralog, HXT3, that arose from the whole genome duplication
FMP23	-1,3503135	Putative protein of unknown function; proposed to be involved in iron or copper homeostasis; the authentic, non-tagged protein is detected in highly purified mitochondria in high-throughput studies
RME1	-1,3515075	Zinc finger protein involved in control of meiosis; prevents meiosis by repressing IME1 expression and promotes mitosis by activating CLN2 expression; directly repressed by a1-alpha2 regulator; mediates cell type control of sporulation; relocalizes from nucleus to cytoplasm upon DNA replication stress
YOL014W	-1,354939	Putative protein of unknown function; mCherry fusion protein localizes to the cytosol and nucleus
TKL2	-1,355691	Transketolase; catalyzes conversion of xylulose-5-phosphate and ribose-5-phosphate to sedoheptulose-7-phosphate and glyceraldehyde-3-phosphate in the pentose phosphate pathway; needed for synthesis of aromatic amino acids; TKL2 has a paralog, TKL1, that arose from the whole genome duplication
OLE1	-1,356025	Delta(9) fatty acid desaturase; required for monounsaturated fatty acid synthesis and for normal distribution of mitochondria
MPC1	-1,369938	Highly conserved subunit of mitochondrial pyruvate carrier (MPC); MPC is a mitochondrial inner membrane complex that mediates pyruvate uptake and comprises Mpc1p and Mpc2p during fermentative growth, or Mcp1p and Mpc3p during respiratory growth; null mutant displays slow growth that is complemented by expression of human or mouse ortholog; mutation in human ortholog MPC1 is associated with lactic acidosis and hyperpyruvatemia
PRM7	-1,3721395	Pheromone-regulated protein; predicted to have one transmembrane segment; promoter contains Gcn4p binding elements; in W303 strain one continuous open reading frame comprising of YDL037C, the intergenic region and YDL039C encodes the IMI1
PPM2	-1,37458255	AdoMet-dependent tRNA methyltransferase; also involved in methoxycarbonylation; required for the synthesis of wybutosine (yW), a modified guanosine found at the 3'-position adjacent to the anticodon of phe-tRNA; similarity to Ppm1p
NUT2	-1,3745935	Subunit of the RNA polymerase II mediator complex; associates with core polymerase subunits to form the RNA polymerase II holoenzyme; required for transcriptional activation and has a role in basal transcription; protein abundance increases in response to DNA replication stress
NSL1	-1,3764425	Essential component of the MIND kinetochore complex; joins kinetochore subunits contacting DNA to those contacting microtubules; required for accurate chromosome segregation; complex consists of Mtw1p Including Nnf1p-Nsl1p-Dsn1p (MIND)
GLT1	-1,3784565	NAD(+)-dependent glutamate synthase (GOGAT); synthesizes glutamate from glutamine and alpha-ketoglutarate; with Gln1p, forms the secondary pathway for glutamate biosynthesis from ammonia; expression regulated by nitrogen source; assembles into filaments as cells approach stationary phase and under cytosolic acidification and starvation conditions
RTN2	-1,380998	Reticulon protein; involved in nuclear pore assembly and maintenance of tubular ER morphology; promotes membrane curvature; regulates the ER asymmetry-induced inheritance block during ER stress; role in ER-derived peroxisomal biogenesis; interacts with Sec6p, Yip3p, and Sbh1p; less abundant than RTN1; member of RTNLA (reticulon-like A) subfamily; protein increases in abundance and relocalizes to plasma membrane upon DNA replication stress
SNU114	-1,391261	GTPase component of U5 snRNP involved in mRNA splicing via spliceosome; binds directly to U5 snRNA; proposed to be involved in conformational changes of the spliceosome; similarity to ribosomal translocation factor EF-2
CAF120	-1,39547	Part of the CCR4-NOT transcriptional regulatory complex; involved in controlling mRNA initiation, elongation, and degradation; contains a PH-like domain; CAF120 has a paralog, SKG3, that arose from the whole genome duplication
YNL277W-A	-1,4013395	Putative protein of unknown function

GTT1	-1,404703	ER associated glutathione S-transferase capable of homodimerization; expression induced during the diauxic shift and throughout stationary phase; functional overlap with Gtt2p, Grx1p, and Grx2p
YKL151C	-1,4056325	Widely-conserved NADHX dehydratase; converts (S)-NADHX to NADH in ATP-dependent manner; YKL151C promoter contains STREs (stress response elements) and expression is induced by heat shock or methyl methanesulfonate; downstream intergenic region drives antisense expression and mediates coordinated regulation of YKL151C and GPM1 phosphoglycerate mutase; protein abundance increases in response to DNA replication stress; homolog of Carkd in mammals and C-terminus of YjeF in E.coli
GZF3	-1,407723	GATA zinc finger protein; negatively regulates nitrogen catabolic gene expression by competing with Gat1p for GATA site binding; function requires a repressive carbon source; dimerizes with Dal80p and binds to Tor1p; GZF3 has a paralog, DAL80, that arose from the whole genome duplication
ECI1	-1,408996	Peroxisomal delta3,delta2-enoyl-CoA isomerase; hexameric protein that converts 3-hexenoyl-CoA to trans-2-hexenoyl-CoA, essential for the beta-oxidation of unsaturated fatty acids, oleate-induced; ECI1 has a paralog, DCI1, that arose from the whole genome duplication
PIG1	-1,4122595	Putative targeting subunit for type-1 protein phosphatase Glc7p; tethers Glc7p to Gsy2p glycogen synthase; PIG1 has a paralog, GAC1, that arose from the whole genome duplication
PEX18	-1,412973	Peroxin; required for targeting of peroxisomal matrix proteins containing PTS2; interacts with Pex7p; partially redundant with Pex21p; primarily responsible for peroxisomal import during growth on oleate, and expression is induced during oleate growth
MDJ2	-1,4179825	Constituent of the mitochondrial import motor; associated with the presequence translocase; function overlaps with that of Pam18p; stimulates the ATPase activity of Ssc1p to drive mitochondrial import; contains a J domain
ADI1	-1,4251635	Acireductone dioxygenease involved in methionine salvage pathway; transcribed as polycistronic mRNA with YMR010W and regulated post-transcriptionally by RNase III (Rnt1p) cleavage; ADI1 mRNA is induced in heat shock conditions; human ortholog ADI1 can complement yeast adi1 mutant
GPP1	-1,4256325	Constitutively expressed DL-glycerol-3-phosphate phosphatase; also known as glycerol-1-phosphatase; involved in glycerol biosynthesis, induced in response to both anaerobic and osmotic stress; GPP1 has a paralog, GPP2, that arose from the whole genome duplication
ATO2	-1,43568	Putative transmembrane protein involved in export of ammonia; ammonia is a starvation signal that promotes cell death in aging colonies; phosphorylated in mitochondria; member of the TC 9.B.33 YaaH family; homolog of Y. lipolytica Gpr1p; ATO2 has a paralog, ADY2, that arose from the whole genome duplication
NRG2	-1,438968	Transcriptional repressor; mediates glucose repression and negatively regulates filamentous growth; activated in stochastic pulses of nuclear localization in response to low glucose
DIA3	-1,4458425	Protein of unknown function; involved in invasive and pseudohyphal growth
FAT3	-1,4481485	Protein required for fatty acid uptake; protein abundance increases in cortical patches in response to oleate exposure; the authentic, non-tagged protein is detected in a phosphorylated state in highly purified mitochondria in high-throughput studies; FAT3 has a paralog, YLR413W, that arose from the whole genome duplication
CPA2	-1,4491575	Large subunit of carbamoyl phosphate synthetase; carbamoyl phosphate synthetase catalyzes a step in the synthesis of citrulline, an arginine precursor
MUD2	-1,4523465	Protein involved in early pre-mRNA splicing; component of the pre-mRNA-U1 snRNP complex, the commitment complex; interacts with Msl5p/BBP splicing factor and Sub2p; similar to metazoan splicing factor U2AF65
CRC1	-1,454439	Mitochondrial inner membrane carnitine transporter; required for carnitine-dependent transport of acetyl-CoA from peroxisomes to mitochondria during fatty acid beta-oxidation; human homolog SLC25A20 complements yeast null mutant
YLR415C	-1,4565015	Putative protein of unknown function; YLR415C is not an essential gene
GPA2	-1,4602305	Nucleotide binding alpha subunit of the heterotrimeric G protein; interacts with the receptor Gpr1p, has signaling role in response to nutrients; required for the recruitment of Ras-GTP at the plasma membrane and in the nucleus
SPO21	-1,4610005	Component of the meiotic outer plaque of the spindle pole body; involved in modifying the meiotic outer plaque that is required prior to prospore membrane formation; SPO21 has a paralog, YSW1, that arose from the whole genome duplication

MIH1	-1,461483	Protein tyrosine phosphatase involved in cell cycle control; regulates the phosphorylation state of Cdc28p; homolog of S. pombe cdc25
SKP2	-1,464027	F-box protein of unknown function; predicted to be part of an SCF ubiquitin protease complex; involved in regulating protein levels of sulfur metabolism enzymes; may interact with ribosomes, based on co-purification experiments
YPS1	-1,464374	Aspartic protease; hyperglycosylated member of the yapsin family of proteases, attached to the plasma membrane via a glycosylphosphatidylinositol (GPI) anchor; involved in nutrient limitation-induced cleavage of the extracellular inhibitory domain of signaling mucin Msb2p, resulting in activation of the filamentous growth MAPK pathway; involved with other yapsins in the cell wall integrity response; role in KEX2-independent processing of the alpha factor precursor
PTR2	-1,466146	Integral membrane peptide transporter; mediates transport of di- and tri-peptides; conserved protein that contains 12 transmembrane domains; PTR2 expression is regulated by the N-end rule pathway via repression by Cup9p
SCW11	-1,4677115	Cell wall protein with similarity to glucanases; may play a role in conjugation during mating based on its regulation by Ste12p
YGR201C	-1,46839	Putative protein of unknown function
SLZ1	-1,473574	Sporulation-specific protein with a leucine zipper motif; subunit of the MIS complex which controls mRNA methylation during during the induction of sporulation
NQM1	-1,491285	Transaldolase of unknown function; transcription is repressed by Mot1p and induced by alpha-factor and during diauxic shift; NQM1 has a paralog, TAL1, that arose from the whole genome duplication
HPF1	-1,492138	Haze-protective mannoprotein; reduces the particle size of aggregated proteins in white wines
ERG25	-1,497264	C-4 methyl sterol oxidase; catalyzes the first of three steps required to remove two C-4 methyl groups from an intermediate in ergosterol biosynthesis; mutants accumulate the sterol intermediate 4,4-dimethylzymosterol; human MSMO1 functionally complements the growth defect caused by repression of ERG25 expression
ALD3	-1,5021665	Cytoplasmic aldehyde dehydrogenase; involved in beta-alanine synthesis; uses NAD+ as the preferred coenzyme; very similar to Ald2p; expression is induced by stress and repressed by glucose
VTC4	-1,507292	Vacuolar membrane polyphosphate polymerase; subunit of the vacuolar transporter chaperone (VTC) complex involved in synthesis and transfer of polyP to the vacuole; regulates membrane trafficking; role in non-autophagic vacuolar fusion; protein abundance increases in response to DNA replication stress
FCY2	-1,508819	Purine-cytosine permease; mediates purine (adenine, guanine, and hypoxanthine) and cytosine accumulation; relative distribution to the vacuole increases upon DNA replication stress
FMP40	-1,509119	Putative protein of unknown function; proposed to be involved in responding to environmental stresses; the authentic, non-tagged protein is detected in highly purified mitochondria in high-throughput studies
RGI2	-1,512175	Protein of unknown function; involved in energy metabolism under respiratory conditions; expression induced under carbon limitation and repressed under high glucose; RGI2 has a paralog, RGI1, that arose from the whole genome duplication
HOM3	-1,5280305	Aspartate kinase (L-aspartate 4-P-transferase); cytoplasmic enzyme that catalyzes the first step in the common pathway for methionine and threonine biosynthesis; expression regulated by Gcn4p and the general control of amino acid synthesis
DIA1	-1,5337535	Protein of unknown function; involved in invasive and pseudohyphal growth; green fluorescent protein (GFP)-fusion protein localizes to the cytoplasm in a punctate pattern
DAL80	-1,5388365	Negative regulator of genes in multiple nitrogen degradation pathways; expression is regulated by nitrogen levels and by Gln3p; member of the GATA-binding family, forms homodimers and heterodimers with Gzf3p; DAL80 has a paralog, GZF3, that arose from the whole genome duplication
RNR3	-1,5411995	Minor isoform of large subunit of ribonucleotide-diphosphate reductase; the RNR complex catalyzes rate-limiting step in dNTP synthesis, regulated by DNA replication and DNA damage checkpoint pathways via localization of small subunits; RNR3 has a paralog, RNR1, that arose from the whole genome duplication
GLO4	-1,5473935	Mitochondrial glyoxalase II; catalyzes the hydrolysis of S-D-lactoylglutathione into glutathione and D-lactate; GLO4 has a paralog, GLO2, that arose from the whole genome duplication
GRX4	-1,5499395	Glutathione-dependent oxidoreductase; hydroperoxide and superoxide-radical responsive; monothiol glutaredoxin subfamily

		member along with Grx3p and Grx5p; protects cells from oxidative damage; with Grx3p, binds to Aft1p in iron-replete conditions, promoting its dissociation from promoters; mutant has increased aneuploidy tolerance; transcription regulated by Yap5p; GRX4 has a paralog, GRX3, that arose from the whole genome duplication
GUT2	-1,5535685	Mitochondrial glycerol-3-phosphate dehydrogenase; expression is repressed by both glucose and cAMP and derepressed by non-fermentable carbon sources in a Snf1p, Rsf1p, Hap2/3/4/5 complex dependent manner
ALT2	-1,555595	Catalytically inactive alanine transaminase; expression is repressed in the presence of alanine and repression is mediated by Nrg1p; ALT2 has a paralog, ALT1, that arose from the whole genome duplication
QDR3	-1,557201	Multidrug transporter of the major facilitator superfamily; member of the 12-spanner drug:H(+) antiporter DHA1 family; has a role in polyamine homeostasis; involved in spore wall asembly; sequence similarity to DTR1 and QDR1, and the triple mutant dtr1 qdr1 qdr3 exhibits reduced dityrosine fluorescence relative to the single mutants; expression is upregulated under polyamine stress; required for resistance to quinidine, barban, cisplatin, and bleomycin
ARG80	-1,559729	Transcription factor involved in regulating arginine-responsive genes; acts with Arg81p and Arg82p
SPO19	-1,562944	Meiosis-specific prospore protein; required to produce bending force necessary for proper assembly of the prospore membrane during sporulation; identified as a weak high-copy suppressor of the spo1-1 ts mutation; SPO19 has a paralog, YOR214C, that arose from the whole genome duplication
PAR32	-1,569313	Protein of unknown function; hyperphosphorylated upon rapamycin treatment in a Tap42p-dependent manner; green fluorescent protein (GFP)-fusion protein localizes to the cytoplasm; PAR32 is not an essential gene
DSE2	-1,5734895	Daughter cell-specific secreted protein with similarity to glucanases; degrades cell wall from the daughter side causing daughter to separate from mother; expression is repressed by cAMP
PHM7	-1,5742195	Protein of unknown function; expression is regulated by phosphate levels; green fluorescent protein (GFP)-fusion protein localizes to the cell periphery and vacuole; protein abundance increases in response to DNA replication stress
ADE17	-1,57603	Enzyme of 'de novo' purine biosynthesis; contains both 5-aminoimidazole-4-carboxamide ribonucleotide transformylase and inosine monophosphate cyclohydrolase activities; ADE17 has a paralog, ADE16, that arose from the whole genome duplication; ade16 ade17 mutants require adenine and histidine
YKR041W	-1,5854405	Protein of unknown function; localizes to the mitotic spindle; overexpression of YKR041W affects endocytic protein trafficking
FAA2	-1,592291	Medium chain fatty acyl-CoA synthetase; activates imported fatty acids; accepts a wide range of fatty acid chain lengths with a preference for medium chains, C9:0-C13:0; localized to the peroxisome; comparative analysis suggests that a mitochondrially targeted form may result from translation starting at a non-canonical codon upstream of the annotated start codon
PHO81	-1,6201725	Cyclin-dependent kinase (CDK) inhibitor; regulates Pho80p-Pho85p and Pcl7p-Pho85p cyclin-CDK complexes in response to phosphate levels; inhibitory activity for Pho80p-Pho85p requires myo-D-inositol heptakisphosphate (IP7) generated by Vip1p; relative distribution to the nucleus increases upon DNA replication stress
HAL5	-1,6226585	Putative protein kinase; overexpression increases sodium and lithium tolerance, whereas gene disruption increases cation and low pH sensitivity and impairs potassium uptake, suggesting a role in regulation of Trk1p and/or Trk2p transporters; HAL5 has a paralog, KKQ8, that arose from the whole genome duplication
PUN1	-1,63177	Plasma membrane protein with a role in cell wall integrity; co-localizes with Sur7p in punctate membrane patches; null mutant displays decreased thermotolerance; transcription induced upon cell wall damage and metal ion stress
YAT1	-1,633346	Outer mitochondrial carnitine acetyltransferase; minor ethanol-inducible enzyme involved in transport of activated acyl groups from the cytoplasm into the mitochondrial matrix; phosphorylated
CAT2	-1,646026	Carnitine acetyl-CoA transferase; present in both mitochondria and peroxisomes; transfers activated acetyl groups to carnitine to form acetylcarnitine which can be shuttled across membranes
YGR067C	-1,646284	Putative protein of unknown function; contains a zinc finger motif similar to that of Adr1p
GDH3	-1,6506475	NADP(+)-dependent glutamate dehydrogenase; synthesizes glutamate from ammonia and alpha-ketoglutarate; rate of alpha-ketoglutarate utilization differs from Gdh1p; expression regulated by nitrogen and carbon sources; GDH3 has a paralog, GDH1, that arose from the whole genome duplication

OPI3	-1,651039	Methylene-fatty-acyl-phospholipid synthase; catalyzes the last two steps in phosphatidylcholine biosynthesis; also known as phospholipid methyltransferase
SIP4	-1,660047	C6 zinc cluster transcriptional activator; binds to the carbon source-responsive element (CSRE) of gluconeogenic genes; involved in the positive regulation of gluconeogenesis; regulated by Snf1p protein kinase; localized to the nucleus
MOG1	-1,6707275	Conserved nuclear protein that interacts with GTP-Gsp1p; stimulates nucleotide release from Gsp1p; involved in nuclear protein import; nucleotide release is inhibited by Yrb1p
GCV1	-1,6768555	T subunit of the mitochondrial glycine decarboxylase complex; glycine decarboxylase is required for the catabolism of glycine to 5,10-methylene-THF; expression is regulated by levels of levels of 5,10-methylene-THF in the cytoplasm
GLN1	-1,6840805	Glutamine synthetase (GS); synthesizes glutamine from glutamate and ammonia; with Glt1p, forms the secondary pathway for glutamate biosynthesis from ammonia; expression regulated by nitrogen source and by amino acid limitation; forms filaments of back-to-back stacks of cylindrical homo-decamers at low pH, leading to enzymatic inactivation and storage during states of advanced cellular starvation; relocalizes from nucleus to cytoplasmic foci upon DNA replication stress
DCI1	-1,694686	Peroxisomal protein; identification as a delta(3,5)-delta(2,4)-dienoyl-CoA isomerase involved in fatty acid metabolism is disputed; DCI1 has a paralog, ECI1, that arose from the whole genome duplication
YPL113C	-1,69529	Glyoxylate reductase; acts on glyoxylate and hydroxypyruvate substrates; YPL113C is not an essential gene
MDH2	-1,709373	Cytoplasmic malate dehydrogenase; one of three isozymes that catalyze interconversion of malate and oxaloacetate; involved in the glyoxylate cycle and gluconeogenesis during growth on two-carbon compounds; interacts with Pck1p and Fbp1
PLB2	-1,7213965	Phospholipase B (lysophospholipase) involved in lipid metabolism; displays transacylase activity in vitro; overproduction confers resistance to lysophosphatidylcholine
YIR014W	-1,7243725	Putative protein of unknown function; green fluorescent protein (GFP)-fusion protein localizes to the vacuole; expression directly regulated by the metabolic and meiotic transcriptional regulator Ume6p; YIR014W is a non-essential gene
ARG4	-1,7293545	Argininosuccinate lyase; catalyzes the final step in the arginine biosynthesis pathway
GIP1	-1,7410965	Meiosis-specific regulatory subunit of the Glc7p protein phosphatase; regulates spore wall formation and septin organization, required for expression of some late meiotic genes and for normal localization of Glc7p
MCH2	-1,7531545	Protein with similarity to mammalian monocarboxylate permeases; monocarboxylate permeases are involved in transport of monocarboxylic acids across the plasma membrane but mutant is not deficient in monocarboxylate transport
MLS1	-1,7573655	Malate synthase, enzyme of the glyoxylate cycle; involved in utilization of non-fermentable carbon sources; expression is subject to carbon catabolite repression; localizes in peroxisomes during growth on oleic acid, otherwise cytosolic; can accept butyryl-CoA as acyl-CoA donor in addition to traditional substrate acetyl-CoA
YPT53	-1,769614	Stress-induced Rab family GTPase; required for vacuolar protein sorting and endocytosis; involved in ionic stress tolerance; similar to Vps21p and Ypt52p; functional homolog of Vps21p; mammalian Rab5 homolog; YPT53 has a paralog, VPS21, that arose from the whole genome duplication
TOG1	-1,7751375	Transcriptional activator of oleate genes; regulates genes involved in fatty acid utilization; zinc cluster protein; deletion confers sensitivity to Calcufluor white, and prevents growth on glycerol or lactate as sole carbon source
PXA1	-1,776968	Subunit of heterodimeric peroxisomal ABC transport complex, with Pxa2p; required for import of long-chain fatty acids into peroxisomes; similar to human adrenoleukodystrophy transporters ABCD1and ABCD2, and ALD-related proteins; mutations in ABCD1 cause X-linked adrenoleukodystrophy (X-ALD), a peroxisomal disorder; human ABCD1 and ABCD2 can each partially complement yeast pxa1 pxa2 double null mutant
SPG1	-1,815379	Protein required for high temperature survival during stationary phase; not required for growth on nonfermentable carbon sources; the authentic, non-tagged protein is detected in highly purified mitochondria in high-throughput studies
CYB2	-1,823	Cytochrome b2 (L-lactate cytochrome-c oxidoreductase); component of the mitochondrial intermembrane space, required for lactate utilization; expression is repressed by glucose and anaerobic conditions
NDT80	-1,829803	Meiosis-specific transcription factor; required for exit from pachytene and for full meiotic recombination; activates middle sporulation genes; competes with Sum1p for binding to promoters containing middle sporulation elements (MSE)

BOP2	-1,837399	Protein of unknown function
SNO4	-1,8382835	Possible chaperone and cysteine protease; required for transcriptional reprogramming during the diauxic shift and for survival in stationary phase; similar to bacterial Hsp31 and yeast Hsp31p, Hsp32p, and Hsp33p; DJ-1/ThiJ/PfpI superfamily member; predicted involvement in pyridoxine metabolism; induced by mild heat stress and copper deprivation
DSE1	-1,851357	Daughter cell-specific protein; may regulate cross-talk between the mating and filamentation pathways; deletion affects cell separation after division and sensitivity to alpha-factor and drugs affecting the cell wall; relocalizes from bud neck to cytoplasm upon DNA replication stress
PXA2	-1,8663965	Subunit of heterodimeric peroxisomal ABC transport complex, with Pxa1p; required for import of long-chain fatty acids into peroxisomes; similar to human adrenoleukodystrophy transportesr ABCD1 and ABCD2, and ALD-related proteins; mutations in ABCD1 cause X-linked adrenoleukodystrophy (X-ALD), a peroxisomal disorder; human ABCD1 and ABCD2 can each partially complement yeast pxa1 pxa2 double null mutant
DIP5	-1,8728615	Dicarboxylic amino acid permease; mediates high-affinity and high-capacity transport of L-glutamate and L-aspartate; also a transporter for Gln, Asn, Ser, Ala, and Gly; relocalizes from plasma membrane to vacuole upon DNA replication stress
IME1	-1,8746305	Master regulator of meiosis that is active only during meiotic events; activates transcription of early meiotic genes through interaction with Ume6p; degraded by the 26S proteasome following phosphorylation by Ime2p; transcription is negatively regulated in cis by the IRT1 long noncoding antisense RNA
CPS1	-1,880455	Vacuolar carboxypeptidase S; expression is induced under low-nitrogen conditions
RCR1	-1,8939795	Protein of the ER membrane involved in cell wall chitin deposition; may function in the endosomal-vacuolar trafficking pathway, helping determine whether plasma membrane proteins are degraded or routed to the plasma membrane; RCR1 has a paralog, RCR2, that arose from the whole genome duplication
HEF3	-1,9071175	Translational elongation factor EF-3; member of the ABC superfamily; stimulates EF-1 alpha-dependent binding of aminoacyl-tRNA by the ribosome; normally expressed in zinc deficient cells; HEF3 has a paralog, YEF3, that arose from the whole genome duplication
PNS1	-1,9202895	Protein of unknown function; has similarity to Torpedo californica tCTL1p, which is postulated to be a choline transporter, neither null mutation nor overexpression affects choline transport
ENT4	-1,9309815	Protein of unknown function; contains an N-terminal epsin-like domain; proposed to be involved in the trafficking of Arn1p in the absence of ferrichrome
ERR2	-1,937724	Enolase, a phosphopyruvate hydratase; catalyzes the conversion of 2-phosphoglycerate to phosphoenolpyruvate; complements the growth defect of an ENO1 ENO2 double mutant
PUG1	-1,9474505	Plasma membrane protein involved in protoprophyrin and heme transport; roles in the uptake of protoprophyrin IX and the efflux of heme; expression is induced under both low-heme and low-oxygen conditions; member of the fungal lipid-translocating exporter (LTE) family of proteins
ARK1	-1,9555465	Serine/threonine protein kinase; involved in regulation of the cortical actin cytoskeleton; involved in control of endocytosis; ARK1 has a paralog, PRK1, that arose from the whole genome duplication
FAA4	-1,9636685	Long chain fatty acyl-CoA synthetase; activates fatty acids with a preference for C12:0-C16:0 chain lengths; role in the competitive import of long-chain fatty acids and sphingoid long-chain bases; role in stationary phase survival; localizes to lipid particles and the plasma membrane; role in sphingolipid-to-glycerolipid metabolism; forms cytoplasmic foci upon replication stress; faa1 faa4 double null complemented by any of human ACSBG1, ACSL1, 3, 4, 5, 6, SLC27A2, or 4
CTA1	-1,9671045	Catalase A; breaks down hydrogen peroxide in the peroxisomal matrix formed by acyl-CoA oxidase (Pox1p) during fatty acid beta-oxidation
YAT2	-1,972345	Carnitine acetyltransferase; has similarity to Yat1p, which is a carnitine acetyltransferase associated with the mitochondrial outer membrane
YMR084W	-1,974989	Putative protein of unknown function; YMR084W and adjacent ORF YMR085W are merged in related strains, and together are paralogous to glutamine-fructose-6-phosphate amidotransferase GFA1

OPT2	-1,98066	Oligopeptide transporter; localized to peroxisomes and affects glutathione redox homeostasis; also localizes to the plasma membrane (PM) and to the late Golgi, and has a role in maintenance of lipid asymmetry between the inner and outer leaflets of the PM; member of the OPT family, with potential orthologs in S. pombe and C. albicans; also plays a role in formation of mature vacuoles and in polarized cell growth
YGL117W	-2,0517855	Putative protein of unknown function
YLR412C-A	-2,052162	Putative protein of unknown function
YGR122W	-2,0540475	Protein that may be involved in pH regulation; probable ortholog of A. nidulans PalC, which is involved in pH regulation and binds to the ESCRT-III complex; null mutant does not properly process Rim101p and has decreased resistance to rapamycin; GFP-fusion protein is cytoplasmic; relative distribution to cytoplasm increases upon DNA replication stress
YLR053C	-2,0649875	Putative protein of unknown function
SSU1	-2,0681445	Plasma membrane sulfite pump involved in sulfite metabolism; required for efficient sulfite efflux; major facilitator superfamily protein
ICL1	-2,0760025	Isocitrate lyase; catalyzes the formation of succinate and glyoxylate from isocitrate, a key reaction of the glyoxylate cycle; expression of ICL1 is induced by growth on ethanol and repressed by growth on glucose
OSW2	-2,1302375	Protein of unknown function reputedly involved in spore wall assembly
ICL2	-2,1835325	2-methylisocitrate lyase of the mitochondrial matrix; functions in the methylcitrate cycle to catalyze the conversion of 2-methylisocitrate to succinate and pyruvate; ICL2 transcription is repressed by glucose and induced by ethanol
HMS1	-2,183972	bHLH protein with similarity to myc-family transcription factors; overexpression confers hyperfilamentous growth and suppresses the pseudohyphal filamentation defect of a diploid mep1 mep2 homozygous null mutant
PHO11	-2,1847995	One of three repressible acid phosphatases; glycoprotein that is transported to the cell surface by the secretory pathway; induced by phosphate starvation and coordinately regulated by PHO4 and PHO2; PHO11 has a paralog, PHO12, that arose from a segmental duplication
UBP13	-2,189864	Ubiquitin-specific protease that cleaves Ub-protein fusions; UBP13 has a paralog, UBP9, that arose from the whole genome duplication
POT1	-2,211091	3-ketoacyl-CoA thiolase with broad chain length specificity; cleaves 3-ketoacyl-CoA into acyl-CoA and acetyl-CoA during beta-oxidation of fatty acids
NCA3	-2,2329025	Protein involved in mitochondrion organization; functions with Nca2p to regulate mitochondrial expression of subunits 6 (Atp6p) and 8 (Atp8p) of the Fo-F1 ATP synthase; SWAT-GFP, seamless-GFP and mCherry fusion proteins localize to the vacuole; member of the SUN family; expression induced in cells treated with the mycotoxin patulin; NCA3 has a paralog, UTH1, that arose from the whole genome duplication
DMC1	-2,2599535	Meiosis-specific recombinase required for double-strand break repair; also required for pairing between homologous chromosomes; required for the normal morphogenesis of synaptonemal complex; homolog of Rad51p and the bacterial RecA protein; binds ssDNA and dsDNA, forms helical filaments; stimulated by Rdh54p
VPS36	-2,2602705	Component of the ESCRT-II complex; contains the GLUE (GRAM Like Ubiquitin binding in EAP45) domain which is involved in interactions with ESCRT-I and ubiquitin-dependent sorting of proteins into the endosome; plays a role in the formation of mutant huntingtin (Htt) aggregates in yeast
POX1	-2,261791	Fatty-acyl coenzyme A oxidase; involved in the fatty acid beta-oxidation pathway; localized to the peroxisomal matrix
YKL050C	-2,30713	Protein of unknown function; the YKL050W protein is a target of the SCFCdc4 ubiquitin ligase complex and YKL050W transcription is regulated by Azf1p; YKL050C has a paralog, EIS1, that arose from the whole genome duplication
BAG7	-2,312719	Rho GTPase activating protein (RhoGAP); stimulates the intrinsic GTPase activity of Rho1p, which plays a bud growth by regulating actin cytoskeleton organization and cell wall biosynthesis, resulting in the downregulation of Rho1p; structurally and functionally related to Sac7p; BAG7 has a paralog, SAC7, that arose from the whole genome duplication
MNT4	-2,3323875	Putative alpha-1,3-mannosyltransferase; not required for protein O-glycosylation; SWAT-GFP and mCherry fusion proteins

		localize to the endoplasmic reticulum and vacuole respectively
MEP1	-2,343266	Ammonium permease; belongs to a ubiquitous family of cytoplasmic membrane proteins that transport only ammonium (NH4+); expression is under the nitrogen catabolite repression regulation; human homolog RHCG complements yeast null mutant; mutations in human homolog RHCG implicated in metabolic acidosis; MEP1 has a paralog, MEP3, that arose from the whole genome duplication
YBR285W	-2,3775615	Putative protein of unknown function; YBR285W is not an essential gene
SNZ1	-2,4073975	Protein involved in vitamin B6 biosynthesis; member of a stationary phase-induced gene family; coregulated with SNO1; interacts with Sno1p and with Yhr198p, perhaps as a multiprotein complex containing other Snz and Sno proteins
YCR007C	-2,4099045	Putative integral membrane protein; member of DUP240 gene family; SWAT-GFP and mCherry fusion proteins localize to the cell periphery and vacuole; YCR007C is not an essential gene
RCH1	-2,409968	Putative transporter; localizes to the plasma membrane in response to high levels of extracellular calcium; member of the SLC10 carrier family; identified in a transposon mutagenesis screen as a gene involved in azole resistance; YMR034C is not an essential gene
AQY1	-2,4165075	Spore-specific water channel; mediates the transport of water across cell membranes, developmentally controlled; may play a role in spore maturation, probably by allowing water outflow, may be involved in freeze tolerance
YMR085W	-2,486864	Putative protein of unknown function; YMR085W and adjacent ORF YMR084W are merged in related strains, and together are paralogous to glutamine-fructose-6-phosphate amidotransferase GFA1
PDC6	-2,50302	Minor isoform of pyruvate decarboxylase; decarboxylates pyruvate to acetaldehyde, involved in amino acid catabolism; transcription is glucose- and ethanol-dependent, and is strongly induced during sulfur limitation
ARG1	-2,564618	Arginosuccinate synthetase; catalyzes the formation of L-argininosuccinate from citrulline and L-aspartate in the arginine biosynthesis pathway; potential Cdc28p substrate
SSA3	-2,569389	ATPase involved in protein folding and the response to stress; plays a role in SRP-dependent cotranslational protein-membrane targeting and translocation; member of the heat shock protein 70 (HSP70) family; localized to the cytoplasm; SSA3 has a paralog, SSA4, that arose from the whole genome duplication
YOR385W	-2,583524	Putative protein of unknown function; green fluorescent protein (GFP)-fusion protein localizes to the cytoplasm; YOR385W is not an essential gene
IDP3	-2,6138165	Peroxisomal NADP-dependent isocitrate dehydrogenase; catalyzes oxidation of isocitrate to alpha-ketoglutarate with the formation of NADP(H+), required for growth on unsaturated fatty acids; IDP3 has a paralog, IDP2, that arose from the whole genome duplication
PDH1	-2,627685	Putative 2-methylcitrate dehydratase; mitochondrial protein that participates in respiration; induced by diauxic shift; homologous to E. coli PrpD, may take part in the conversion of 2-methylcitrate to 2-methylisocitrate
PHM6	-2,628395	Protein of unknown function; expression is regulated by phosphate levels
SHH3	-2,7081365	Putative mitochondrial inner membrane protein of unknown function; although similar to paralogous Sdh3p, Shh3p is not a stoichiometric subunit of either succinate dehydrogenase or of the TIM22 translocase; SHH3 has a paralog, SDH3, that arose from the whole genome duplication
ICS2	-2,710527	Protein of unknown function; null mutation does not confer any obvious defects in growth, spore germination, viability, or carbohydrate utilization
FMP45	-2,7181415	Integral membrane protein localized to mitochondria; required for sporulation and maintaining sphingolipid content; similar to SUR7; FMP45 has a paralog, YNL194C, that arose from the whole genome duplication
HBT1	-2,7332935	Shmoo tip protein, substrate of Hub1p ubiquitin-like protein; mutants are defective for mating projection formation, thereby implicating Hbt1p in polarized cell morphogenesis; HBT1 has a paralog, YNL195C, that arose from the whole genome duplication
ATO3	-2,7659655	Plasma membrane protein, putative ammonium transporter; regulation pattern suggests a possible role in export of ammonia from the cell; phosphorylated in mitochondria; member of the TC 9.B.33 YaaH family of putative transporters

PHO89	-2,7728145	Plasma membrane Na+/Pi cotransporter; active in early growth phase; similar to phosphate transporters of Neurospora crassa; transcription regulated by inorganic phosphate concentrations and Pho4p; mutations in related human transporter genes hPit1 and hPit2 are associated with hyperphosphatemia-induced calcification of vascular tissue and familial idiopathic basal ganglia calcification
GAP1	-2,774187	General amino acid permease; Gap1p senses the presence of amino acid substrates to regulate localization to the plasma membrane when needed; essential for invasive growth
YKL107W	-2,809881	Putative short-chain dehydrogenase/reductase; proposed to be a palmitoylated membrane protein
JLP1	-2,9219435	Fe(II)-dependent sulfonate/alpha-ketoglutarate dioxygenase; involved in sulfonate catabolism for use as a sulfur source; contains sequence that resembles a J domain (typified by the E. coli DnaJ protein); induced by sulphur starvation
CRF1	-2,926906	Transcriptional corepressor; involved in repression of ribosomal protein (RP) gene transcription via the TOR signaling pathway which promotes accumulation of Crf1p in the nucleus; role in repression of RP genes varies by strain; CRF1 has a paralog, IFH1, that arose from the whole genome duplication
YLR307C-A	-2,9347615	Putative protein of unknown function
CTT1	-2,955544	Cytosolic catalase T; has a role in protection from oxidative damage by hydrogen peroxide
SHH4	-3,03931	Putative alternate subunit of succinate dehydrogenase (SDH); mitochondrial inner membrane protein; genetic interaction with SDH4 suggests that Shh4p can function as a functional SDH subunit; a fraction copurifies with SDH subunit Sdh3p; expression induced by nitrogen limitation in a GLN3, GAT1-dependent manner; Shh4p has greater similarity to human SDHD (subunit D of SDH, implicated in paraganglioma) than does its paralog Sdh4p
YMR175W-A	-3,0702625	Putative protein of unknown function
NDE2	-3,1607725	Mitochondrial external NADH dehydrogenase; catalyzes the oxidation of cytosolic NADH; Nde1p and Nde2p are involved in providing the cytosolic NADH to the mitochondrial respiratory chain; NDE2 has a paralog, NDE1, that arose from the whole genome duplication
ADH2	-3,2996215	Glucose-repressible alcohol dehydrogenase II; catalyzes the conversion of ethanol to acetaldehyde; involved in the production of certain carboxylate esters; regulated by ADR1
FMP48	-3,301794	Putative protein of unknown function; the authentic, non-tagged protein is detected in highly purified mitochondria in high-throughput studies; induced by treatment with 8-methoxypsoralen and UVA irradiation
GIT1	-3,3422925	Plasma membrane permease; mediates uptake of glycerophosphoinositol and glycerophosphocholine as sources of the nutrients inositol and phosphate; expression and transport rate are regulated by phosphate and inositol availability
CIT3	-3,368834	Dual specificity mitochondrial citrate and methylcitrate synthase; catalyzes the condensation of acetyl-CoA and oxaloacetate to form citrate and that of propionyl-CoA and oxaloacetate to form 2-methylcitrate
AZR1	-3,5050075	Plasma membrane transporter of the major facilitator superfamily; involved in resistance to azole drugs such as ketoconazole and fluconazole
YJL045W	-3,587052	Minor succinate dehydrogenase isozyme; participates in oxidation of succinate and transfer of electrons to ubiquinone; induced during the diauxic shift in a Cat8p-dependent manner; YJL045W has a paralog, SDH1, that arose from the whole genome duplication
PHO5	-3,736264	Repressible acid phosphatase; 1 of 3 repressible acid phosphatases that also mediates extracellular nucleotide-derived phosphate hydrolysis; secretory pathway derived cell surface glycoprotein; induced by phosphate starvation and coordinately regulated by PHO4 and PHO2
PMA2	-3,7834355	Plasma membrane H+-ATPase; isoform of Pma1p, involved in pumping protons out of the cell; regulator of cytoplasmic pH and plasma membrane potential
SPL2	-3,9100215	Protein with similarity to cyclin-dependent kinase inhibitors; downregulates low-affinity phosphate transport during phosphate limitation by targeting Pho87p to the vacuole; upstream region harbors putative hypoxia response element (HRE) cluster; overproduction suppresses a plc1 null mutation; promoter shows an increase in Snf2p occupancy after heat shock; GFP-fusion

		protein localizes to the cytoplasm
SIP18	-3,9421645	Phospholipid-binding hydrophilin; essential to overcome desiccation-rehydration process; expression is induced by osmotic stress; SIP18 has a paralog, GRE1, that arose from the whole genome duplication
YDL218W	-4,3433565	Putative protein of unknown function; YDL218W transcription is regulated by Azf1p and induced by starvation and aerobic conditions; expression also induced in cells treated with the mycotoxin patulin
PHO84	-4,713877	High-affinity inorganic phosphate (Pi) transporter; also low-affinity manganese transporter; regulated by Pho4p and Spt7p; mutation confers resistance to arsenate; exit from the ER during maturation requires Pho86p; cells overexpressing Pho84p accumulate heavy metals but do not develop symptoms of metal toxicity
GRE1	-5,4754885	Hydrophilin essential in desiccation-rehydration process; stress induced (osmotic, ionic, oxidative, heat shock and heavy metals); regulated by the HOG pathway; GRE1 has a paralog, SIP18, that arose from the whole genome duplication
SPS100	-5,7559415	Protein required for spore wall maturation; expressed during sporulation; may be a component of the spore wall; expression also induced in cells treated with the mycotoxin patulin; SPS100 has a paralog, YGP1, that arose from the whole genome duplication

8.3 Publications and conference proceedings

The data regarding CdS QD effect on yeast cell and mitochondrion, obtained during this Ph.D. course, were published in peer-reviewed journals:

- Marmiroli M., Pagano L., Pasquali F., Zappettini A., Tosato V., Bruschi C.V., Marmiroli N. (2016) A genome-wide nanotoxicology screen of Saccharomyces cerevisiae mutants reveals the basis for cadmium sulphide quantum dot tolerance and sensitivity. Nanotoxicology. 10(1):84-93.

- Pasquali F., Agrimonti C., Pagano L., Zappettini A., Villani M., Marmiroli M., White J.C., Marmiroli N. (2016) Nucleo-mitochondrial interaction of yeast in response to cadmium sulfide quantum dot exposure. Journal Of Hazardous materials. http://dx.doi.org/10.1016/j.jhazmat.2016.11.053.

The data were also presented during several national and international conferences:

- 1st Parma Nanoday, Parma, Italy. Poster session: Pagano L, Marmiroli M, Pasquali F, Marmiroli N "Functional toxicogenomics of CdS QDs in Saccharomyces cerevisiae".

- 2nd Parma Nanoday, Parma, Italy. Poster session: Pasquali F, Agrimonti C, Marmiroli M, Pagano L, Zappettini A, Tosato V, Bruschi CV, Marmiroli N "High-throughput genomic and transcriptomic analysis of CdS QDs response in Saccharomyces cerevisiae".

- 12th International Phytotechnologies Conference - Phytotechnologies for Sustainable Development, Manhattan KS, USA. Presentation: Marmiroli M, Pagano L, Pasquali F,

Zappettini A, Villani M, Tosato V, Bruschi CV, Marmiroli N “Basis for cadmium sulphide quantum dot tolerance and sensitivity: a genome-wide nanotoxicology screening of Saccharomyces cerevisiae mutants”.

- 13th International Phytotechnologies Conference "Plant-Based Solutions for Environmental Problems: From Lab to Field" Marmiroli N, Ruotolo R, Marmiroli M, Imperiale D, Paesano L, Pagano L, Pasquali F, Pira G, Maestri E (2016) ”Mitochondrial Disruption as a Molecular Mechanism of Toxicity of Metal-Containing Nanoparticles”.

- XVII Congresso Nazionale AIBG. Presentation: Marmiroli N, Ruotolo R, Marmiroli M, Imperiale D, Pagano L, Pasquali F, Maestri E (2016) Molecular mechanisms of toxicity of metal-containing nanoparticles in plants: an -omics approach.

1ST PARMA NANO-DAY

WORKSHOP SCIENTIFICO

28 NOVEMBRE 2014

AUDITORIUM PLESSO POLIFUNZIONALE, CAMPUS, PARCO AREA DELLE SCIENZE UNIVERSITÀ DI PARMA

unipr&expo2015

Functional toxicogenomics of CdS QDs in *Saccharomyces cerevisiae*

Luca Pagano[1], Marta Marmiroli[1], Francesco Pasquali[1], A. Zappettini[2], V. Tosato[3], C. V. Bruschi[3], Nelson Marmiroli[1]

[1]*Department of Life Sciences, University of Parma*
[2]*IMEM-CNR, Parma*
[3]*ICGEB, Trieste*

Engineered nanomaterials (NMs) are on the nanoscale level range ca. 1-100 nm, with high reactivity and surface area. NMs showed peculiar physico-chemical properties and are currently used in different areas. Despite some recently acquired knowledge on the effects of NMs on human toxicology and to a lesser extent of their ecotoxicology, very little is known about mechanisms of biological uptake and interaction with cells of living as well as between environmental and biological compartmentalization and chemical behavior in the environment. The aim of this work was to develop a toxicogenomics approach for NMs risk assessment, focusing on CdS QDs using *Saccharomyces cerevisiae* as model system. The approach in yeast was based on a collection of 6000 haploid strains carrying deletions in genes which are not essential for survival. Resistance (or hypersensitivity) to CdS QDs exhibited by a specific strain suggests that the gene deleted in that strain plays a role in the phenotype. Through the complementation of the phenotype of candidate genes identified, we tried to shed light on the possible key role genes involved in mechanisms of response to CdS QDs. Results obtained in yeast could offer a possible answer regarding the mechanism of response in which the CdS QDs are involved and suggested also that CdS QDs and Cd^{2+} can exploit different pathways of response. The approach used can therefore provide information on biological mechanisms and key role genes involved in nanomaterials effects on yeast cells and, more in general, on higher eukaryotes and human.

2ND PARMA NANO-DAY

WORKSHOP SCIENTIFICO

3-4 DICEMBRE 2015

AUDITORIUM PLESSO POLIFUNZIONALE

CAMPUS, AREA DELLE SCIENZE E DELLE TECNOLOGIE

UNIVERSITÀ DEGLI STUDI DI PARMA

Poster

High-throughput genomic and transcriptomic analysis of CdS QDs response in *Saccharomyces cerevisiae*

Francesco Pasquali[1,#], Marta Marmiroli[1], Luca Pagano[1], Caterina Agrimonti[1], Andrea Zappettini[2], Valentina Tosato[3], Carlo V. Bruschi[3], Nelson Marmiroli[1]
[1]*Department of Life Sciences, University of Parma*
[2]*IMEM-CNR, Parma*
[3]*ICGEB, Trieste*
[#]francesco.pasquali@studenti.unipr.it

Nanotechnology is a rapidly growing industry, with a market value expected to reach US$ 49 billion by 2017 (Nanotechnology Market Outlook 2017, RNCOS, May 2013).
Engineered nanomaterials (ENMs) are structures on the range of 1-100 nm, characterized by peculiar properties due to their small size and surface reactivity that make them suitable for several industrial applications. Because of their wide diffusion and of the lack of information about mechanisms of biological uptake and interaction with cells, it's crucial to assess the risks linked to their spread and behaviour in the environment. The aim of this work was to analyse the response of Saccharomyces cerevisiae model system to CdS QDs, exploiting high-throughput genomic and transcriptomic approaches: the former consisted in screening a collection of 6000 haploid strains, with a deletion in genes that are not essential for yeast's survival; the latter consisted in a whole-transcriptome analysis of expression levels through Affymetrix GeneChip Microarray platform.
The data were analysed through different bioinformatics tools to identify the genes and main pathways of response to CdS QDs. In particular, mitochondrial organization and mitosis seemed to be the main biological processes impaired by CdS QDs toxicity.
Results obtained could therefore provide information on biological mechanisms and key role genes involved in nanomaterials response in yeast cells and, more in general, in higher eukaryotes and humans.

ISBN 978-88-941066-1-9

Phytotechnologies for Sustainable Development

12th International Conference
International Phytotechnology Society
2015 September 27-30 Hilton Garden Inn - Manhattan, KS

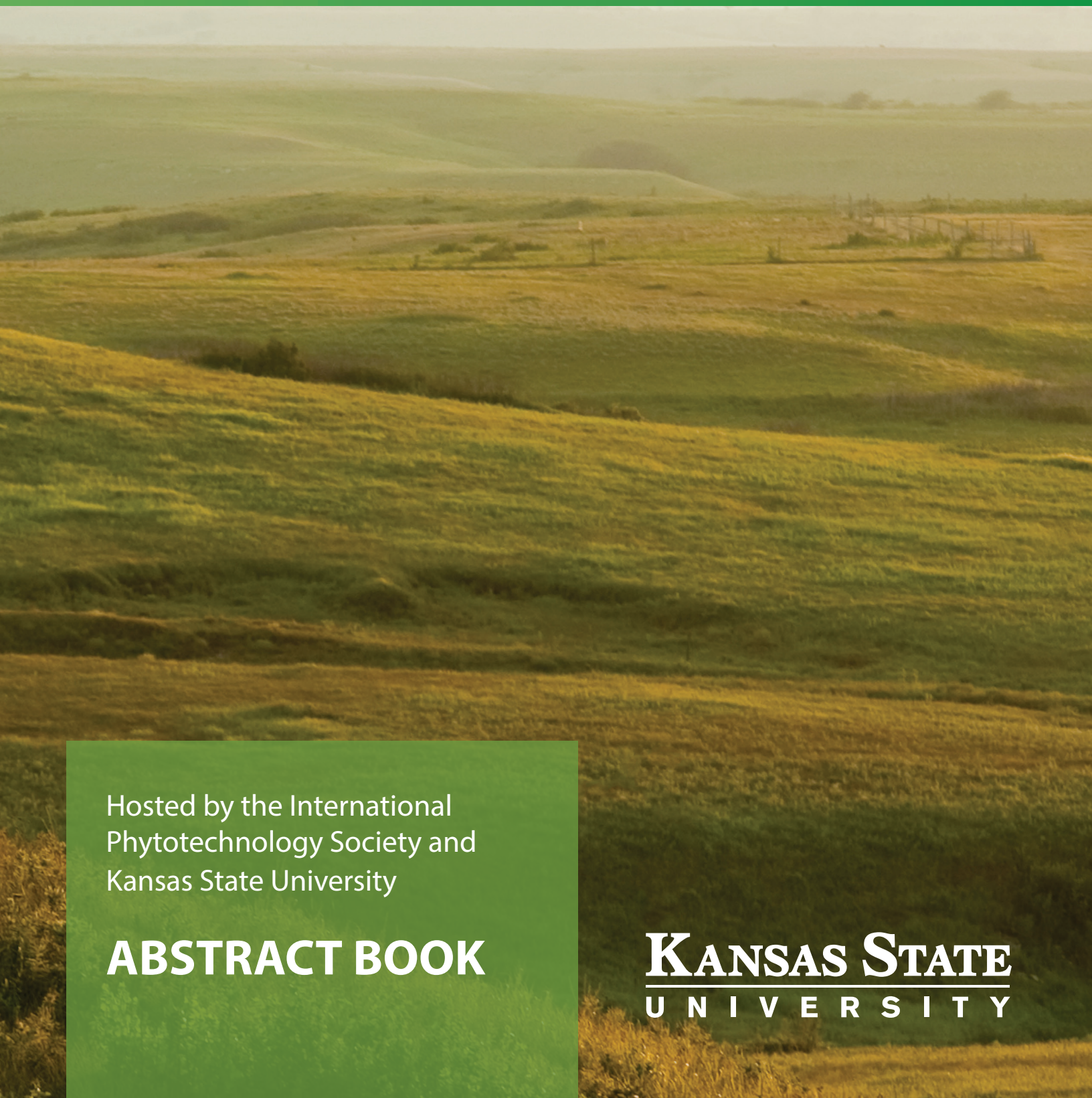

Hosted by the International Phytotechnology Society and Kansas State University

ABSTRACT BOOK

KANSAS STATE UNIVERSITY

Abstract Book

12th International Phytotechnologies Conference

Organized by:
International Phytotechnology Society

Hosted by:
Kansas State University

Editor:
Larry E. Erickson
ISBN 178-0-692-50825-1

Published by:
Kansas State University
Manhattan, KS

84. Marmiroli, Marta

Two cv. of Solanum lycopersicum treated with As and As+Si: differences in As uptake, localization, oxidative stress response and proteomic profile

Marmiroli, Marta*, Davide, limperiale; Francesca, Mussi; Giacomo, Lencioni; Nicola, Cavirani; Nelson, Marmiroli. All authors: Dept. Life Sciences, University of Parma, Parco Area delle Scienze 33/A, 43124 Parma, Italy.

Cultivars Aragon and Gladis of Solanum lycopersicum were sown in punched-wells polystyrene boxes on common garden soil, after several transplants, they were settled (one plant) in 12-L pots in a greenhouse under controlled conditions. One hundred days after sowing (T0), three plants every batch of 12, where harvested: all organs (roots, leaves, stems, fruits). Two batches were treated either with 5mg/L As (AsNaO2) or 5mg/L As (AsNaO2) plus 2mg/L Si (CaSiO3), one was left as control. After 48 hours (T48h) and 15 days (T15d), three replicates for treatment were collected along with their soils. Total As was measured with AAS for each plant organ and soil; TFs, BCFs were calculated accordingly for each organ, time and type of treatment. We measured in leaves and fruits oxidative stress response indicators, such as respiration, chlorophyll and carotenoids, total phenolics, DPPH, ABTS, total GSH (GSSG, GSH in redox state), lipid peroxidation, total ROS. Cross-sections of all organs were analysed for morphological changes at cellular level with optical and ESEM microscopy, SEM/EDX microanalysis was used for As, Si and mineral nutrients localisation within each organ. Total proteins were extracted from fruits and leaves (for each type/time of treatment), separated through 2D-SD-PAGE gels, stained with Comassee blue. Significant spots were cut, de-stained, digested with trypsin, run through MALDI-TOF to obtain peptides mass fingerprints, which were searched and identified in silico. Significant difference were found between cultivars, in all quantities and parameters, depending mostly on the treatment length and Si addition.

Keywords: Arsenic, Tomato cvs., Silicon, As accumulation, plant response to As

*Marrmiroli, Marta, Dept. Life Sciencies, University of Parma, Parco Area delle Scienze 33/A, 43124 Parma, Italy. E-mail: marta.marmiroli@unipr.it

85. Marmiroli, Marta

Basis for cadmium sulphide quantum dot tolerance and sensitivity: a genome-wide nanotoxicology screening of Saccharomyces cerevisiae mutants

* Marmiroli, Marta1, Luca, Pagano1; Francesco Pasquali 1; Andrea, Zappettini2; Valentina, Tosato3; Carlo, Bruschi3; Nelson, Marmiroli1*.
1: Dept. Life Sciences, University of Parma, Parco Area delle Scienze 33/A, 43124 Parma, Italy.
2: IMEM-CNR, Parma, Italy
3: Yeast Molecular Genetics Laboratory, International Centre of Genetic Engineering and Biotechnology, Trieste, Italy.

The use of cadmium sulphide quantum dots (CdS QDs) is increasing, particularly in the electronics industry, but their size (1-10 nm in diameter) is small enough for them to be taken up by living cells. Here, a bakers' yeast (Saccharomyces cerevisiae) deletion mutant collection has been exploited to provide a high-throughput means of revealing the genetic basis for tolerance /susceptibility to CdS QDs exposure. The deletion of 112 genes, some associated with the abiotic stress response, some with various metabolic processes, some with mitochondrial organization, some with transport and some with DNA repair, reduced the level of tolerance to CdS QDs. A geneontology analysis highlighted the role of oxidative stress in determining the cellular response. Transformation of sensitive mutants with centromeric plasmids harbouring DNA from a wild type strain restored the wild type growth phenotype when the complemented genes encoded either HSC82, DSK2 or ALD3. The use of these simple eukaryote knock-out mutants for functional toxicogenomics analysis will inform studies focusing on higher organisms.

Keywords: CdS Quantum Dots, functional toxicology, yeast mutants, gene ontology analysis.

*Marrmiroli, Marta1, Dept. Life Sciencies, University of Parma, Parco Area delle Scienze 33/A, 43124 Parma, Italy. E-mail: nelson.marmiroli@unipr.it

Proceedings of The 13th International Phytotechnologies Conference

Yingming Luo
David Tsao
Jing Song
Jason White
Lee Newman
Longhua Wu
Joel Burken
Pengjie Hu
Stephen Ebbs
Xiaoe Yang
Yanli Gao
Chen Tu
Lizhong Zhu
Shupeng Li

(Editors)

26-29 September, 2016

Hangzhou, China

Mitochondrial Disruption as a Molecular Mechanism of Toxicity of Metal-Containing Nanoparticles

N. Marmiroli, R. Ruotolo, M. Marmiroli, D. Imperiale, L. Paesano, L. Pagano, F. Pasquali, G. Pira & E. Maestri

Department of Life Sciences, University of Parma, Parma, Italy

*Presenting author: elena.maestri@unipr.it

Abstract: One of the main challenges raised by the widespread application of engineered nanomaterials, with the possibility of interfering with their commercial development, is the still perceived lack of knowledge on their potential toxic effects. Even though evidence is accumulating on the biological effects of nanomaterials, at the level of cells, tissues, organisms, the risk assessment procedures are not harmonised and the results obtained so far are not easily comparable. Recent experimentations on disparate organisms, ranging from fungi to plants and animal tissues, have shown that mitochondria are among the main targets of nanomaterials containing metals, such as nano titania, nano zinc oxide, quantum dots and nanosilver. In the effort to provide a unifying picture of the basilar molecular mechanisms of nanomaterial actions, this work reviews the most recent literature, examining all instances of mitochondrial involvement in the response to nanomaterials in eukaryotes, describing the role of the interplay between nuclear and mitochondrial genomes, the effects on mitocondrial morphology and/or functionality, the consequences on cell life or death. The results will highlight the critical features and parameters to consider in the design of safer nanomaterials, as well as provide a standardised battery of tests which can be applied to assess the impact of nanomaterials in general. The focus on metal-containing nanomaterials will be relevant for risk assessment of the most important classes of nanoparticles present in our environment. At the same time, the elucidation of molecular mechanisms for toxicity can provide information necessary for the "safe-by-design" approach to nanotechnologies.

Key words: apoptosis, hazards, nanotechnology, respiration, risk assessment

Acknowledgment: The research has been financed by Local funds, University of Parma.

XVII Congresso Nazionale AIBG

Associazione Italiana di Biologia e Genetica Generale e Molecolare

Atti del Congresso

30 settembre - 1 ottobre 2016 • Cagliari

XVII Congresso Nazionale AIBG

Associazione Italiana di Biologia e Genetica Generale e Molecolare

30 settembre - 1 ottobre 2016 • Cagliari

www.corsiecongressi.com/aibg2016/index.asp

Si ringrazia il collega Angelo Diaz per l'immagine di copertina

Molecular basis of the antitumor activity of delta-tocotrienol in melanoma cells: apoptosis, endoplasmic reticulum stress and cancer cell stemness

R.M. Moretti[1*], M. Marzagalli[1*], E. Messi[1], M. Montagnani Marelli[1], F. Fontana[1], G. Beretta[2], P. Limonta[1#]
[1]Department of Pharmacological and Biomolecular Sciences, University of Milan; [2]Department of Pharmaceutical Sciences, University of Milan *Contributed equally to the work

Malignant melanoma is one of the most aggressive and treatment-resistant human cancers: the prognosis of metastatic disease is still poor.
The interest in nutraceutical compounds is increasing, because of their antitumor activity and lower toxicity with respect to standard therapies. Tocotrienols, vitamin E components, were reported to possess antitumor activity in some tumors.

Preliminary data obtained in our laboratory demonstrate that delta-tocotrienol (δ-TT) exerts an antiproliferative activity in melanoma cells (A375 and BLM), while sparing normal melanocytes. The experiments here described were performed to clarify the molecular basis of this activity.
1) We demonstrated that, in melanoma cells, δ-TT triggers the apoptosis process (cleavage of caspase-3/PARP, increased Bax/Bcl2 ratio, cytochrome c release).
2) The proapoptotic effect of this compound was mediated by activation of the endoplasmic reticulum (ER) stress-related branches: PERK/ATF4/CHOP, IRE1alpha and caspase-4.
3) The A375 melanoma cell line is enriched of cancer stem cells (CSC) overexpressing the CD271 marker. When cultured in appropriate conditions, these cells are able to form melanospheres expressing the embryonic Oct-4 stem cell marker. δ-TT reduced the ability of melanoma cells to form melanospheres. Treatment of stem cells-enriched cultures (melanospheres) with δ-TT resulted in a significant decrease of sphere number and dimensions.

These data demonstrate that δ-TT exerts a proapoptotic activity on melanoma cells, through activation of the ER stress pathways and by reducing the CSCs subpopulation of melanoma cell lines.
(PRIN 2010-2011, FBML, M. Rouge Onlus)

Molecular mechanisms of toxicity of metal-containing nanoparticles in plants: an omics approach

N. Marmiroli, R. Ruotolo, M. Marmiroli, D. Imperiale, L. Pagano, F. Pasquali, E. Maestri[#]
Department of Life Sciences, University of Parma, Parma, Italy

One of the main challenges raised by the widespread application of engineered nanomaterials, with the possibility of interfering with their commercial development, is the still perceived lack of knowledge on their potential toxic effects. Even though evidence is accumulating on the biological effects of nanomaterials, at the level of cells, tissues, organisms, the risk assessment procedures are not harmonised and the results obtained so far are not easily comparable. Recent experimentations on disparate organisms, ranging from fungi to plants and animal tissues, have shown that mitochondria are among the main targets of nanomaterials containing metals, such as nano titania, nano zinc oxide, quantum dots and nanosilver.

In the effort to provide a unifying picture of the basilar molecular mechanisms of nanomaterial actions, this work reviews the most recent literature, examining all instances of mitochondrial involvement in the response to nanomaterials in eukaryotes, describing the role of the interplay between nuclear and mitochondrial genomes, the effects on mitocondrial morphology and/or functionality, the consequences on cell life or death. The results will highlight the critical features and parameters to consider in the design of safer nanomaterials. The focus on metal-containing nanomaterials will be relevant for risk assessment of the most important classes of nanoparticles present in our environment. At the same time, the elucidation of molecular mechanisms for toxicity can provide information necessary for the "safe-by-design" approach to nanotechnologies.